

# CASE FILE COPY

NASA-SP 5110

TECHNOLOGY UTILIZATION

## 55-NITINOL—THE ALLOY WITH A MEMORY: ITS PHYSICAL METALLURGY, PROPERTIES, AND APPLICATIONS

A REPORT



NATIONAL AERONAUTICS AND SPACE ADMINISTRATION



**55-NITINOL—THE ALLOY WITH A MEMORY:  
ITS PHYSICAL METALLURGY,  
PROPERTIES, AND APPLICATIONS**

**A REPORT**

By  
C.M. Jackson, H.J. Wagner, and R.J. Wasilewski,

Prepared under contract for NASA  
by Battelle Memorial Institute



*Technology Utilization Office*

NATIONAL AERONAUTICS AND SPACE ADMINISTRATION

*Washington, D.C.*

1972

NOTICE • This document was prepared under the sponsorship of the National Aeronautics and Space Administration. Neither the United States Government nor any person acting on behalf of the United States Government assumes any liability resulting from the use of the information contained in this document, or warrants that such use will be free from privately owned rights.

---

For sale by the Superintendent of Documents,  
U.S. Government Printing Office, Washington, D.C. 20402  
Price \$1.00

*Library of Congress Catalog Card Number 74-177266*

# Foreword

The National Aeronautics and Space Administration has established a Technology Utilization Program for the rapid dissemination of information on technological developments that have potential utility outside the aerospace community. To assure the greatest possible benefits to the public from the space program, emerging technology and innovations are continuously screened and that which has potential industrial or educational use is presented in a series of NASA publications. This report is one of a series of such publications sponsored by the NASA Technology Utilization Office to help industry and institutions benefit from research and development in the aerospace field.

A series of nickel-titanium alloys (55-Nitinol), which are unique in that they possess a shape "memory," are described in this report. Components made of these materials that are altered in their shapes by deformation under proper conditions will return to predetermined shapes when they are heated to the proper temperature range. The shape memory, together with the force exerted and the ability of the material to do mechanical work as it returns to its predetermined shape, suggest a wide variety of industrial applications for the alloys. This report also includes discussions of the physical metallurgy and the mechanical, physical, and chemical properties of 55-Nitinol; procedures for melting and processing the material into useful shapes; and a summary of applications that have been suggested for these unique alloys.

Director  
Technology Utilization Office

# Acknowledgments

The published information used in preparing this report was obtained from articles in technical journals and reports on Government-sponsored research programs. In locating this material, the following information centers, libraries, and abstract services were searched:

- Defense Metals Information Center
- The Libraries of Battelle-Columbus
- ASM Review of Metal Literature
- Chemical Abstracts

Additional data were obtained by personal contact, telephone, or written communication with 31 individuals representing 19 organizations in the United States and foreign countries. All the information in the report covers the period from 1955 to March 31, 1970.

The contributions of the individuals and organizations indicated above are acknowledged with the authors' appreciation. The assistance of Vernon W. Ellzey, Project Technical Coordinator of Battelle Memorial Institute, is also gratefully acknowledged.

# Contents

	Page
CHAPTER 1. INTRODUCTION .....	1
CHAPTER 2. PHYSICAL METALLURGY .....	3
Equilibrium Phases .....	3
Crystal Structure .....	4
Discussion of Crystal Structures .....	8
Mechanical-Memory Behavior .....	11
CHAPTER 3. PROCESSING PROCEDURES .....	15
Melting and Casting .....	15
Mechanical Working .....	19
Heat Treatment .....	21
Joining .....	22
CHAPTER 4. PHYSICAL PROPERTIES .....	23
Melting Point .....	23
Density .....	23
Electrical Resistivity .....	23
Thermoelectric Power .....	28
Hall Coefficient .....	29
Velocity of Sound .....	30
Damping, Internal Friction, Dynamic Modulus, and Poisson's Ratio .....	35
Heat Capacity and Latent Heat of Transformation .....	42
Magnetic Susceptibility .....	47
Thermal Conductivity .....	47
Thermal Expansion Effects and Shape Memory .....	47
CHAPTER 5. MECHANICAL PROPERTIES .....	57
Stress-Strain Characteristics .....	57
Thermomechanical Recovery Force and Work .....	63
Hardness .....	68
Effects of Alloying .....	70
Impact Toughness .....	71
Fatigue Strength .....	71
Machinability .....	73
CHAPTER 6. CHEMICAL PROPERTIES .....	75
Resistance to Corrosion .....	75
Resistance to Oxidation .....	75
Effect of Hydrogen Absorption .....	76
CHAPTER 7. APPLICATIONS FOR 55-NITINOL .....	77
CHAPTER 8. CONCLUSIONS AND RECOMMENDATIONS .....	81
REFERENCES .....	83



# Introduction

Some 10 years ago, Buehler and Wiley of the U.S. Naval Ordnance Laboratory developed a series of engineering alloys that possess a unique mechanical (shape) "memory" (ref. 1). The generic name of the series of alloys is 55-Nitinol, where Nitinol stands for Nickel Titanium Naval Ordnance Laboratory. These alloys, which have chemical compositions in the range from about 53 to 57 weight percent nickel, balance titanium, are based on the intermetallic compound NiTi.

The memory is such that, given the proper conditions, Nitinol objects can be restored to their original shape even after being "permanently" deformed out of that shape. The return to the original shape is triggered by heating the alloy to a moderate temperature. Considerable force is exerted, and mechanical work can be done, by the material as it "snaps back" to its original shape. This mechanical (shape) memory, which is otherwise unknown in engineering alloy systems, furnishes design engineers with the opportunity to design on the basis of an entirely new principle.

The potential of these alloys in a wide variety of industrial and Government applications prompted the NASA Technology Utilization Office to sponsor the preparation of this literature review by the Columbus Laboratories of Battelle Memorial Institute. Significant research on 55-Nitinol has been funded by NASA.

The concept of a shape memory is new. Accordingly, a brief description of this memory and how it is imparted to Nitinol objects will be given first.

The steps in the Nitinol shape memory process are shown in figure 1 (ref. 2). The material is first obtained in a basic shape such as wire, rod, sheet, tube, extrusion, and casting (step 1). This shape is then formed into the shape that the alloy will later be called upon to "remember," i.e., its "memory configuration" (step 2). Next, the Nitinol shape is clamped in a fixture that constrains it in the memory configuration (step 3). The Nitinol, restrained from

moving by the fixture, is given a heat treatment to impart the memory and is then cooled (step 4). (Drennen, Jackson, and Cross found 900° F to be the optimum heat treatment temperature for several 55-Nitinol compositions (refs. 3 and 4). It was later found that 900° F is also the optimum memory heat treatment temperature for a number of other compositions of 55-Nitinol.) After the Nitinol part, in the memory configuration, has cooled to below the transformation temperature range (to be defined), the part is strained to form the "intermediate shape" (step 5). The intermediate shape is the shape that the part is to retain until it is heated to restore it to the memory configuration (step 6). The temperature to which the part must be heated to return it to the memory configuration depends on the chemical composition of the alloy.

Buehler and Wang have shown that the transformation temperature on heating, which corresponds approximately to the top of the temperature range through which the material must be heated to restore it to its memory configuration, varies in binary nickel-titanium alloys from about -50° to +166° C (ref. 5). Furthermore they showed that, by substituting cobalt for some of the nickel in the alloy, the transformation temperature can be decreased to about -238° C (ref. 5).

Of considerable interest to potential users of the alloy is the fact that the memory process (steps 5 through 7 in fig. 1) can be repeated many times. That is, after the part has recovered its memory configuration upon heating (step 6 in fig. 1) and cooled to below its transformation temperature range (step 7), it can be deformed again to an intermediate shape (step 5) and then heated to restore it to the memory configuration (step 6). This repeatability of the shape-memory effect has been demonstrated on samples that have been subjected to steps 5, 6, and 7, thousands and even millions of times.

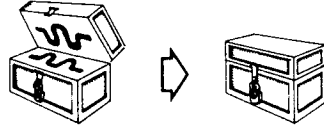
As the 55-Nitinol part, in its intermediate shape, is heated to return it to its memory configuration, the

(1) OBTAIN 55-NITINOL IN A BASIC SHAPE: wire, rod, sheet, tube, extrusion, casting, etc.

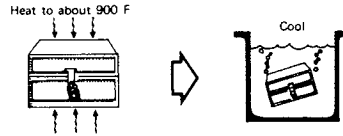
(2) FORM THE DESIRED "MEMORY CONFIGURATION"



(3) CLAMP MEMORY CONFIGURATION IN A FIXTURE



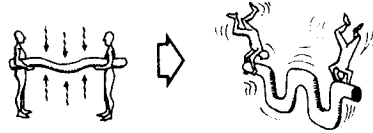
(4) GIVE MEMORY HEAT TREATMENT (MHT)



(5) STRAIN TO THE INTERMEDIATE SHAPE



(6) GIVE RESTORATIVE HEAT TREATMENT (RHT) (+300 to +275 F., depending on composition)



(7) COOL TO AMBIENT TEMPERATURE



This cycle is called a Strain-Heat-Cool (SHC) Cycle.

FIGURE 1.—Steps in the Nitinol shape memory process.

alloy exerts very considerable force and can do significant mechanical work. Accordingly, the applications that have been envisioned for 55-Nitinol utilize not only the shape change but also these force and work capacities. Other applications are based on the unusual changes in damping capacity and electrical resistivity that occur over the transformation-temperature range.

In the following chapters consideration will be given to the physical metallurgy, processing, properties, and potential applications of 55-Nitinol—"The Alloy With a Memory." It is extremely impor-

tant to keep in mind, when considering data on the properties of 55-Nitinol, that these properties are very sensitive—much more so than are the properties of other nickel- or titanium-base alloys—to the chemical composition of the alloy. These properties are also sensitive to the methods by which the alloy is processed and heat treated. Thus, data of different investigators, measured on material that is nominally the same, are often in disagreement. Through careful control of the chemical composition and processing history of these alloys, however, reproducible results can be obtained.

## Physical Metallurgy

## EQUILIBRIUM PHASES

The existence of the equiatomic compound NiTi was first reported by Laves, who suggested the structure to be ordered, CsCl (B2) type (ref. 6). Later work on the phase equilibria in the system Ti-Ni established (1) that NiTi melts congruently, (2) that the next titanium-rich compound  $Ti_2Ni$  forms by a peritectic reaction, and (3) that a eutectic reaction takes place between NiTi and the congruently melting  $Ni_3Ti$  (refs. 7 and 8). In addition, both investigations indicated an essentially vertical NiTi-phase-field boundary on the titanium-rich side of the equiatomic composition. Significant discrepancies, however, are present in the reported melting and peritectic temperatures, and the proposed boundaries of the single-phase NiTi field. Basic differences arose in the interpretation of the observations below approximately 800° C. Margolin and Ence suggested NiTi was stable over a wide composition range down to room temperature (ref. 7). Poole and Hume-Rothery suggested NiTi would "undergo a low temperature decomposition into  $Ti_2Ni + Ni_3Ti$ " (ref. 8) in agreement with the earlier suggestion of Duwez and Taylor (ref. 9), who placed the eutectoid temperature at >800° C. Subsequent work by Purdy and Parr did not confirm the existence of the eutectoid reaction (ref. 10). They suggested that there was a significant contraction of the NiTi single-phase field at temperatures <800° C, and also they were the first to uncover the presence of a new structure ( $\pi$ ) forming at 36° C in compositions containing <50 atomic percent (<55 weight percent) nickel.

The three versions of the proposed equilibrium diagram in the vicinity of the equiatomic composition are shown schematically in figure 2 (Buehler and Wiley) (ref. 11). In critically evaluating these, it was first noted that the broad homogeneity range suggested by Margolin et al. (ref. 7) was based on very

scanty data, hence the later determination (ref. 10) of the NiTi composition limits is preferred. In later work, some observations have been rationalized on the assumption of the eutectoid reaction (refs. 11 to 15) and other observations on the assumption of its absence (refs. 16 to 24); at times both assumptions were successively used by the same investigators.

A definitive evaluation of the published data is at present handicapped by the grossly inadequate characterization of the materials on which the observations were made. It is probable that most of the experimental specimens were significantly contaminated with interstitials—in particular, oxygen and the extent to which such contamination may affect the binary phase equilibria has not been determined. An extensive investigation of the equilibrium diagram close to the equiatomic composition suggests the following (ref. 24):

(1) Maximum congruent melting occurs at  $50.8 \pm 0.2$  atomic percent Ni, rather than (as previously assumed) at the equiatomic composition.

(2) The nickel-rich phase boundary is in close agreement with that determined by Purdy and Parr (ref. 10). The homogeneity range of the NiTi below 500° C is very limited.

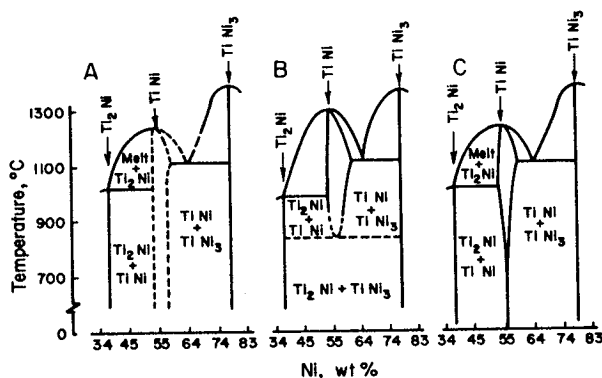


FIGURE 2.—The NiTi equilibrium diagram showing three different versions of the TiNi-phase boundary.

(3) A new phase, of approximate composition  $\text{Ni}_3\text{Ti}_2$ , forms (probably by a peritectoid reaction) at  $625 \pm 20^\circ\text{C}$  in nickel-rich compositions. Its structure is closely related to that of  $\text{Ni}_3\text{Ti}$ , and its formation can be suppressed very readily.

(4) A diffusionless structural transformation takes place in  $\text{NiTi}$  at approximately  $60^\circ\text{C}$ .

The above conclusions are basically in agreement with the equilibrium diagram proposed by Purdy and Parr, and the resulting diagram is shown in figure 3. On the basis of the observations on low-interstitial compositions heat treated in the  $600^\circ\text{C}$  temperature range (ref. 21), the existence of the eutectoid composition can be ruled out. The diagram in figure 3, however, cannot be considered as completely established. In particular, there are indications that other structures may also form in annealing the metastable, nickel-rich, compositions at temperatures below  $500^\circ\text{C}$ , in addition to (or perhaps instead of) the  $\text{Ni}_3\text{Ti}_2$  phase (ref. 24).

Significant segregation can be expected on solidification of the equiatomic melt, with the resultant presence of fine  $\text{Ti}_2\text{Ni}$  phase in the solid (fig. 3). This has, in fact, been generally observed. Homogenizing the cast material at  $1000^\circ\text{C}$  or (preferably) alternate hot working and annealing in this temperature range can be used to obtain essentially phase-pure  $\text{NiTi}$ , provided the interstitial content is kept low. The  $\text{Ti}_2\text{Ni}$  structure, however, is stabilized by oxygen (refs. 21 and 25) and nitrogen (ref. 26), and the precipitate may be present even in nickel-rich compositions containing sufficient interstitials.

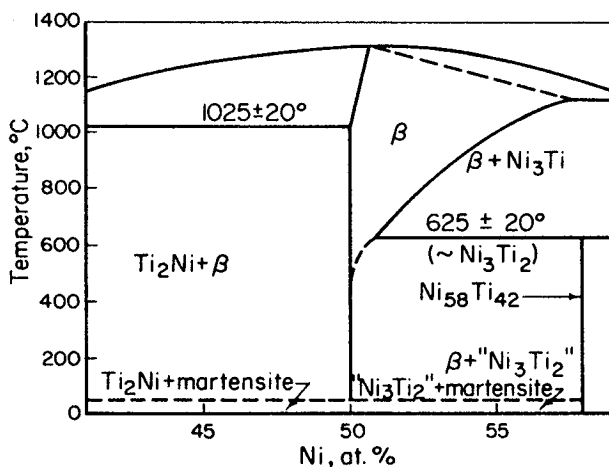


FIGURE 3.—Proposed equilibrium diagram of the  $\text{NiTi}$  binary system in the vicinity of the equiatomic composition.

The essentially vertical phase field boundary on the titanium-rich side suggests no major effects of prior thermal history in the titanium-rich compositions. In contrast, the fact that the nickel solubility in the  $\text{NiTi}$  phase increases rapidly with temperature presents a "precipitation-hardening" type of phase diagram. The sluggishness of the precipitation of  $\text{Ni}_3\text{Ti}$  at higher temperatures and of  $\text{Ni}_3\text{Ti}_2$  below  $625^\circ\text{C}$  makes it very easy to retain the metastable, supersaturated  $\text{NiTi}$  phase at room temperature. The hardenability of nickel-rich compositions, first reported by Buehler and Wiley is due to solid solution and/or precipitation hardening, depending on the heat treatment (refs. 11 and 12).

The precipitation of an intermediate phase of the approximate composition  $\text{Ni}_3\text{Ti}_2$  at  $625^\circ\text{C}$  and below, has been positively established (ref. 24). Whether this phase is representative of the equilibrium conditions, however, is not clear. Both the  $\text{Ni}_3\text{Ti}_2$  and other related structures observed to precipitate at  $<500^\circ\text{C}$  may be transition structures in the formation of  $\text{Ni}_3\text{Ti}$  equilibrium precipitates. The peritectic reaction proposed by Wasilewski et al. in figure 3 must be considered tentative at this time, and other possibilities (e.g., spinodal decomposition) cannot be ruled out (ref. 24).

Standard metallographic examination of the microstructures of nickel-titanium compositions near stoichiometric  $\text{NiTi}$  so far has been of very limited significance. This is due primarily to the apparently featureless structure of the martensitic phase, and also to the generally present minor second-phase precipitates in the (nominally single phase)  $\text{NiTi}$  compositions. In the "commercial-purity" material, titanium carbide, oxide and/or oxycarbide inclusions are also common. In addition, the apparent structure may depend sensitively on the mode of preparation of the metallographic section (ref. 11).

It is considered that the few published examples of structures are not sufficiently representative to warrant a more detailed discussion. A meticulous investigation of this area is indicated, preferably in conjunction with replica- and transmission-electron microscopy.

## CRYSTAL STRUCTURE

### $\text{Ti}_2\text{Ni}$ and $\text{Ni}_3\text{Ti}$

The structures of the nonequatomic compounds previously reported have been well established.  $\text{Ti}_2\text{Ni}$

is cubic, face-centered (Fd3m), with a cell containing 32 formula units (96 atoms) and a parameter given as  $a_0 = 11.328$  (ref. 9), 11.320 (ref. 8), or 11.3193Å (ref. 25). The ternary, oxygen-containing  $Ti_4Ni_2O$  crystallizes in the same structure, but with a lattice parameter of  $a_0 = 11.3279\text{Å}$ , indicating only a small (if any) lattice expansion on the inclusion of the 16 oxygen atoms in the unit cell (ref. 25).

$Ni_3Ti$  has a hexagonal structure,  $DO_{24}$  type,  $D6_3/mmc$ , consisting of an ABAC stacking of hexagonal close packed (hcp) planes. The lattice parameters reported were

(1)  $a = 5.1010\text{Å}$ ;  $c = 8.3067\text{Å}$  (ref. 27)

(2)  $a = 5.104\text{Å}$ ;  $c = 8.292\text{Å}$  (ref. 9)

(3)  $a = 5.110\text{Å}$ ;  $c = 8.319\text{Å}$  (ref. 8)

(4)  $a = 5.108\text{Å}$ ;  $c = 8.321\text{Å}$  (ref. 28)

Both  $Ti_2Ni$  and  $Ni_3Ti$  are believed to have very narrow homogeneity ranges, and no lattice-parameter variation with composition has been reported.

### NiTi

The structure of the equiatomic compound was stated by Laves and Wallbaum to be of CsCl type (B2), but with no lattice-parameter data or evidence of ordering (ref. 6). Subsequent investigations reported  $a_0 = 2.986$  (ref. 9), 3.011 (ref. 29), 3.013 (ref. 8), and 3.010Å (ref. 30). Observations based on "very diffuse lines" obtained on quenched powders were interpreted as indicating a lattice parameter increase from 2.986Å at 46 atomic percent to 3.012Å at 51 atomic percent titanium (ref. 30), but this is an overstatement of the experimental results presented; the actual variation ranged from 3.00 to 3.012Å only. Purdy and Parr reported, however, no significant lattice-parameter variation (ref. 10).

The earliest explicit proof of the ordered structure was reported by Pietrokowsky and Youngkin, who observed the presence of only the (100) superlattice reflection, in a pattern obtained with monochromatic  $CuK\alpha$  radiation (ref. 31). A similar observation was subsequently reported by Gilfrich, who used MoK radiation and observed the (100) reflection at temperatures up to 1000°C, thus concluding that no order-disorder reaction occurs below that temperature (ref. 14).

A major novel structural investigation was carried out by Wang and co-workers, who reported successful growth of NiTi (nominal composition: 51 atomic percent nickel) single crystals by a modified strain-

anneal technique (ref. 32). The subsequent structure investigation by single-crystal diffraction methods was interpreted as follows (refs. 17 and 33):

(1) Contrary to previously accepted views, the NiTi structure is not a simple CsCl type, but has a large cubic cell corresponding to a superlattice structure, with  $a_0 = 9\text{Å}$ . The unit cell thus consists of 27 subcells of the CsCl structure. This superlattice is stable at moderately elevated temperatures only, and is designated NiTi II. Its proposed atom arrangement is shown in figure 4 (ref. 17).

(2) At a temperature between 600° and 700° C this superlattice structure becomes disordered, and the compound becomes simple body-centered cubic, with random atom distribution, and  $a_0 = 3\text{Å}$ . This structure is designated NiTi I.

(3) The NiTi II large-cell superlattice structure undergoes a displacive structural transformation (fig. 5) on cooling below 40° C, in the compound containing 51 atomic percent Ni. The resulting structure, denoted by NiTi III, was postulated to exhibit a more metallic (nondirectional) bond character than the NiTi II, the latter exhibiting predominantly a covalent (directional) bond. (See ref. 17.)

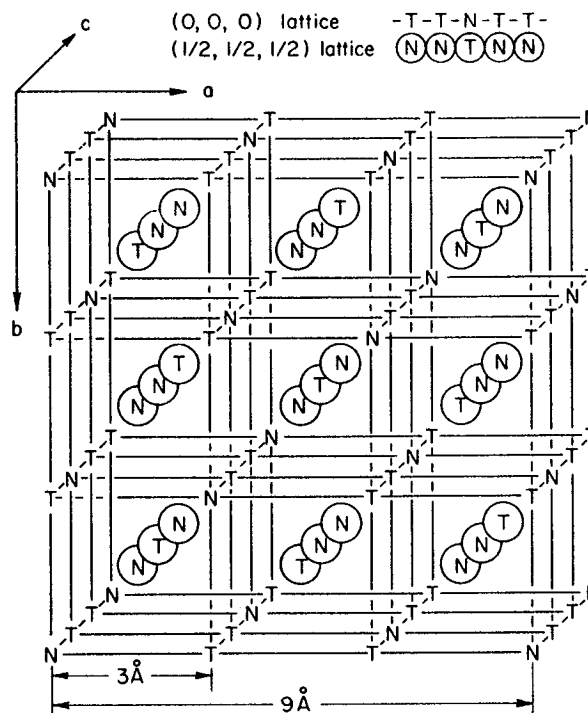


FIGURE 4.—The unit cell of the TiNi (II) phase: The lattice is composed of two distinct simple cubic networks, (0,0,0) and (1/2,1/2,1/2) whose linear atomic sequences are -Ti-Ti-Ni-Ti-Ti- and -Ni-Ni-Ti-Ni-Ni-, respectively.

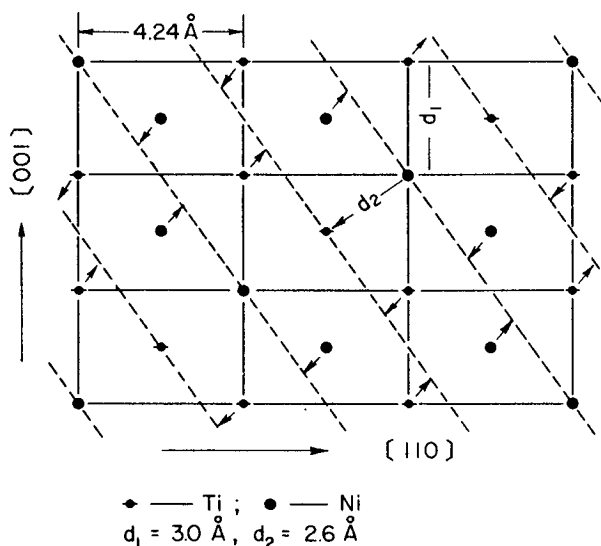


FIGURE 5.—The (110) plane of the TiNi (II) structure whose orientation is shown in figure 4. (The approximate directions of the atomic movements initiated at the 40° C transition are indicated by arrows. The dotted lines indicate the final positions of the atoms which are not yet attained at -70° C.)

(4) The transition NiTi II  $\rightarrow$  NiTi III for the 51 atomic percent nickel composition is reported to start, on cooling, at 40° C. The atom displacement continues on continuing cooling, and the postulated final positions are not attained even at -70° C. Considering the transformation as martensitic, therefore,  $M_s$  is 40° C and  $M_f$  must be below -70° C.

Wang et al. do not give the cell parameters or the atom positions in the final martensitic structure they suggest. The cooperative atom movement they postulate, however (fig. 5), is interpreted as a "unique martensitic pseudo-order-disorder transition." According to the qualitative argument proposed, the true structure should be rhombohedral, both in NiTi II and in NiTi III, inasmuch as one of the cubic  $\langle 111 \rangle$  directions must differ from the remaining ones. The pseudocubic symmetry observed is explained in terms of random occurrence of the four possible structure variants.

In X-ray and electron-diffraction, transmission electron-microscopy, and electrical-resistivity studies of polycrystalline materials, Dautovich and Purdy obtained somewhat different results (ref. 18). They investigated compositions containing 51.0, 50.4, and 50.0 atomic percent nickel, the nickel-rich compositions having been prepared by levitation melting and warm rolling. The interstitial content was not deter-

mined. Their findings can be summarized as follows:

(1) The 51 percent nickel composition, as recrystallized (15 min at 700° C), is single phase, CsCl structure, with faint but sharp superlattice lines. The comparison of X-ray and pycnometric densities indicates that excess nickel is present as antistructure atoms on the titanium sublattice, rather than causing the formation of vacancies on titanium sites.

(2) Subsequent annealing at 500° C causes the Widmanstatten precipitation of a second phase, assumed to be coherent Ti<sub>2</sub>Ni. Selected-area-diffraction (SAE) patterns of the matrix usually showed CsCl symmetry. Occasionally, however, additional spots were observed, which could be indexed on the basis of a unit cell of  $a_0 = 3 \times 3.01 = 9.03 \text{ \AA}$ . This was tentatively ascribed to the ordering of the excess nickel atoms, with an ideal "ordered" defect structure corresponding to 51.8 percent nickel. No corresponding diffraction lines were observed in (polycrystal) X-ray-diffraction patterns.

(3) The displacive transformations were followed by X-ray and electron diffraction, and by electrical-resistivity measurements. It was considered that the transformation takes place in two stages, viz. Cubic NiTi  $\rightarrow$  transition structure, observed to form gradually on cooling from 50° to 23° C. The patterns obtained at 23° C could be indexed as either of the following:

(a) Monoclinic structure,  $a = 4.41 \text{ \AA}$ ;  $b = 3.01 \text{ \AA}$ ;  $c = 4.14 \text{ \AA}$ ;  $\beta = 92.3^\circ$ , or

(b) Rhombohedral structure,  $a = 6.02 \text{ \AA}$ ;  $\alpha = 90.7^\circ$ .

Both of these structures are consistent with the observed doubling of the [110] interplanar spacing observed by SAE. The rhombohedral structure was preferred because of the better intensity agreement between calculated and observed values, and the nonsplitting of the strong (220) reflection. At 20° C an abrupt transformation veers into a martensitic product, reported of triclinic symmetry from electron-diffraction patterns. The unit cell proposed has:  $a = 4.60 \text{ \AA}$ ;  $b = 2.86 \text{ \AA}$ ;  $c = 4.11 \text{ \AA}$ ;  $\alpha = 90.1^\circ$ ;  $\beta = 90.0^\circ$ ;  $\gamma = 96.7^\circ$ ; and SAE patterns suggest the approximate orientation relationships:  $(010)_m \parallel (010)_{\text{cubic}}$ ;  $(001)_m \parallel (101)_{\text{cubic}}$ . The authors identify the martensite with the  $\pi$  phase of Purdy and Parr (ref. 10).

The X-ray diffraction results of Wasilewski et al. confirmed the existence of a diffusionless transformation of the NiTi structure, which was believed to be

“closely related to the CsCl structure” (ref. 21). The structure of the martensitic product was not determined, but was suggested to be complex and of low symmetry. In specimens normalized by annealing for 1 hr at 650° C and furnace cooling, differences in the martensitic patterns were observed in different compositions. These were interpreted as suggesting the formation of two distinct martensitic structures, one forming in compositions containing <50.2 percent Ni, and the other at >50.8 percent Ni. The authors also considered the nature of the reaction taking place in the vicinity of 650° C and found it occurs only in nickel-rich compositions. They concluded that in view of the rather high heat of formation of NiTi (8100 cal/mole) the order-disorder reaction is unlikely to be involved (ref. 34).

It should be stressed that the conclusion of two different martensites forming, depending on the composition, can be considered suspect in view of the reported presence of preferred orientation in the specimens investigated (ref. 21). Furthermore, only one type of martensite was observed by Dautovich and Purdy, though on differently heat-treated materials (500° C anneal) (ref. 18). Martensitic structure varying with composition was, however, unambiguously determined in another CsCl structure: AuCd (Chang and Read (ref. 35)).

Hanlon et al. reported the variation of the transition temperature with composition (ref. 22). As shown in figure 6, the results of three independent investigations of the effect of composition on the martensitic-transition temperature differ markedly, although the reasons for such discrepancy are not obvious.

Additional work on crystal structures was reported in a series of papers by Marcinkowski and co-workers, who used predominantly transmission-electron microscopy. The presence of two distinct martensitic structures was reported in a “well-annealed,” equiatomic NiTi deformed “a few percent at room temperature” (ref. 36). The shear movements of the atoms leading to the two alternative product structures (fig. 7) were given. It was concluded that the martensites form by two distinct simple shear displacements, in the  $[\bar{1}11]_{B2}$  direction and the  $(1\bar{1}2)_{B2}$  plane. As the result, the parent structure above the plane of shear is converted into a monoclinic martensite denoted  $M'_0$  in figure 7, while below the shear plane the (also monoclinic) martensite  $M_0$  is formed. The  $c$  parameters of both martensites are

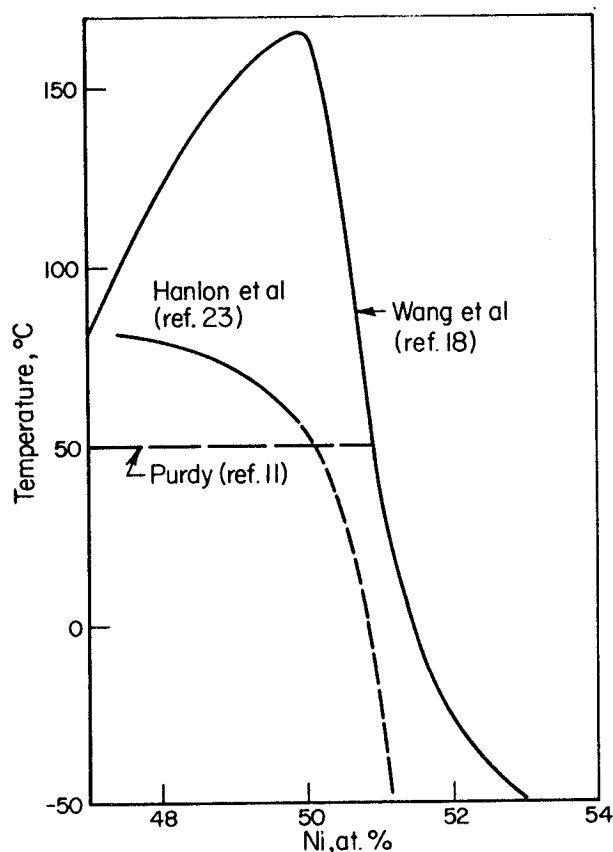


FIGURE 6.—The effect of chemical composition on the martensitic transformation temperature of binary NiTi alloys (refs. 10, 17, and 22).

nearly equal to  $a_0 \sqrt{2}$  of the  $B2$  unit cell. When the lamellae of the two martensite variants are equal in width, the shears almost exactly compensate each other, so that no lattice deformation by slip or twinning is required to accommodate the transformation shear. This almost complete shear compensation is suggested to account (qualitatively) for the revision of the deformed material to its original shape upon reversion to the  $B2$  structure. No other unit-cell parameters ( $a$ ,  $c$ , or  $\beta$ ) are given.

With respect to these conclusions it must be noted that a certain ambiguity is inherent in the method of specimen preparation used. From prior investigations, it may be reasonably concluded that the equiatomic NiTi undergoes a martensitic transformation above 25° C, even though the exact transition temperatures vary. The need for some plastic deformation to develop the martensitic structures observed seems, therefore, unexpected; and the effects of such deformation on either the structures or the morphology of the martensite may be significant.

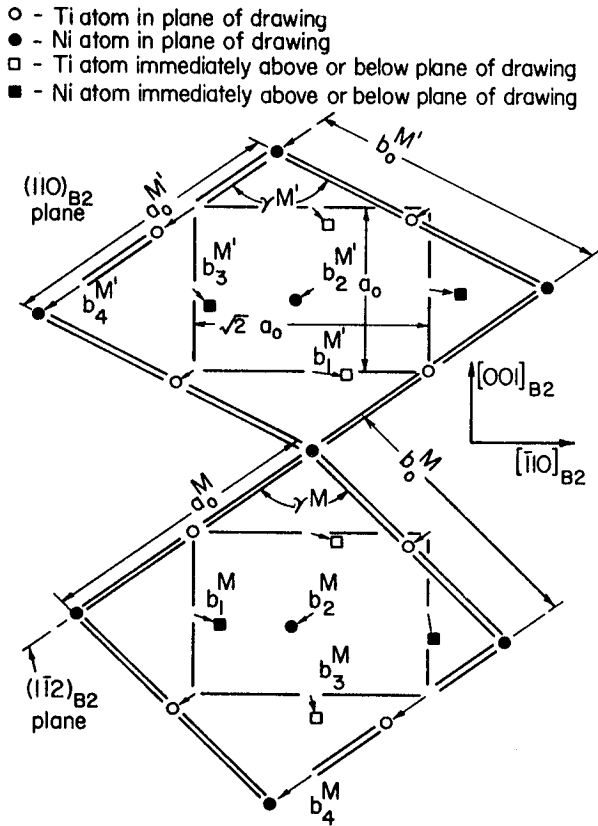


FIGURE 7.—Atom movements which produce true martensitic structures in NiTi.

A more extensive investigation further developing these concepts was reported by Marcinkowski et al. (ref. 37). Transmission-electron microscopy was the main experimental technique used, and the equiatomic (nominal) composition NiTi was investigated. The specimens were heat treated as thin strips, about 0.004 in. thick, in evacuated quartz ampoules, at 1050° C, and quenched from either 1050° C, or from some lower temperature above 650° C.

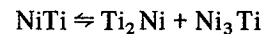
While somewhat more documented, this work presents essentially the same conclusions as the earlier one (ref. 36). It is pointed out that the martensitic structures may be considered as distorted HCP, if the atom species are considered equivalent. The two martensitic structures may be arranged either in bands, or as a checker pattern. In the latter case, any transformation-related macroscopic shear distortions are "almost perfectly eliminated." Although the shears involved in the martensitic formation may be expressed in terms of dislocation formalism (the partial dislocation having a Burgers vector of  $b = (14/88) a_0 [11\bar{1}]$ , referred to the B2 lattice), the

authors pointed out that "nothing is gained by describing the shuffles in terms of dislocation motion, since they give rise to no net shear." The parameters of the martensitic structures are given as

(1)  $M'$ :  $a = 5.19\text{\AA}$ ;  $b = 5.51\text{\AA}$ ;  $c = 4.25\text{\AA}$ ;  $\beta = 116^\circ$ .

(2)  $M$ :  $a = 5.19\text{\AA}$ ;  $b = 4.96\text{\AA}$ ;  $c = 4.25\text{\AA}$ ;  $\beta = 99^\circ$ .  
 A subsequent paper deals with some aspects of the deformation behavior of NiTi, on the basis of the above structures (ref. 38).

In their most recent paper the nature of the  $\sim 650^\circ$  C reactions is considered by Koskimaki et al. (ref. 16). Two compositions, stated as the equiatomic and one containing 54.4 atomic percent nickel, were investigated. The authors conclude that the eutectoid reaction



occurs at  $640^\circ \pm 10^\circ$  C and approximately 51 atomic percent nickel. This eutectoid decomposition is preceded by the formation of an intermediate, large unit-cell (fcc,  $a_0 = 15.2$  to  $15.9\text{\AA}$  transition precipitate. The basic character of the equilibrium reaction, however, is thus in agreement with that proposed in figure 2(b) (refs. 8 and 9). The authors' conclusions regarding the existence of the eutectoid, however, were questioned in discussion by Wasilewski et al. (ref. 23).

### $\text{Ni}_3\text{Ti}_2$

This phase, found to form below 625° C, is suggested to have a structure related to that of  $\text{Ni}_3\text{Ti}$ , consisting of a stacking sequence of ten, rather than four, hcp layers, in a composition analyzed by electron microprobing as  $\text{Ni}_{58}\text{Ti}_{42}$  (ref. 24). The structure determination was based on the earlier patterns for such stacking variants in the Ti-Ni-Cu ternary system by Pfeifer et al. (ref. 39). These investigators found that, apart from the  $\text{Ni}_3\text{Ti}$  structure (which they denote as A4, indicating four-layer stacking), variants A9, A10, and A21 can also form. Wasilewski et al. indicated that A9 and A21 structures may form at temperatures below 500° C, but conclusive confirmation was not obtained (ref. 24).

## DISCUSSION OF CRYSTAL STRUCTURES

In view of the wide disagreement between the reported crystal structure observed at, and in the

vicinity of, the equiatomic NiTi, an attempt will be made to consider (1) the probable causes for such variations, (2) the equilibrium diagram features and the crystal structures reliably established, and (3) conclusions regarding the experimental work required to clarify the existing controversies.

It is believed that the principal reason for the discrepancies in the observed behavior is the all but complete lack of even minimal characterization of the experimental materials. In the majority of published works, the materials investigated are merely referred to as NiTi, not even the nominal composition being given. Furthermore, the impurity content has seldom been determined; at best, the manufacturer's typical analysis of the starting materials, i.e., nickel and titanium, used for the initial synthesis of the compound, is given. The only published work in which somewhat more extensive—but still far from adequate—material characterization had been attempted is that of Butler et al. (refs. 21, 22 and 24), and the calorimetric study of the martensitic transition by Dautovich et al. (ref. 40).

The inadequate characterization is of particular importance in NiTi for two reasons. First, even with high purity and composition control of initial synthesis, the compound is readily contaminated by oxygen in the subsequent processing into suitable specimen shapes. The usual laboratory purification methods cannot be assumed to be effective in interstitial removal from NiTi, e.g., the low-interstitial compound prepared by levitation melting (ref. 18) subjected to double electron-beam zone melting "purification" showed an increase in oxygen content from the very low starting value of  $\sim 100$  ppm (ref. 40) to 1500 ppm (ref. 41). Therefore, the nominal purity of the starting materials may be of little significance in determining that of the experimental specimens. Also, there is indirect evidence that some volatilization (or reaction) takes place during vacuum anneals at temperatures of the order of  $1000^\circ\text{C}$ . This leads to an apparent, or real, change in surface composition and might be particularly significant in the heat treatment of powder, or thin strip, material. This effect can be minimized, however, by annealing bulk, rather than high surface-to-volume ratio, specimens.

Second, for reasons of convenient martensitic transition-temperature range, compositions with a slight excess of nickel (50.5 to 51 percent) have most frequently been sought in the work to date (refs. 11

and 12). Their behavior was considered as representative of the inherent behavior of the "ideal" NiTi structure, in spite of the presence of a large concentration of the structural defects ( $\sim 2$  percent anti-structure nickel atoms, according to ref. 18). This assumption is not necessarily justified. In addition, it is questionable whether equilibrium conditions can be readily attained at, or close to, room temperature in nickel-rich compositions, in view of the diffusion-controlled reactions occurring in the vicinity of  $650^\circ\text{C}$  (ref. 21).

If the experimental materials are, in fact, in a metastable, nonequilibrium condition, their behavior can be expected to be highly nonreproducible; the chances of duplicating the exact degree of nonequilibrium are obviously very slight. Most recent results of Wasilewski et al. indicate this is most probably the major factor (ref. 24).

The following equilibrium diagram features can be considered established:

(1) TiNi melts congruently at a composition slightly nickel-rich, rather than equiatomic. The triple points are:

(a)  $\text{Ti}_2\text{Ni} - \text{NiTi} - \text{liq}$ :  $1025 \pm 20^\circ\text{C}$ ,  $49.75 \pm 0.25$  atomic percent Ni.

(b)  $\text{NiTi} - \text{Ni}_3\text{Ti} - \text{liq}$ :  $1120 \pm 20^\circ\text{C}$ ,  $58.0 \pm 1.0$  atomic percent Ni.

(2) The titanium-rich phase boundary is essentially vertical below the peritectic temperature of  $1025^\circ\text{C}$ .

(3) The nickel-rich phase boundary slopes sharply from 58.0 percent Ni at  $1120^\circ\text{C}$  to 51 percent Ni at  $625^\circ\text{C}$ . The cubic nickel-rich structure can be readily retained by quenching from the single-phase field.

(4) The high-temperature NiTi structure is either an ordered-CsCl type or one very closely related to it. Neutron diffraction work by Freise strongly suggests the former (ref. 42).

(5) The CsCl-structure NiTi undergoes a diffusionless transformation slightly above  $25^\circ\text{C}$ . The  $M_s$  temperature and the temperature range  $M_s$  to  $M_f$  may vary with composition and with prior thermal history, which indicates nonequilibrium behavior. The most probable equilibrium transition temperature is approximately  $60^\circ\text{C}$ , and independent of composition (ref. 24).

(6) The diffusion-controlled reactions close to  $625^\circ\text{C}$  in nickel-rich compositions involve the precipitation of one or more nickel-rich phases intermediate between NiTi and  $\text{Ni}_3\text{Ti}$ . The precipitate

structures are closely related to that of  $\text{Ni}_3\text{Ti}$ . These reactions are very sluggish, and can be easily suppressed by moderately fast cooling.

(7) The structures and/or the number of the martensitic products formed have not been unambiguously determined. Only the existence of the transition and its diffusionless character were established.

The single-crystal diffraction work by Wang et al., presents the first major effort at determining the various crystal structures present (refs. 17 and 33). The work was carried out predominantly on a noncharacterized, nominal 51 percent nickel composition, and the geometry of the shear transformation appears consistent. The results are interpreted in terms of the ideal, equiatomic composition. There are, however, some inconsistencies between the proposed interpretation and the experimental data. Some of these results include:

(1) Strain-anneal single-crystal growth, by repeated cycling over the  $500^\circ$  to  $900^\circ$  C range of a nickel-rich composition, involves repeated crossing of the diffusion-controlled reaction range. It is possible that the streaks observed in the zone photographs (ref. 17) may be due to a modulated structure (ref. 43) rather than to the proposed "displacement disorder." In addition, the Laue patterns shown were not, in fact, those of true single crystals.

(2) The pseudocubic 9A superlattice structure, resulting from the random distribution of the four variants of the rhombohedral domains, could be readily confirmed by the appearance of (111) reflections. The interpretation based only on the zero-layer precession patterns of poor quality cannot be accepted as fully convincing. In addition, the agreement between the observed and the calculated interplanar spacings given in table 1 of reference 17 is poor, in some cases (lines 1, 10, 13, 14, 17, 29, 33), unacceptably so.

(3) The gradual transition to the martensitic product proposed is not in agreement with either the "burst" type martensite formation, or the nucleation-and-growth type martensites.

(4) The suggested coexistence of two or three structures at the same composition over a temperature range, proposed in reference 33 is thermodynamically impossible in a binary system.

These single crystal observations should, therefore, be treated with considerable caution, unless more conclusive corroborating evidence is forthcoming. Similar caution should be exercised in the evaluation

of subsequent work, based on the acceptance of these observations, as e.g., the postulated irreversible critical range in the martensitic transition. (ref. 44).

The X-ray and electron-diffraction results given in reference 18 show the presence of a regular striped contrast in the 51 percent Ni compound annealed at  $700^\circ$  C, i.e., close to the single-phase field boundary. This, again, may have been due to a structure modulation (ref. 43). The annealing of specimens in thin-strip form may also have caused a significant shift of the chemical composition of the specimen. As regards the proposed transition phase and martensitic structures, the agreement between the calculated and the observed polycrystal-diffraction patterns is obviously fair. It is doubtful, however, whether other than rigorous single-crystal data on such complex structures can be accepted as significant. Much the same reservations can be voiced in respect to the interpretation of the observations by Marcinkowski et al., even though the transformation shears proposed are a highly possible qualitative rationalization of some aspects of the transformation behavior (refs. 15 and 36 to 38).

The largely inconclusive results of Wasilewski et al. (at least with regard to the crystal structures) reflect the relative inferiority of the standard experimental methods as compared with transmission electron microscopy (refs. 21 to 24). The use of relatively large specimens, however, permitted them to carry out a relatively extensive characterization of the materials actually examined. The parallel investigation in which more than one experimental technique was used on a range of compositions has shown convincingly that differences in prior treatment can significantly affect both the microstructures and the properties of NiTi compositions. Also, the investigation showed that the major effects can be obtained in nickel-rich NiTi.

In view of the apparent great variety of possible structures reported to date in the NiTi system it seems the clarification of the existing discrepancies will require further work on carefully characterized material. It is essentially mandatory that the behavior over a significant range of composition, with respect to two or more properties, be investigated. The conclusions based on one property alone may be inconclusive. The comparison of these conclusions with observations on differently prepared materials may be misleading. Unquestionably, additional single-crystal research on very rigorously characterized

material seems essential for the firm determination of equilibrium structures.

### MECHANICAL-MEMORY BEHAVIOR

The "mechanical-memory" behavior first reported by Buehler et al. is based on the fact that this material, when deformed below the transition temperature, will return to its original undeformed shape on heating through the transition range (ref. 13). The deformed shape is not reversible on subsequent cooling into the martensitic range. The mechanical- and physical-property variation over the transformation range will be discussed in detail in subsequent chapters. Only the suggested rationalizations for this anomalous behavior and some reported observations on the atomic displacements in the transition range will be discussed here.

The original observation of the memory behavior was rationalized in terms of stress-sensitive decomposition of NiTi. It was indicated that  $Ti_2Ni$  forms preferentially under tensile stress, and  $Ni_3Ti$  under compressive stress (ref. 13). It was further suggested that both of these structures revert to the original NiTi on heating to about  $65^\circ C$ . X-ray-diffraction data interpreted as confirming this hypothesis were reported (ref. 14). It is now, however, generally accepted that this hypothesis is incorrect, and that the memory behavior is in some manner related to the diffusionless-structure transformation.

Qualitatively similar anomalous behavior had been previously observed in the martensitic transformations of the compounds AuCd (ref. 45) and InTl (ref. 46). Both of these compounds, when severely deformed in the martensitic structure under some conditions, revert to the original configuration on heating above the transition temperature. This effect has been most extensively studied in single-crystal Au-47.5 Cd. The semiquantitative rationalization indicated that the martensite forms in two twin-related orientations (refs. 47 and 48). On application of stress, one of the twin orientations, more favorably oriented with respect to the sense of stress, can grow at the expense of the other. This growth may be reversible (in some cases) on the removal of stress; but even when permanent deformation of the twinned martensite is affected, the original shape is regained on heating into the B2 structure range. The memory effect, therefore, may result from (1) an invariant orientation relationship between the B2

parent structure and the twinned martensitic product and (2) the strain accommodation by the growth of one twin orientation at the expense of the other. Whether this is correct, however, cannot yet be definitely stated. In particular, the possible significance of the atom shuffles, known to be involved in the martensitic formation, is yet to be determined (ref. 48).

The situation in NiTi is far less clear. Although substructures, interpreted as probable twins, have been reported, it is not yet established whether or not the deformation in the martensitic product structure is a prerequisite for the memory behavior (ref. 21). On the basis of the published interpretations, the following alternatives may be considered possible:

(1) The deformation must occur in a partly transformed material. This would be consistent with the very extensive ( $M_s$ - $M_f$ ) range proposed by Wang et al. (ref. 17) and with the suggested "strain-martensite" formation in rationalization of the low-yield behavior (ref. 19).

(2) The deformation must occur above the  $M_s$  (but below the  $M_d$ ) temperature. As shown by Ball et al in their investigation of polycrystalline  $Ni_{52}Ti_{48}$ , the plastic strain "due to the formation of strain martensite" could be repeatedly recovered on subsequent heating to  $200^\circ C$  (ref. 49). (In all tests, however, a substantial part of the total strain was irreversible, and ascribed to dislocation flow.) A similar assumption has been implied, though not explicitly stated, by deLange and Zijdeveld (ref. 50). They suggested that a thermal martensite is formed as a random distribution of all the possible crystallographic orientations with respect to the parent lattice. Such random distribution would minimize the strains arising from the (unknown) martensitic shear. When martensite is formed in the presence of an applied stress, however, some orientations will be favored, and a preferred martensitic orientation (texture) will result. This is schematically illustrated in figure 8.

(3) The deformation must occur below the  $M_f$  temperature. In this case the twinned martensitic hypothesis may apply, but the possibility of other alternatives cannot be excluded (ref. 48).

There is, at present, very little reliable information to permit an unequivocal choice between the above alternatives, and a significant amount of work is required to throw further light on the memory phenomenon. It is probable that, by analogy with Au-47.5Cd, deformation in the martensitic product

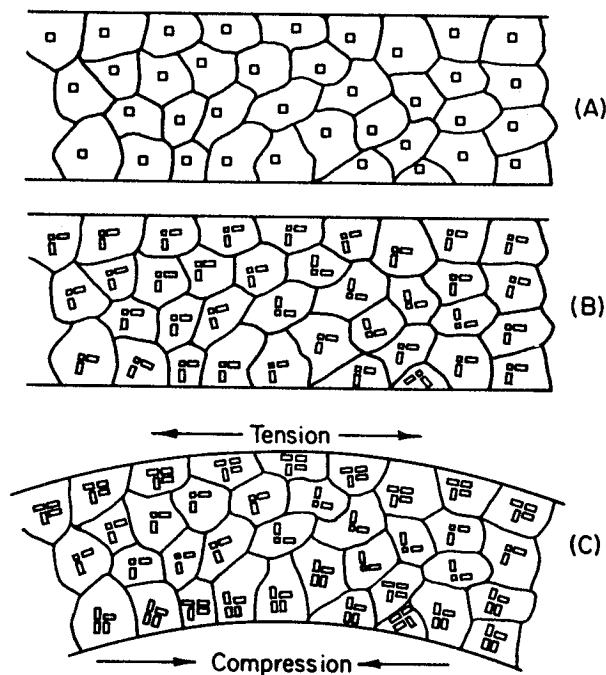


FIGURE 8.—Schematic representation of the martensitic transformation (hypothetical): (a) at 100° C: high-temperature phase with random orientation, (b) after cooling to 20° C: martensite with random orientation has formed in the high-temperature phase, and (c) after deformation at 20° C: (the plastic deformation is realized by the formation of martensite of preferred orientation. The tension and compression sides of the specimen show different textures of the martensite.

phase is a necessary prerequisite. This, however, cannot now be accepted as established beyond doubt, particularly since essentially none of the martensitic transformation parameters ( $M_s$ ,  $M_f$ ,  $M_d$ ,  $A_s$ , and  $A_f$  composition effects) is now unquestionably certain.

In the following section it will be assumed only that the memory behavior is directly related to the martensitic transformation. The observations pertaining to the nature of the structure change involved will be discussed briefly.

#### Martensitic Transformation

As proposed by Wang et al. this reaction consists of a progressive departure from the parent NiTi II structure, hence, a second-order transition (ref. 17). The authors, however, state that "a considerable amount (5.78 cal/g, which corresponds to about 307 cal/g atom for the alloy considered) of latent heat (is) involved at the . . . transition." Since second-order reactions are defined as involving a discontinuity in

the first derivative of the energy vs temperature relationship, the existence of latent heat is not consistent with the proposed reaction order.

Dantovich and Purdy indicated that the intermediate transition structure is formed by a second-order transformation mechanism, but leave open the question of the order of the martensite formation (ref. 18). The observations by Wang et al. (ref. 44) are interpreted as confirming the second-order character of the transition above the martensitic transformation temperature range; but whereas this transition to an intermediate structure was found to exhibit no hysteresis in reference 40, Wang et al. reported it to be irreversible, and to occur only on cooling. Subsequent interpretation of calorimetric data by Dautovich et al. (fig. 9), implies that a discontinuity in  $C_p$  was assumed on martensite formation; the order of the martensitic reaction was not explicitly established (ref. 40).

X-ray-diffraction, calorimetric, dilatation, and physical-property observations reported by Wasilewski et al. were interpreted as indicating a first-order reaction, and latent heat determined at  $370 \pm 20$  cal/g atom (refs. 21, 22, and 24). It is usually accepted that martensitic reactions are, in general, first-order transformations (ref. 48). The most recent work confirms that the order of the transformation does not change depending on the product structure observed (ref. 24).

The above conflicting interpretations are all based on comparably differing experimental behavior of the (nominally the same) compositions investigated. Was-

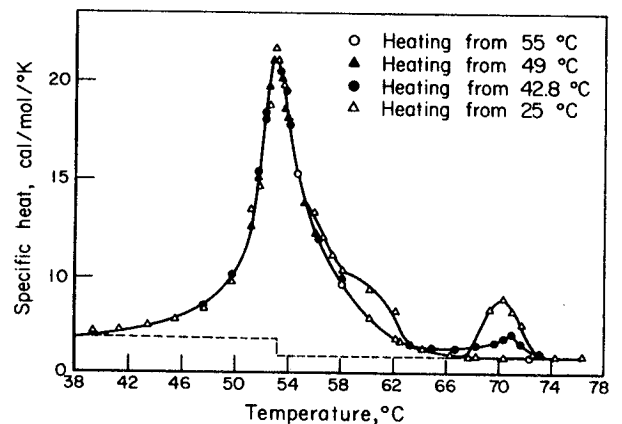


FIGURE 9.—Calorimetric data obtained during heating from the temperatures indicated. (Each heating run was preceded by heating the sample to 95° C or above. The broken line indicates the base values used in the graphical integration.)

ilewski et al. concluded that most of the observations, particularly those on the most commonly used nickel-rich compositions, had been made on nonequilibrium materials (ref. 24). This would account for the wide disagreement between different sets of observations. The extent to which the nonequilibrium condition of the material may affect the transition temperature, the transition temperature range, and possibly the nature of the product has not been investigated to date.

The atom displacements involved in the martensitic transition of the second order, as proposed by Wang have already been mentioned (ref. 17). Additional hypotheses, obtained basically by transmission-electron-microscopy methods and due to Marcinkowski and co-workers have also been referred to (refs. 15 and 36 to 38).

Chandra and Purdy, while giving no detailed atom movements, suggest that the premartensitic-transition structure is characterized by large-amplitude, short-wavelength-atom displacements from their CsCl lattice sites, reflecting incipient instability (ref. 51). This interpretation of the observed streaks in the electron-diffraction patterns does not agree with the results of X-ray diffraction concurrently obtained on other samples of the same (low-oxygen, typically 100 to 200 ppm) material, in that either the triclinic martensite or the rhombohedral transition-structure pattern was observed in these (ref. 18). (If only the atom displacements from their equilibrium positions were involved, the symmetry of the X-ray pattern would not change. For random vibration variation, all the lines should merely become uniformly more diffuse, as with increasing temperature.)

In considering the possible sequence of events at the martensitic transition, the prior heat treatment may also be of significance. Iwasaki and Hasiguti observed the presence of antiphase-domain boundaries in NiTi containing 50.3 percent nickel and in the ternary composition 47Ni-6Co-47Ti (ref. 52). The electron-diffraction pattern showed clearly many spots not possible for the simple CsCl structures, but no clear-cut structure was established. Antiphase

boundaries were observed in dark-field images, with a superlattice reflection, in both "as-annealed" and "as-deformed (in tension)" material. The antiphase boundaries were found to lie on  $[112]$   $B2$  planes. The domains were some three times larger and much more sharply defined in the annealed specimens than in the deformed material.

A precipitation phenomenon in both the stoichiometric and nickel-rich (51 percent nickel) material was reported by Otsuka and Shimizu (ref. 53). The precipitates observed were not  $Ti_2Ni$  and  $Ni_3Ti$ , and in both compositions all the extra spots identified as due to the precipitate lay in  $[112]$   $B2$  reciprocal lattice planes. In both compositions the spacing and the stacking sequence of the reciprocal lattice planes constructed were the same as those of  $B2$  lattice, and had a period of six layers. The arrangement of the reciprocal lattice points, however, was different in the two compositions. In the equiatomic compound, the pattern was indexed as monoclinic, while the nickel-rich precipitate structure was indexed as orthorhombic. The equiatomic composition appeared single phase, hence, the authors suggested that an "early stage of precipitation" may have been involved. The structure of the nickel-rich compound (annealed 72 hours at  $500^\circ C$ ) showed the presence of plate-like precipitate, in agreement with the observations in reference 24 and figure 3.

It is noted that a common feature of all the transmission-electron-microscopy observations is the significance of  $[112]$   $B2$  planes whether interpreted as antiphase domain boundaries (ref. 52), precipitate planes (ref. 53), or the plane of shear (ref. 38). In conclusion, it appears that the information on the martensitic transformation in NiTi is at present highly inadequate. Assuming that the memory behavior is directly connected with this transformation, a considerable amount of additional experimental work is required before reproducible behavior can be reliably expected. Most, if not all, of the interpretations to date must be considered as largely speculative, and should be used with considerable caution in future work, whether fundamental or applied.



# Processing Procedures

## MELTING AND CASTING

The melting and casting of 55-Nitinol to obtain sound, homogeneous material of the proper composition was once a critical problem in the utilization of this unique alloy. Initially, in order to obtain material for research projects the alloy was nonconsumable-arc melted (ref. 12) or levitation melted (ref. 10). Vacuum-induction melting and consumable-arc methods were introduced later, because they better fit commercial production conditions.

The principal features of each method, as regards the end product are summarized in table 1 (ref. 54). The arc and induction methods are discussed in detail in the following paragraphs.

## Vacuum Induction Melting

### Crucible

Vacuum-induction-melting methods worked out by Buehler and co-workers at the U.S. Naval Ordnance Laboratory entailed the use of a high-purity graphite crucible because it was found that molten NiTi would absorb only a very limited amount of carbon (ref. 54). Typically, the ingot will contain about 0.03 to 0.08 wt percent C (ref. 55). For vacuum-induction melting 70- to 80-lb heats, Drennen, Jackson, and Wagner reported on the use of ATJ graphite, a high-density, low-porosity form of graphite (ref. 56). The melting crucible, which had a 100-lb capacity, was designed so that the crucible and

TABLE 1.—Alloy Melting Methods for the Preparation of NiTi and Associated Transition Element Compounds.

Property	Melting method			
	Levitation	Nonconsumable arc	Consumable arc	Vacuum Induction <sup>1</sup>
Melt purity	Superior	Very good	Excellent	Satisfactory
Chemical homogeneity	Excellent <sup>2</sup>	Very good <sup>2</sup>	Fair	Excellent
Composition control	Excellent	Excellent	Fair	Excellent <sup>3</sup>
Configuration casting	Good	Fair	Fair	Excellent
Quantity production	Very limited	Limited	Good	Excellent
Relative cost/lb	Highest	High	Medium	Lowest

<sup>1</sup> Employing a high purity graphite crucible and proper melt sequencing.

<sup>2</sup> Homogeneity limited to very small melts.

<sup>3</sup> Empirical charge factors must be determined in advance.

pouring lip were mechanically joined in such a way that the molten alloy never contacted any other material than graphite during melting and pouring.

The major disadvantage of the graphite crucible is that it will react with either molten nickel or titanium. Carbon is highly soluble in molten nickel, and has a well-known affinity for titanium. On the other hand, NiTi does not have any appreciable solubility for carbon. Procedures for avoiding contact with the pure molten ingredients are described below. Because of this disadvantage of graphite, other crucible materials have been explored, though in each case the results were not satisfactory. Buehler, for example, prepared some Nitinol in a 99 percent-MgO crucible by melting the nickel first and then charging the titanium (ref. 54). He found that the oxygen level in the Nitinol had increased to about 0.08 to 0.18 percent, whereas only 0.05 percent would be expected from the analysis of the sponge titanium used as a charge material. As a result of this work it was indicated that the method might be used satisfactorily, but would require rapid melt sequencing.

Wasilewski et al. reported that melting in alumina crucibles resulted in appreciable oxygen contamination (ref. 21). Drennen et al. (ref. 56) experimented with a thoria crucible, since thermodynamic considerations and experimental data (ref. 8) indicated that  $\text{ThO}_2$  would not be reduced by molten NiTi. Because thoria is very sensitive to thermal shock, however, its use as a crucible (or even as a thermocouple protection tube) led to procedural difficulties.

#### Melting Procedures

The best way to vacuum-melt Nitinol appears to be to start the melt with a piece of Nitinol of known composition, and then add nickel and titanium mixed together in the proper proportion (refs. 56 and 57). In cases when the Nitinol starter material was not available however, an alternate procedure was used to limit contact between molten nickel or titanium and the graphite crucible. Specifically, thin nickel sheet, formed into a closed-end tube, was set vertically (with the closed end down) in the crucible, and a mixture of nickel and titanium was placed in the tube as the initial charge material (ref. 56).

High-quality ingots weighing 65 lb were prepared by the following procedure (ref. 56):

(1) Place a 5 to 10 lb "starter" piece of Nitinol of known composition in the bottom of the crucible.

(2) Place a mixture of titanium and nickel in the tower of the vacuum furnace. (EL-90 grade electrolytic titanium crystal, commonly called "sponge," and electrolytic nickel were used as the charge materials by Drennen et al. (ref. 56).)

(3) Pump furnace down to a pressure of 1 to 10 microns ( $1$  to  $10 \times 10^{-3}$  torr).

(4) When the Nitinol starter piece has melted, the chamber is blanked off from the vacuum pumps and back filled with high-purity argon to a pressure of 1/6 atmosphere.

(5) Add the nickel and titanium mixture from the charging tower at a rate about equal to the dissolution rate.

(6) After the melting is complete, gradually lower the chamber pressure to about 1 to 12 microns, and allow the melt to outgas gently.

(7) Measure the temperature with a Pt-Pt/10Rh thermocouple sheathed in an ATJ graphite protection tube. Maintain the melt temperature at  $1400^\circ$  to  $1470^\circ$  C.

(8) Blank off the furnace and pour the metal into a graphite mold. Leave 5 to 10 lb of material in the furnace.

(9) If another heat is to be made immediately, start with step 2. If not, pour the remaining material into a graphite mold for use as the starting charge in a subsequent heat.

Drennen reported that if the melt-down of the titanium and nickel was conducted under a full vacuum in the order of 10 microns, the evolution of gas, especially from the nickel, was extremely violent and tended to blow the molten nickel out of the melt and onto the upper part of the crucible (ref. 56). Because this part of the crucible was relatively cool, the metal tended to solidify and build up around this area. Vacuum degassing of the nickel-melting stock reduced the gas evolution somewhat; backfilling with argon reduced the gas evolution and splattering to practically nil. The removal of the gas that is absorbed in the melt during melting under argon is carried out in vacuum (step 6, above).

#### Ingot Quality

Four aspects of ingot quality are important, especially if Nitinol is considered for commercial production. These are:

*Surface quality and internal soundness.*—Drennen, Jackson, and Wagner found that casting of Nitinol

into tapered graphite molds with hot tops produced sound 65-lb ingots, free of secondary pipe and with an excellent surface (fig. 56). One of the ingots obtained is shown in figure 10. This ingot is 14.25 in. long with a 5.5-in. hot top. The ingot diam is 5 in. at the top and 3.5 in. at the bottom. This taper produced properly controlled directional solidification, and no secondary pipe. Earlier investigators, using a different ingot design, produced ingots of a similar size but with a very considerable amount of secondary pipe.

*Composition control.*—Composition control is important whenever Nitinol is being used in applications which make use of the sharp changes in properties with temperature. For example, Nitinol which has been memory-heat treated will return to its memory shape after being heated through a certain temperature range, called the transition temperature range. For convenience, the end of this range (when no further shape change occurs) is known as the “transition temperature.” It is very sensitive to the chemical composition of the Nitinol.

In Battelle's development of melting and casting procedures it was found that the transition temperature was perhaps a more sensitive measure of the composition of the alloy than was the chemical analysis (ref. 56). This point is illustrated in figure 11, which shows the relationship of transition temperature to both the analyzed and the intended (i.e., charge) compositions. Considerable scatter may be seen in the data that relate to analyzed compositions. This is not too surprising, inasmuch as the accuracy of the titanium analysis is estimated to be about  $\pm 0.23$  percent for material with these contents of titanium. Since a 0.3 percent variation in titanium content might be responsible for a change of  $30^{\circ}$  to  $55^{\circ}$  C in transition temperature, it would be difficult, if not impossible, to use chemical analysis in quality control procedures for the transition temperature.

*Homogeneity.*—In later work, the Battelle-Columbus investigators determined that a 65-lb as-cast ingot was very homogeneous (ref 58). Specifically, an ingot (analyzed titanium content: 45.1 weight percent) similar to that shown in figure 10 was sectioned longitudinally and examined in ten locations for evidence of micro- and macrosegregation. Five experimental techniques were used in the examination: (1) X-ray spectrography, (2) “wet” chemical analysis, (3) electron-microprobe analysis, (4) metallography, and (5) microhardness measurements. All

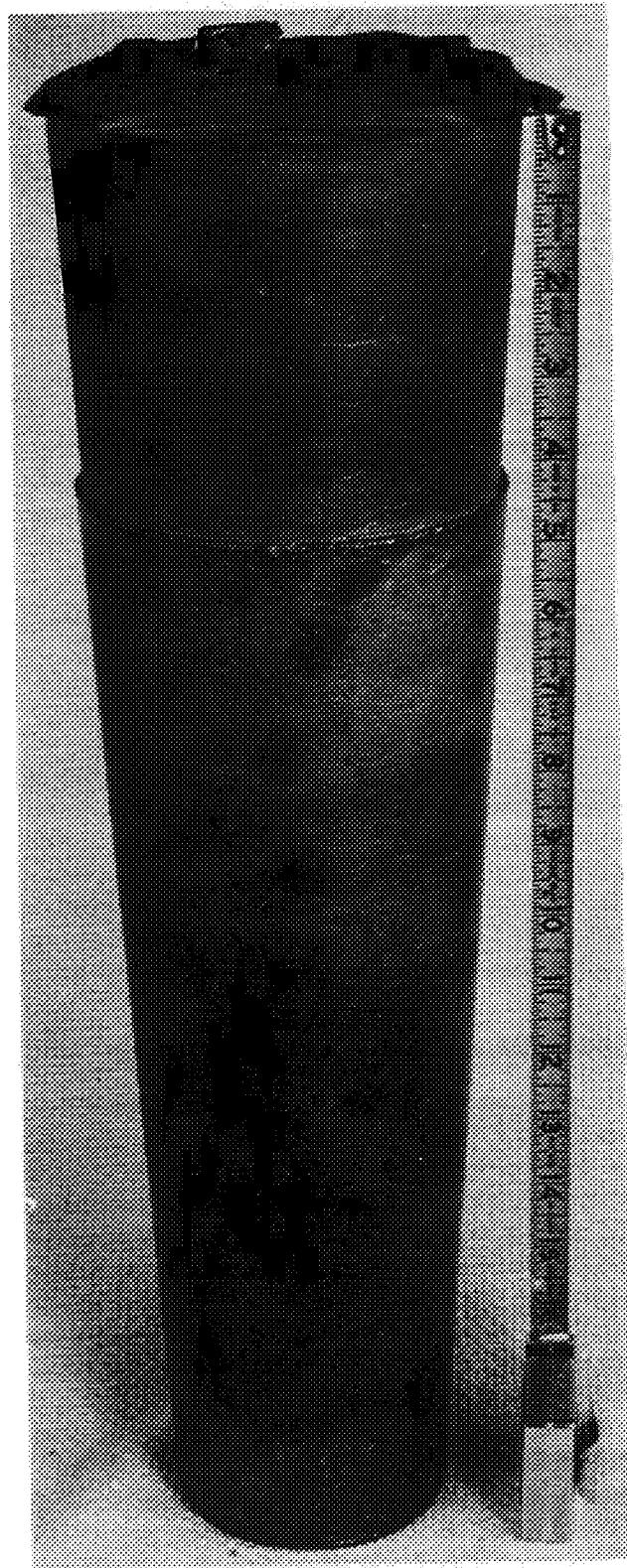


FIGURE 10.—Photograph of 65-lb ingot of Nitinol nickel-base alloy.

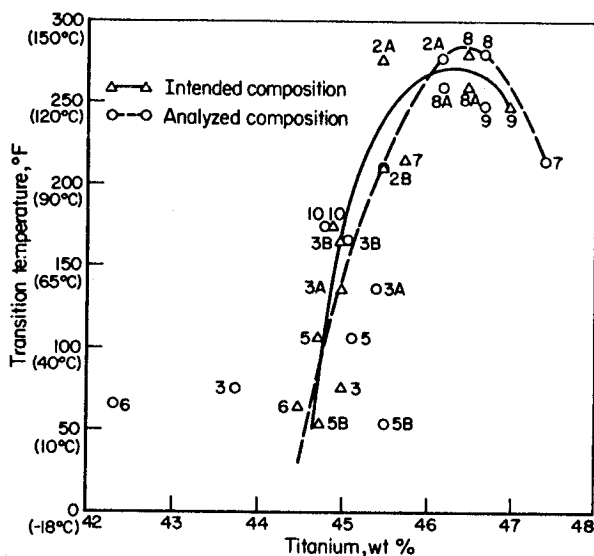


FIGURE 11.—Relationship between the intended and analyzed compositions and the transition temperature of experimental Nitinol alloys.

measurements indicated that the ingot was quite homogeneous. For instance, the maximum difference between the mean and any single titanium wet chemical analysis was 0.03 weight percent. By way of comparison, Buehler indicated that to obtain homogeneity by consumable-arc methods requires several remelts (ref. 55). The degree of homogeneity achieved in the vacuum induction melted ingot is indicative of the homogeneity of the melt and proper solidification of the ingot.

#### Consumable- and Nonconsumable-Arc Melting

Little has been written about consumable-arc remelting of Nitinol. Since the process is "remelting," the major problem is to obtain the electrode, which is preferably solid Nitinol of the same composition as the desired ingot. In some cases, compacts of nickel and titanium are used as the electrode. As stated previously, arc melting has the disadvantage of requiring several remelts to obtain homogeneous ingots. On the other hand, few impurities are introduced because there are no crucible reactions.

Rozner and Wasilewski found that laboratory quantities of Nitinol could be melted by the consumable-electrode method, under an atmosphere of gettered argon, in a water-cooled copper mold 2.25 in. in diameter (ref. 19). The electrode material was solid Nitinol prepared by nonconsumable-arc melting titanium iodide and premelted electrolytic nickel.

There was less than 0.01 percent loss of material, so that the composition of the button was essentially the same as that of the starting material mixture.

Buehler and Wiley used a nonconsumable electrode (water-cooled tungsten) to prepare about 1.5-lb ingots by vacuum-arc remelting small buttons (ref. 12). Initially the buttons (about 15 g each) were prepared by mixing the nickel and titanium well, and using enough power to maintain almost the entire button molten. This produced buttons that were said to be chemically homogeneous. They were then arc-cut into smaller segments and charged a few at a time into a copper water-cooled crucible 2.25 in. deep and 2.25 in. in diameter. After these button-segments had been nonconsumably melted, new segments were added and completely fused to the previously melted portion of the billet. In this manner, 1.5-lb ingots were prepared that were homogeneous and free of any seams.

Nonconsumable-arc melted buttons were prepared under 0.5 atm of gettered argon by Wasilewski, Hanlon, and Butler (refs. 21 and 59). Starting with titanium iodide (>99.92 percent Ti and 0.027 to 0.030 percent oxygen) and vacuum-premelted carbonyl nickel (>99.95 percent Ni), they reported that the product contained 0.015 percent oxygen, which would be in keeping with the amount of oxygen in the titanium charge material.

#### Single-Crystal Growing

Wang et al. in need of a single crystal of NiTi for X-ray diffraction studies, described a method of recrystallizing polycrystalline wire to form a single crystal (refs. 60 and 61). The ends of the wire were spot welded to tungsten leads and vacuum sealed in a Pyrex-glass tube (fig. 12). When the wire was heated electrically and cycled a few dozen times between

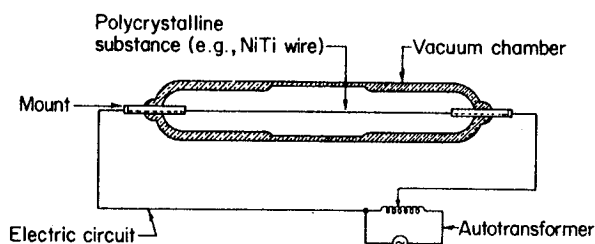


FIGURE 12.—Schematic diagram of equipment used in experiments directed toward preparing single crystals of NiTi.

500° and 900° C, single crystal growth was observed. The cycling, about 8 times a minute, introduced sufficient fast stress-strain alternation (caused by expansion and contraction) to allow a single grain to nucleate and grow.

## MECHANICAL WORKING

### *Hot Working*

Generally speaking, 55-Nitinol alloys are readily hot worked, and various methods are mentioned in the literature. The main precautions to be observed are (1) to carry out the hot working at temperatures below which incipient melting of secondary phases can occur, and (for certain alloys) (2) to homogenize the alloy by holding at elevated temperature for an extended period in order to put certain nonequilibrium phases into solution.

Buehler and Wang indicated that the Nitinol alloys can be hot worked by rolling, forging, extrusion, or swaging at 700° to 900° C, with 800° C being the preferred temperature (ref. 54). They stated that above 900° C the alloy may be hot short because of the low melting point and reduced strength of the NiTi + Ti<sub>4</sub>Ni<sub>2</sub>O eutectic; furthermore, there may be interstitial oxygen contamination when the alloy is heated about 900° C (ref. 26). In earlier work these same investigators reported working the alloy in air at temperatures of 650° to 1000° C, with 700° C preferred (ref. 62). Bars were swaged at 850° C to 0.3 or 0.2-in. diameter for a program sponsored (ref. 63); from these sizes down to 0.140 in., the rods were swaged at 800° C, using 10 percent reduction per swaging die (ref. 73).

To prevent oxygen contamination, some investigators have canned the Nitinol billets in mild steel for hot working, later removing the can by pickling in an HNO<sub>3</sub>/HCL solution. Wasilewski et al. used this technique for swaging (ref. 21), forging (ref. 59), Dynapak extrusion at 120 in./sec (ref. 19), and conventional extrusion at 6 in./sec (ref. 19). Extrusion was carried out at 900° C using extrusion ratios of 4:1 to 16:1. Wasilewski found that the canned billets could be extruded or swaged at 800° to 950° C, and warm worked at 600° to 300° C, with no oxygen pickup or iron contamination (ref. 21).

Beuhring, Jackson, and Wagner press forged 65-lb ingots at 850° C in air after a homogenizing treatment of 24 hours at 800° C (ref. 64). Drennen and

Jackson also observed that the 65-lb workpieces were somewhat difficult to work and handle under a forging hammer, and that press forging at 850° C was preferred (ref. 65).

Buehler and his associates at the U.S. Naval Ordnance Laboratory, in rolling strip reported that for initial passes the rolling temperature was 850° C, but that the temperature was gradually lowered to 700° C as the strip became thinner (refs. 63 and 66). Hot rolling was halted at 0.040-in. thickness. Warm rolling to foil gages was conducted by heating the strip to 650° C in a tube furnace mounted ahead of the rolls; the strip was reheated after each pass. Up to 5 mils of "screw down" was used for each pass on approximately 0.040-in. strip; as the 0.006-in. thickness was approached, as many as 4 or 5 passes were made at a given mill setting to achieve the desired reduction.

Schuerch reported hot rolling of thin strip in a special rolling mill with copper rolls through which electrical current passed to keep the strip at a dull red heat during rolling (ref. 67).

In rolling plate, Drennen and Jackson started with a forged slab 1.3×4×33 in. (ref. 65). The slab was held at 850° C for 45 min and then rolled to 0.58-in. thickness, taking about a 10 percent reduction in thickness per pass. After the last reduction the material was annealed at 850° C for 30 min in preparation for cold rolling.

### *Conditioning After Hot Working*

Before proceeding with cold working, the hot-worked material should be cleaned of all oxide, and any small surface checks should be ground out. The oxide, said to be mostly an adherent TiO<sub>2</sub>, is best removed mechanically by grinding or grit blasting. Acid pickling is quite slow, and may attack the material unevenly if care is not taken to stir the solution. Oxide removal can be carried out satisfactorily in a room-temperature solution of 1 HNO<sub>3</sub>:2 H<sub>2</sub>O:1/8HF.

Before proceeding with cold drawing, the alloy should be annealed at 700° to 800° C for 6 to 10 min in order to soften the alloy and preoxidize it so that it will hold the lubricant. The 700° C treatment will result in a thinner oxide than will treatment at a higher temperature, and is therefore preferable. If the material is to be cold rolled, it should be annealed before (rather than after, as in the case of cold

drawing) being cleaned of oxide according to the procedures discussed in the previous paragraph.

#### *Cold Working and Annealing*

Cold working of Nitinol alloys is relatively straightforward, provided that the alloy is worked considerably below its transition temperature  $M_s$ , and that proper lubricants are used. A unique explosive behavior has been reported when Nitinol is cold worked under certain conditions, and more will be said about this later (ref. 68).

*Wire drawing.*—Typically, the maximum reduction in area between anneals when drawing is about 30 percent. Considerable latitude is allowed, however, and reductions up to 60 percent have been reported (refs. 4 and 55). Annealing to soften the drawn wire should be carried out at temperatures between 600° and 800° C, for short times (refs. 54 and 69). Only a short time is necessary because instead of recovery and recrystallization, the annealing depends primarily on transformation of the martensitic structure to the high-temperature structure, in which case the atoms must move through relatively small distances. Some change in dimensions occurs during annealing, however, because of the shape memory effect; for example, drawn wire will shorten 3 to 5 percent and increase in diameter correspondingly as the wire is heated through its transition-temperature range (ref. 55).

Recrystallization and grain growth can be brought about by heating for 1 hr at 600° to 1000° C. Grain growth depends on the amount of prior cold work. Details are presented in the section entitled "Heat Treatment."

The drawing schedule used by Battelle-Columbus for producing wire can be taken as typical (refs. 55, 63, and 70). Since the end of the transition temperature range of one of the alloys was below room temperature, however, a special procedure was developed for drawing this composition. For the wire with a transition temperature above room temperature, the following procedure was recommended (ref. 71):

(1) Draw alloys with 10 percent reduction per die down to a diameter of 0.032 in. Process anneal at 700° C and air cool after each draw. Some alloys may be capable of being drawn 2 dies (10 percent each) between anneals. Carbide dies may be used.

(2) Starting at a diameter of 0.032 in., draw the alloys with a 20 percent reduction per die, using

diamond dies. Process anneal at 700° C and air cool after each draw.

While many lubricants work well, and lanolin has been recommended in particular (ref. 55), Battelle-Columbus has preferred a water-soluble lubricant such as Syntergent "A," which can be washed off easily before the process anneals. Preoxidation at 700° to 800° C is important, if the lubricant is to adhere well; otherwise, die chatter may occur.

Pointing the wires can be done by (1) cold swaging after annealing (preferably, the swaged point is annealed again to minimize breakage during drawing), (2) grinding before annealing, or (3) dipping the end of the wire in a 50HNO<sub>3</sub>-50HF solution with an applied dc potential of 2 volts (ref. 71). Roll pointing has not been very successful (ref. 55).

For the alloy with a transition-temperature range from -23° to -7° C, Battelle-Columbus developed a special procedure that allowed the wire to be drawn at temperatures in the neighborhood of -29° C (ref. 71). Cooling could, of course, be accomplished easily by passing the wire through a dry ice-acetone mixture. In this case, however, the problem of lubricating the wire would have necessitated a second bath with consequent heating effects. Furthermore, the lanolin would be very viscous at these low temperatures. Battelle found that a mixture of Dow Polyglycol P-400 and dry ice served as a cooling bath for the wire. At the same time the polyglycol adhered to the wire and had sufficient viscosity and lubricity to serve as the lubricant. Thus, in a single pass through a tank of the polyglycol-dry ice mixture the wire was cooled and lubricated just prior to entering the drawing die (ref. 71).

In pointing the wire with the low transition temperature, it was found that hot swaging was preferred over cold swaging. Grinding or chemical action could also be used, as with other Nitinol alloys.

Drawing rate is determined by the extent to which the wire can be kept cool during drawing; that is, it should be kept from heating above its transition temperature during drawing. The maximum drawing rate in production, accordingly, will depend on the type of lubrication, auxiliary die cooling, wire-transition temperature range, die design (conventional or roller dies), and the amount of area reduction in going through the die. Hot drawing, at temperatures considerably above the transition temperature range, could probably also be used.

*Cold rolling.*—Little has been written about the cold rolling of Nitinol, since the material has mostly been used in the form of wire. Foil (0.006- and 0.003-in. thickness) was prepared by warm rolling (see above), and given only a few sizing passes at room temperature.

Experience at Battelle-Columbus indicated that, for thin strip, nominal reductions of about 10 percent per pass can be taken and that the material should be annealed after about 10 percent reduction in thickness. In making plate 4-in. wide by 0.5-in., Battelle found that thickness reductions of about 9 percent could be taken on annealed plate from 0.58- to about 0.56-in. thickness, on a 16-in. diam by 24-in.-wide 2-high rolling mill (ref. 65). The reductions were about 5 percent per pass to a thickness of 0.533 in.; then, the mill setting was lowered at the rate of 0.0005 in. per pass until 0.526-in. thickness was reached. The plate was then annealed at 700° C for 1 hr and air cooled; as a result of passing through the transition-temperature range, the thickness increased to 0.547 in. It was then cold rolled to a thickness of 0.500 in. by reducing the mill setting about 10 mils per pass.

Buehler and Wang reported that the stoichiometric NiTi composition can explode when rolled in a particular way (ref. 68). They found that when strip (0.040-in. thick by 3/8-in. wide) was inserted into a

rolling mill with “the rolls forced tightly together” the strip “explodes intermittently” as it progresses through the rolls. A sketch of the experimental set-up is shown in figure 13. The explosions that occurred were not only noisy but also gave off light. High-velocity fragments, estimated to be traveling at 500 to 1000 ft/sec, struck the Plexiglas shield shown in figure 13. The phenomenon was explained in terms of the stress-induced martensitic transformation that occurs as the NiTi is deformed by the rolls. By the time the material reaches the outlet side of the rolls, it is heated and reverts back to the *B2* structure “explosively.” (Another explanation, based on the exothermic nature of the *B2* → martensite transformation, has also been postulated.) Warming the strip to 100° C before rolling prevented the explosive phenomenon, presumably because this temperature was above  $M_d$  and, therefore, the stress-induced martensitic transformation could not occur.

#### *Effect of Cold Work on Properties*

Cold working of Nitinol by rolling, drawing, or swaging can cause marked changes in the mechanical and physical properties of this alloy. Contraction and expansion behavior is discussed in Chapter 4, “Physical Properties,” (refs. 11, 68, 72, and 73). Effects of working on mechanical properties are discussed in chapter 5, “Mechanical Properties.”

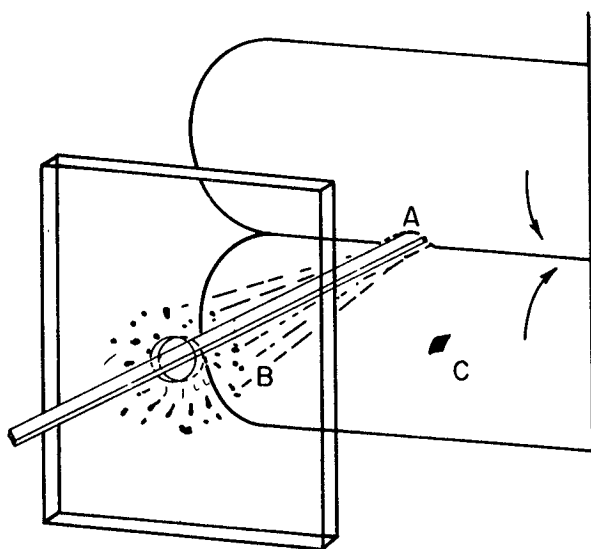


FIGURE 13.—Schematic drawing showing the experimental arrangement during drastic cold working: ((a) point at which strip enters mill, (b) scarred Plexiglas shield caused by fragmentation, and (c) piece of spent specimen adhering to roll.)

## HEAT TREATMENT

The literature contains several distinctly different types of heat treatments that have been used for Nitinol alloys. On the one hand, various investigators have sought equilibrium microstructures, and have therefore annealed the material at high temperatures and attempted to homogenize and solution-treat it. In other investigations, the purpose was to measure properties of samples in which the martensitic structure was present. These experiments entailed lower temperatures, and various temperature cycles. In yet another series of investigations, the objective was to optimize the shape-memory response, and thus empirical methods were developed. The various heat treatments are covered in the sections dealing with the specific property of interest.

Annealing to permit further cold working has already been discussed, and it was pointed out that recrystallization is not necessary since a martensitic

shear movement was involved. Nevertheless, investigators have reported that recrystallization and grain growth do occur as in other metallic materials, but the recrystallization temperature was practically independent of the amount of prior cold work (ref. 12). In these investigations, the specimens were cold rolled at various degrees from about 5 to 22 percent and then annealed for 1 hr at various temperatures. The hardness curves in figure 14 show that all specimens, regardless of the amount of deformation, showed a sharp drop in hardness after annealing for 1 hr at 600° C. Metallographic examination confirmed that recrystallization had occurred.

Normal grain growth behavior was observed, as shown in figure 15 (ref. 12). The specimens that had received the least amount of cold work grew larger grains at 800° and 1000° C than did the more severely worked specimens.

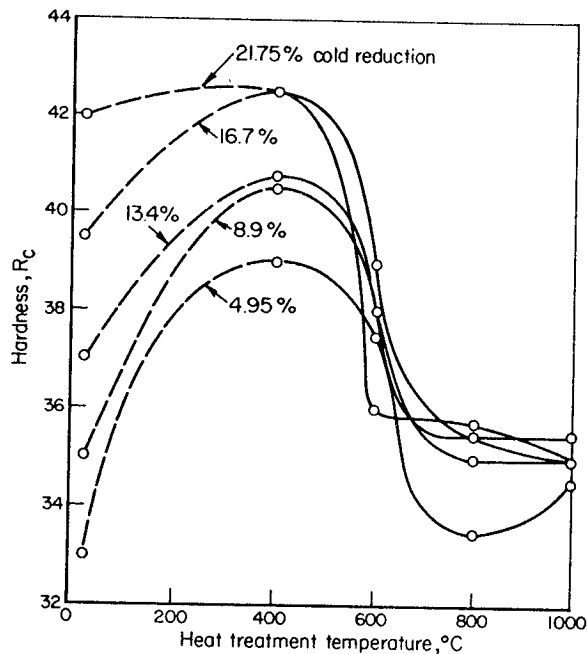


FIGURE 14.—Hardness of NiTi specimens after heat treatment for 1 hr at selected temperatures.

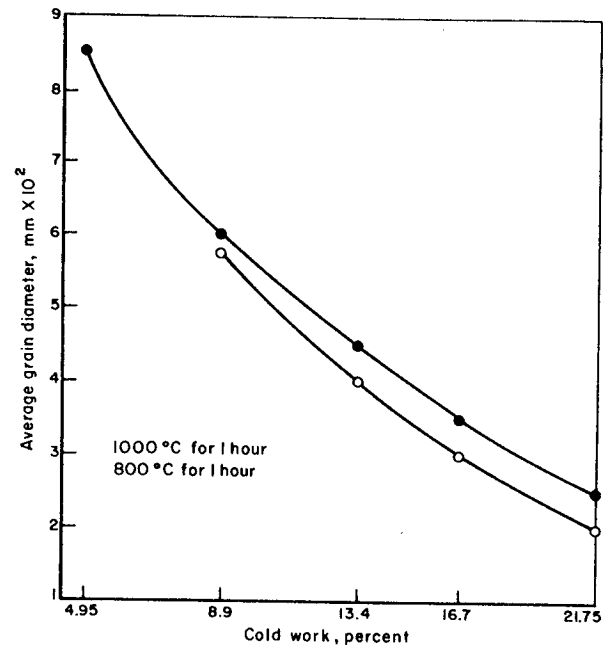


FIGURE 15.—Effect of 1-hr heat treatment at 800° and 1000° C on the grain size of NiTi, as a function of the degree of prior cold working.

## JOINING

Not a great deal has been reported on the welding or brazing of Nitinol, but preliminary experiments indicate that the alloy can be readily fusion welded and spot or seam welded.

Buehler and Wiley reported on the gas-tungsten-arc (GTA) butt welding of 1/8-in.-thick hot-rolled plate using Nitinol as the filler rod (ref. 74). They reported that little difficulty was encountered in making the joint, and that it was free of cracks and porosity. The microstructure of the fusion zone was that of a typical cast structure consisting of fine dendrites. Some extraneous phases (angular or star shaped) were detected, however, these phases were probably caused by some contamination during welding.

Drennen and Jackson also found that 55-Nitinol can be welded using GTA techniques (ref. 4). They were also successful in resistance-spot welding 55-Nitinol, using an argon cover.

# Physical Properties

## MELTING POINT

The melting temperature of the 55.1 weight percent Ni alloy has been observed as 1240° to 1310° C (ref. 74). This is not a temperature range, but rather reflects the uncertainties in establishing the phase diagram. NiTi, being a congruent melting compound, should show a clear melting point.

## DENSITY

The density of the 55.1 weight percent Ni alloy at 25° C was found by Buehler and Wiley to be 6.45 g/cm<sup>3</sup> (ref. 74). Dautovich reported 6.55 g/cm<sup>3</sup> for a 51 atomic percent Ni alloy (ref. 18).

## ELECTRICAL RESISTIVITY

Hanlon et al. measured the electrical resistivity of NiTi over the composition range from 48 to 52 atomic percent Ti at temperatures from -268° C to +900° C (ref. 59). The change in electrical resistivity with temperature in the 15° to 110° C range on heating and cooling for a 50 atomic percent Ti sample is shown in figure 16. Above 75° C, this sample was stated to have essentially the *B2* structure, while below 0° C it was completely in the low-temperature phase. The change in resistivity of a 50.7 atomic percent Ti sample that has the low temperature structure at room temperature is illustrated in figure 17. The resistivity decreases normally with decreasing temperature. The residual resistance at 4.2° K (-268.8° C), 19 microhm-cm, is said to be relatively high and indicative of the persistence of a considerable amount of lattice distortion well below the martensitic-transformation-temperature range. Also, the low-temperature behavior for a sample containing 48.8 atomic percent Ti is shown in figure 17. In the figure the characteristic heating/cooling hysteresis seen in the 50 atomic percent Ti sample has not only

shifted to lower temperatures in the 48.8 atomic percent Ti sample, but also has broadened its temperature range. The extensive hysteresis was said to be characteristic of the low-temperature transformations in nickel-rich samples, but samples containing less than 48 or 49 atomic percent Ti showed no clear-cut transformation.

The electrical resistivity of the high- and low-temperature forms of NiTi (50.0 atomic percent Ti) extrapolated to ~70° C are (ref. 59):

CsCl( <i>B2</i> ) structure	Low-temperature structure
82 microhm-cm	76 microhm-cm

These data apply only to samples annealed 1 hr at 900° C and water quenched.

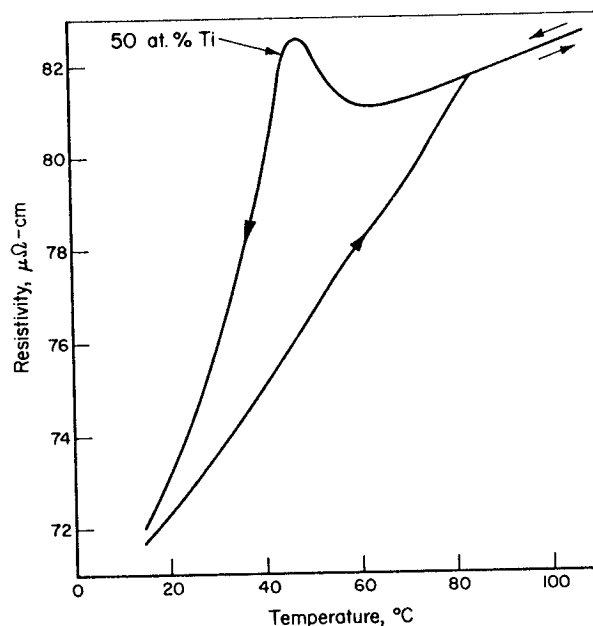


FIGURE 16.—Electrical resistivity of NiTi (50 atomic % Ti) over the temperature range of the martensitic phase transformation.

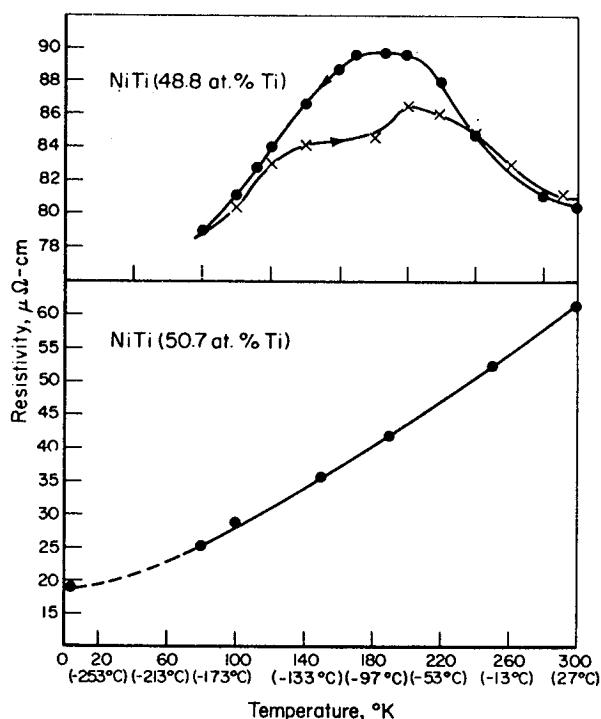


FIGURE 17.—Low-temperature resistivity of NiTi (48.8 and 50.7 atomic % Ti).

Wang carried out experiments on specimens with 51 atomic percent Ni that were free of deformation and of sustained tensile and compressive stresses (ref. 44). Because of the diffusion-type transformation from NiTi I to NiTi II, postulated by Wang to occur in the  $600^{\circ}$  to  $700^{\circ}$  C range as discussed in the section titled "Crystal Structure," prolonged annealing at  $600^{\circ}$  C was believed to be essential if pure NiTi II is desired. The electrical resistivity curve of an alloy annealed at  $610^{\circ}$  C for 4 days followed by furnace cooling to room temperature is shown in figure 18(a). Annealing above  $700^{\circ}$  C was said to result in a structure consisting of both NiTi I and NiTi II, with the fraction of NiTi I increasing as the annealing temperature is raised. The electrical resistivity curves for the alloy annealed at  $700^{\circ}$ ,  $800^{\circ}$ , and  $900^{\circ}$  C, respectively, (oil quenched) are also given in figure 18.

The triangular shape of the resistivity vs temperature curve is not a hysteresis effect, according to Wang (ref. 44). (A hysteresis involves a lag behind the equilibrium state due to a time of relaxation when the temperature is changing.) Rather, the shape of the curve is said to be indicative of a martensitic transition between NiTi II and NiTi III. (NiTi I is

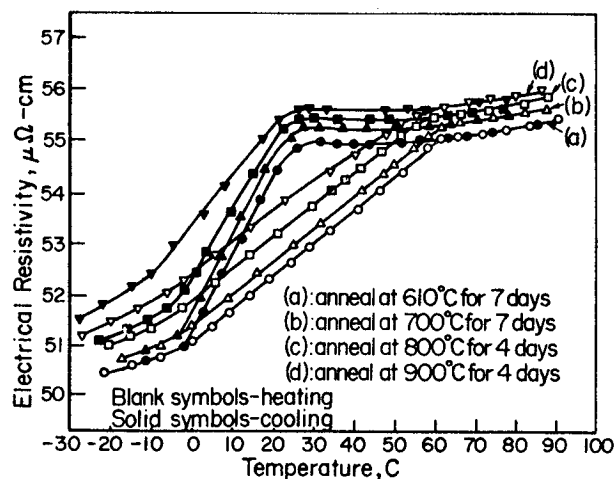


FIGURE 18.—Effect of annealing temperature on the electrical resistivity of NiTi (51 atomic % Ni) at and around the martensitic transition temperature.

believed to be unable to transform directly to NiTi III.) Thus, the decrease in the triangular areas with increasing annealing temperature, as shown in curves b, c, and d of figure 18, was presumed to be a manifestation of the decreasing amount of NiTi II that was thought to be available to undergo the martensitic transformation to NiTi III.

The effect of various types of thermal cycling on electrical resistivity is shown in figure 19. The cooling path  $M_s'-M_s'$  and the heating path  $M_s'-A_s$  are irreversible.\* That is, if the direction of temperature change were to be reversed while traversing these paths, the resistivity curve would not retrace its original path. In contrast to this behavior, the cooling path  $A_s-M_s$  is reversible. The triangular form and the irreversible nature of the cycle are said to be totally independent of the rate of heating or cooling.

In Wang's work, thermal cycles carried beyond the range  $M_s'$  to  $A_s$  without any reversals in the range  $M_s'-A_s$  on heating or  $M_s-M_s'$  on cooling are called "complete" cycles (ref. 44). The triangular portion of the curve will remain unaltered through an indefinite number of complete cycles, according to Wang. On the other hand, when thermal cycling was carried out within the irreversible ranges  $M_s'-A_s$  or  $M_s-M_s'$ , the triangular form of the resistivity curve was altered.

\*The terms  $A_s$  and  $M_s$  appear to have been used by analogy to the nomenclature used in steel technology for martensitic reactions. It should be noted, however, that microstructural examinations at various temperatures would be required before the exact significance of the  $A_s$  and  $M_s$  temperatures identified in reference 45 could be proven.

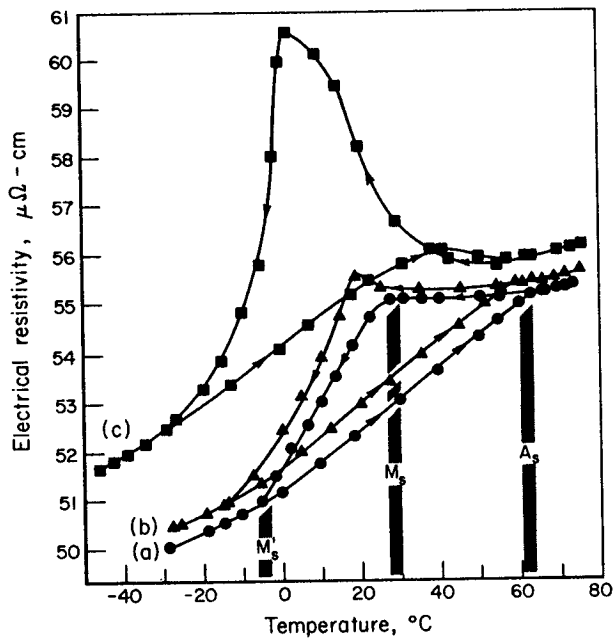


FIGURE 19.—Effect of “incomplete” cycles on the electrical resistivity of NiTi (51 atomic % Ni) at and around the martensitic transition temperature (cycling direction is indicated by arrows: (a) without incomplete cycling, (b) after six incomplete cycles, and (c) after several hundred incomplete cycles) (ref. 44).

After six such incomplete cycles, the resistivity curve (b) shown in figure 19 was obtained. After a few hundred such cycles, the curve (c) was obtained. Thus, as the number of incomplete cycles was increased, a progressive overall increase in resistivity was observed, along with an increase in the area of the triangular portion of the curve and a shift (to lower temperatures) of the maximum resistivity on cooling. The curve (c) in figure 19 could be restored to curve (a) only after prolonged reannealing of the alloy at 600° C or above.

Buehler and Wiley measured the electrical resistivity of Nitinol alloys containing 54.5 and 55.1 weight percent Ni (ref. 12). The materials had been arc melted by the nonconsumable method, hot rolled between 700° and 1050° C, and slit so that the specimen was a strip, measuring about 0.125 to 0.186-in. wide by 0.010-in. thick and 5.5 in. long. In figure 20 are plotted the electrical resistivity data for a 54.5 weight percent Ni alloy, hot rolled and annealed (at 1050° C) between -57° and +99° C. Data for the resistivity change of the 55.1 weight percent Ni alloy at temperatures to 900° C were “too scattered to be capable of interpretation,” but the resistivity showed a sharp increase (on heating) at

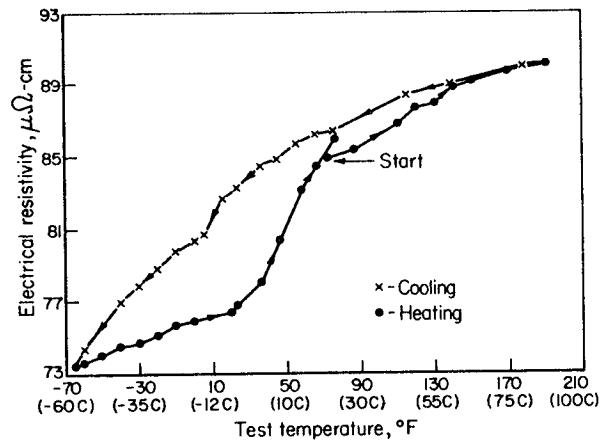


FIGURE 20.—Electrical resistivity as a function of temperature for a 54.5 weight % NiTi alloy.

about 700° C. At 900° C, it reached 132 microhm-cm.

The room-temperature resistivity of the 55.1 weight percent Ni composition was measured in order to obtain some indication of the structure (order-disorder, in particular) of variously quenched specimens. Two specimens were furnace cooled from 593° C, then heated to various temperatures and quenched. Their electrical resistivities are shown in figure 21. Similarly, two specimens were air cooled after hot rolling to 0.020 in. at 700° C, and then reheated to various temperatures and quenched. Their resistivities are shown in figure 22.

In each case, it was found that the resistivity

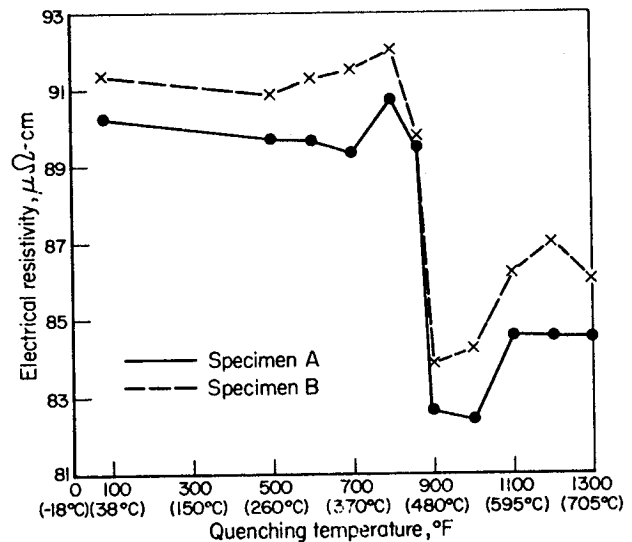


FIGURE 21.—Room-temperature electrical resistivity of NiTi (55.1 weight % Ni) strip heated to various temperatures and quenched.

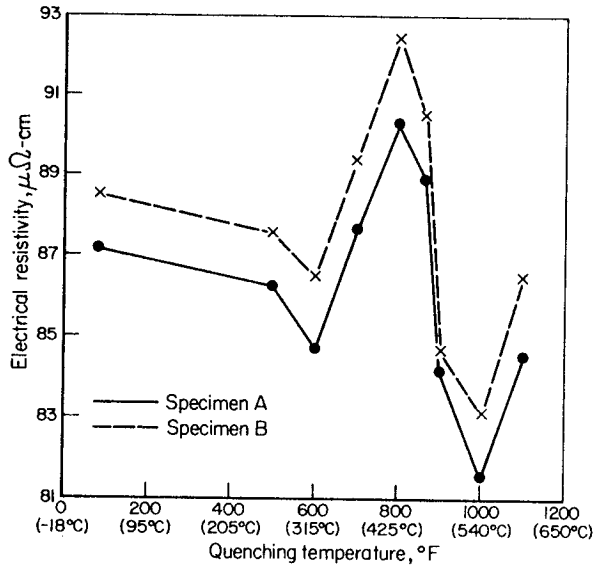


FIGURE 22.—Room-temperature electrical resistivity of NiTi (55.1 weight % Ni) strip heated to various temperatures and quenched. (Initial condition of specimen; hot rolled to 0.020 in. at 700° C.)

reached a maximum at about 427° C, dropping sharply to a minimum at about 480° to 540° C. A relationship of these data to an order-disorder transformation was discussed, but no conclusions were reached. The electrical resistivity of stoichiometric NiTi and its alloys containing copper or excess nickel was investigated by Goff in the temperature range from -270° to +27° C (ref. 75). The composition and grain size of the samples are given in table 2.

TABLE 2.—Composition and Grain Size of Samples

Sample	Solute	Solute concentration, atomic %	Grain size, μ
TiNi	—	—	42
TiNi-2 Cu	Cu	1.7	46
TiNi-8 Cu	Cu	8.1	54
TiNi-18 Ni	Ni	18.3	—

The electrical resistivity of each alloy is shown as a function of temperature in figure 23. Goff interpreted the curves of figure 23 in terms of Matthiessen's rule,

$$\rho = \rho_o + \rho_i,$$

where  $\rho_o$  and  $\rho_i$  are the residual and ideal resistivities, respectively (ref. 75);  $\rho_i$  is an intrinsic property of the

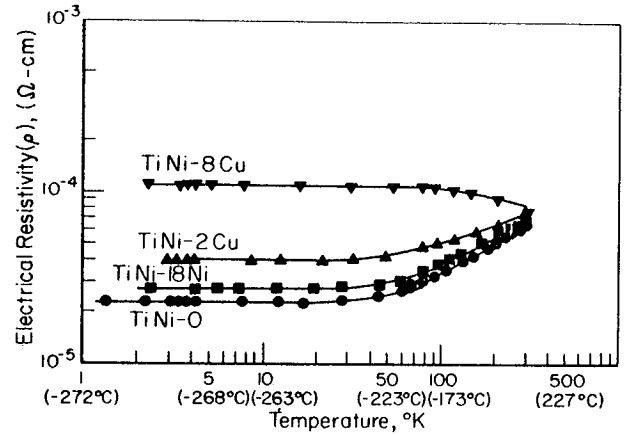


FIGURE 23.—The electrical resistivity of selected NiTi-base alloys, as a function of temperature.

material and depends directly on some power of  $T$ . At some low temperature it becomes negligible with respect to the temperature-independent  $\rho_o$ . The concentration dependence of  $\rho_o$  is shown in figure 24. From the data, it appears that  $\rho_o$  can be expressed as

$$\rho_o = \rho_{ox} + \rho_{oo},$$

where  $\rho_{ox}$  is due to the solute and  $\rho_{oo}$  is an intrinsic property of the NiTi matrix.

Because of the large values of  $\rho_o$ , it was not possible to separate  $\rho_i$  from  $\rho$  at temperatures above -243° C, and not at all for the TiNi-8Cu sample. The values obtained for  $\rho_i$  are given in figure 25, where they show a dependence on  $T^1$  above -153° C and on  $T^2$  below -173° C. The  $T^1$  dependence is usually observed in transition metals and indicates that the electron-phonon scattering has entered the Debye

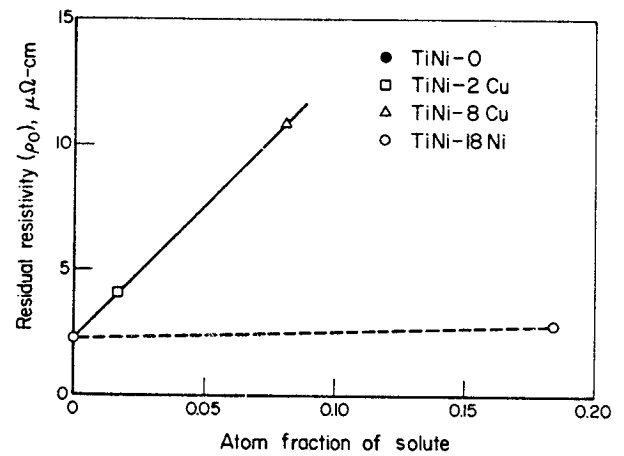


FIGURE 24.—The effect of the atomic fraction of solute on the residual resistivity of NiTi-base alloys.

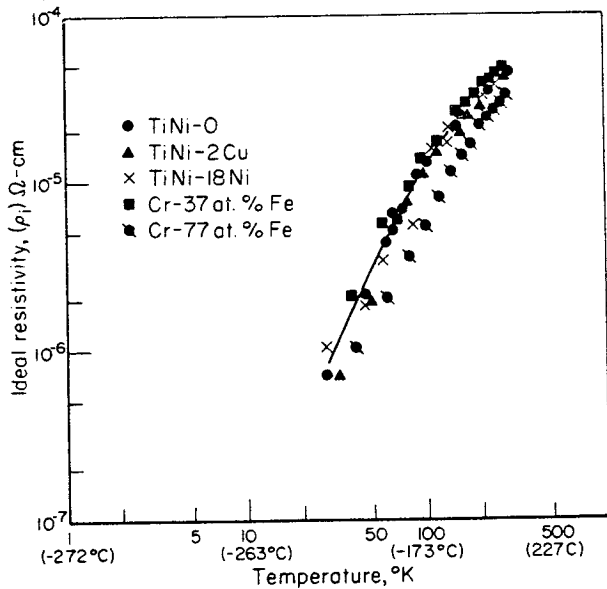


FIGURE 25.—Ideal electrical resistivity of NiTi and CrFe alloy specimens.

elastic range. The  $T^2$  dependence is unusual. Goff related these observations to the Fermi energy, effective mass, and relative valences of the solutes.

Dautovich and Purdy related some of the electrical resistivity data to the X-ray-diffraction patterns, as shown in figure 26 (ref. 18). The material used was 50 atomic percent Ni prepared by arc melting by Buehler and co-workers at the U.S. Naval Ordnance Laboratory. The ingots were hot rolled in air (maxi-

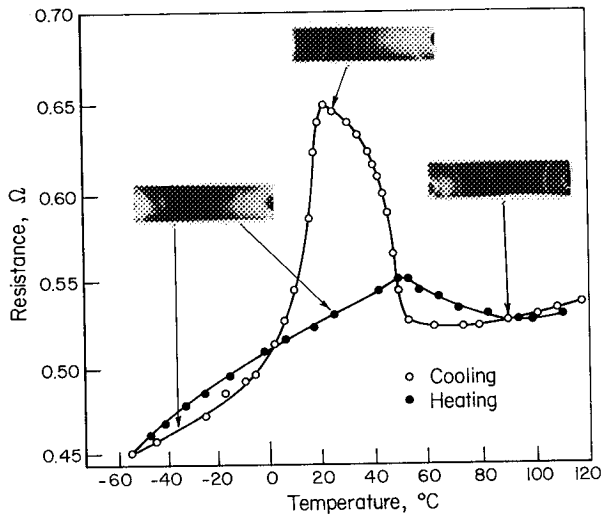


FIGURE 26.—Electrical resistance as a function of temperature for NiTi (50 atomic % Ni), X-ray-diffraction patterns superimposed.

mum temperature 700° C) and electropolished to remove scale and the oxygen-diffusion zone. Wire 0.020 in. in diameter was used for the resistivity measurements, and (after electropolishing to a 0.005-in. diameter) for the X-ray powder diffraction studies. On cooling from 125° C, the resistance begins to rise to 50° C, a change that is accompanied by a change in crystal structure (fig. 26). These results were interpreted as indicating the existence of a premartensitic-transition structure, as discussed in the section, "Crystal Structure."

Cross, et al. found that the shape of the resistivity vs temperature curve for drawn wire depended strongly on the heat-treatment temperature used for giving the wire a straight memory (ref. 63). The resistivity-temperature curves also varied with the chemical composition of the alloy, form (wire or strip), and dimension (diameter or thickness). Three different materials were investigated, the compositions and other characteristics of which are given in table 3. Some of the results obtained are shown in figures 27 through 31. The electrical-resistivity behavior is correlated with the bend-recovery behavior of wire memory, heat treated at various temperatures. The bend recovery of wire was found to have been most complete after the 500° C anneal.

This same annealing temperature caused the greatest area enclosed by the resistance vs temperature curve as it was cycled from about -46° to + 121° C. The correlation of bend recovery with the area enclosed within the resistivity-profile loop applied to all forms and sizes tested.

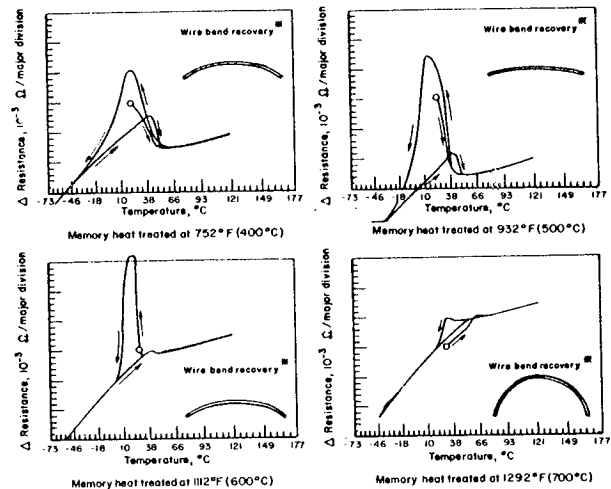


FIGURE 27.—Effect of memory heat-treatment temperature on electrical resistance and bend-recovery behavior.

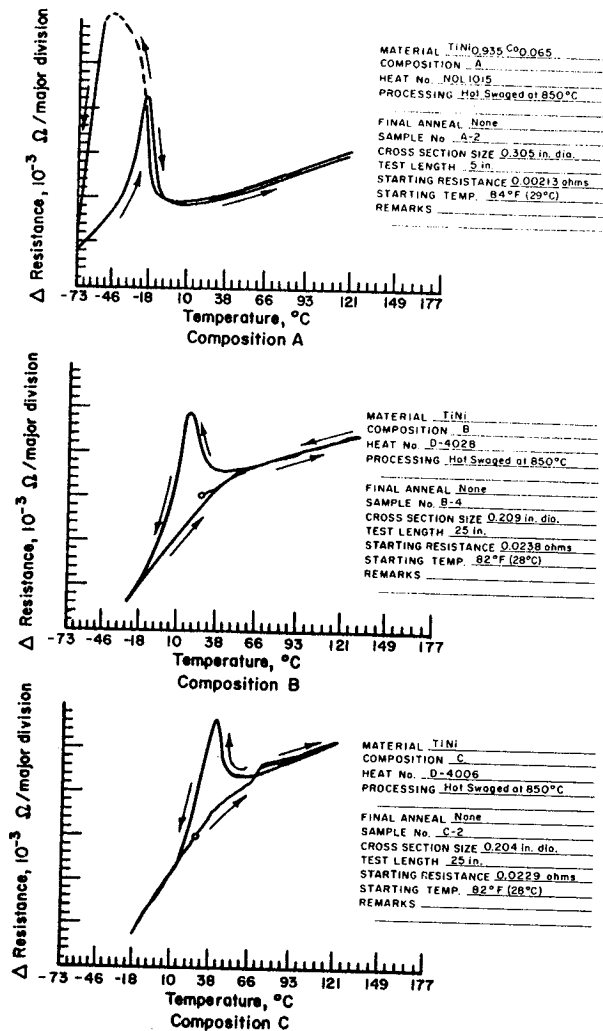


FIGURE 28.—Effect of temperature on the electrical resistance of swaged rods.

TABLE 3.—Materials Used in Goodyear Aerospace Corporation's Nitinol Study for NASA (Refs. 63 and 70).

Chemical composition	Heat No. <sup>a</sup>	$M_s$ temperature, °C <sup>b</sup>		
		Swaged rod	3-mil foil	6-mil foil
A — TiNi <sub>0.935</sub> Co <sub>0.065</sub> <sup>c</sup>	NOL-1015	-51	-65	-62
B — C 0.07, Ni 55.0, Ti balance <sup>d</sup>	D-4028	18	24	24
C — C 0.06, Ni 54.6, S 0.006, Ti balance <sup>d</sup>	D-4006	41	41	41

<sup>a</sup>All heats were induction melted in a graphite crucible.

<sup>b</sup>Determined from electrical resistance vs temperature measurements made on "as-received" material in the case of the swaged rod and on final annealed material in the case of foil. The  $M_s$  temperature is defined in the typical curve shown in figure 19.

<sup>c</sup>Charge composition as reported by the U.S. Naval Ordnance Laboratory.

<sup>d</sup>Chemical analysis.

The resistance change with temperature for hot-swaged rod of the three compositions is shown in figure 28. The curves for memory-heat-treated material in various forms and sizes are given in figures 29 to 31.

## THERMOELECTRIC POWER

The thermoelectric power of NiTi (50.6 atomic percent Ti and 50.0 atomic percent Ti) was reported by Wasilewski, Hanlon and Butler (ref. 21), and by Hanlon, Butler, and Wasilewski (ref. 59), respectively. The change in thermoelectric power with temperature is shown in figures 32 and 33. In addition, the way thermoelectric power (at room temperature) varies with the titanium content of the alloy and with the heat treatment is shown in figure 33. The variation of thermoelectric power with composition reflects primarily a change in crystal structure. Although the magnitude of the thermoelectric power varies with heat treatment, it is always less in the B2 structure.

Metallographic and electron-microprobe studies showed that a nickel-rich phase precipitated during the time the sample was held at 600° C, thus decreasing the nickel content of the matrix. When the sample was stored (at room temperature) for about a year, an increase in the thermoelectric power resulted, but no microstructural changes were observed as a result of aging which correlate with the change in thermoelectric power.

For a specimen with 50.0 atomic percent Ti, annealed at 900° C for 1 hr and water quenched, Hanlon et al. reported the following values of thermo-

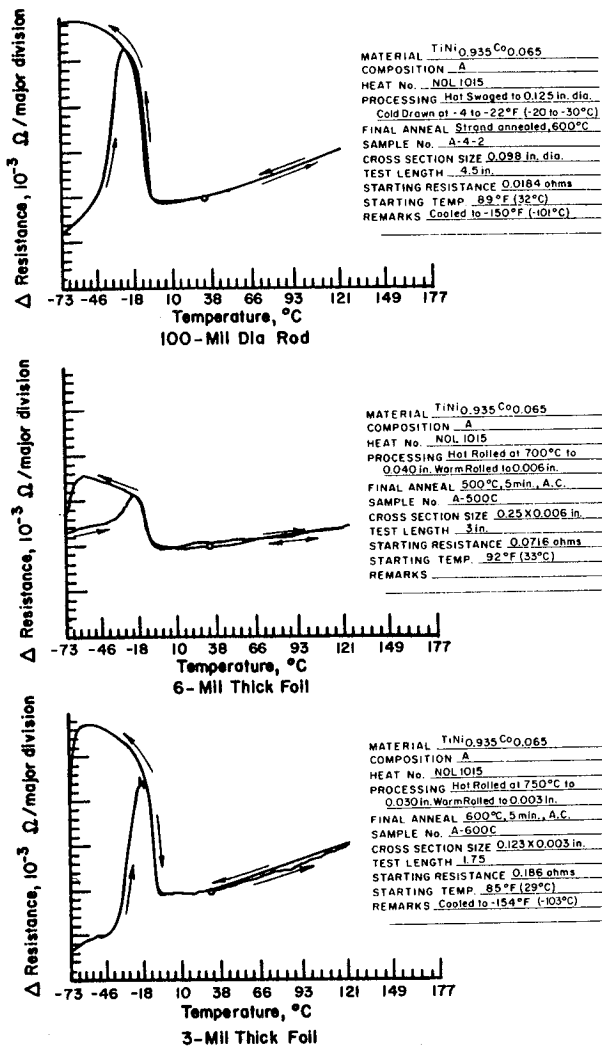


FIGURE 29.—Effect of temperature on the electrical resistance of composition-A materials.

electric power for the high-temperature CsCl(B2) structure and the low-temperature structure, both at about 70° C (ref. 59). To obtain these values, the temperature dependent properties were extrapolated to the transition midpoint, ~70° C.

CsCl(B2) at ~70° C	Low temperature structure at ~70° C
--------------------	-------------------------------------

Thermoelectric power $\mu V/^\circ C$	+6	+10
---------------------------------------	----	-----

Goff investigated the influence of copper additions to NiTi on the thermoelectric power from -270° to +27° C (ref. 75). His results are plotted in figure 34 in which the absolute thermoelectric power based on measurements of NiTi against copper, copper against

lead, and the absolute thermoelectric power of lead are shown. Goff indicated that the values for TiNi-2Cu are probably too large because of some calibration trouble during the measurements.

HALL COEFFICIENT

Hanlon et al. measured the Hall coefficient and ac resistivity of NiTi at 20 Hz (ref. 59). The temperature dependence for stoichiometric NiTi is shown in figure 35. Above 75° C, the structure of this sample was essentially B2, and below 0° C, it was completely in the low-temperature phase. The Hall coefficient was positive (p-type) in both crystallographic modifications, but increased by a factor of about 3.5 in going from the high-temperature state to the low one. Also shown in figure 35 is the Hall coefficient (at room temperature) for a 49 atomic percent titanium NiTi alloy. This sample is in the B2 structure at room temperature; its Hall coefficient is about 20 percent greater than that of the stoichiometric composition in the B2 structure. For stoichiometric NiTi, Hanlon et al. found the Hall coefficients to be  $+0.5 \times 10^{-4}$  cm<sup>3</sup>/coulomb for the B2 structure and  $+1.8 \times 10^{-4}$  for the low temperature structure (ref. 59). This number is based on extrapolation of temperature-dependent properties to about 70° C (the transition midpoint) for a sample annealed at 900° C for 1 hr and water quenched.

Wang et al. used a rectangular specimen 0.1 X 3.5 X 14.8 mm for Hall effect measurements using standard dc techniques (refs. 44 and 77). In figure 36 (top) the Hall coefficient ( $R_H$ ) is given as  $1.8 \times 10^{-4}$  cm<sup>3</sup>/coulomb below the  $M_s'$  and  $0.4 \times 10^{-4}$  cm<sup>3</sup>/coulomb above the  $A_s$  temperature both complete and incomplete cycles. (See section on "Electrical Resistivity" for a description of incomplete and complete cycles.

The Hall mobility,  $\mu_H$ , was calculated from the measured electrical resistivity,  $\rho$ , and the Hall coefficient,  $\mu = R_H/\rho$ , and is given in figure 36 (bottom). Because there is a difference in the resistivity peak between the complete cycles and incomplete cycles, there is also a difference in Hall mobility; however, the difference is hardly significant. Wang concluded from this that the overall Hall-mobility change is due primarily to a change in the effective number of carriers  $N_h$  rather than from changes in the effective mass of electrons and holes,  $m^*$ , or in  $\bar{T}$ , the mean relaxation time.

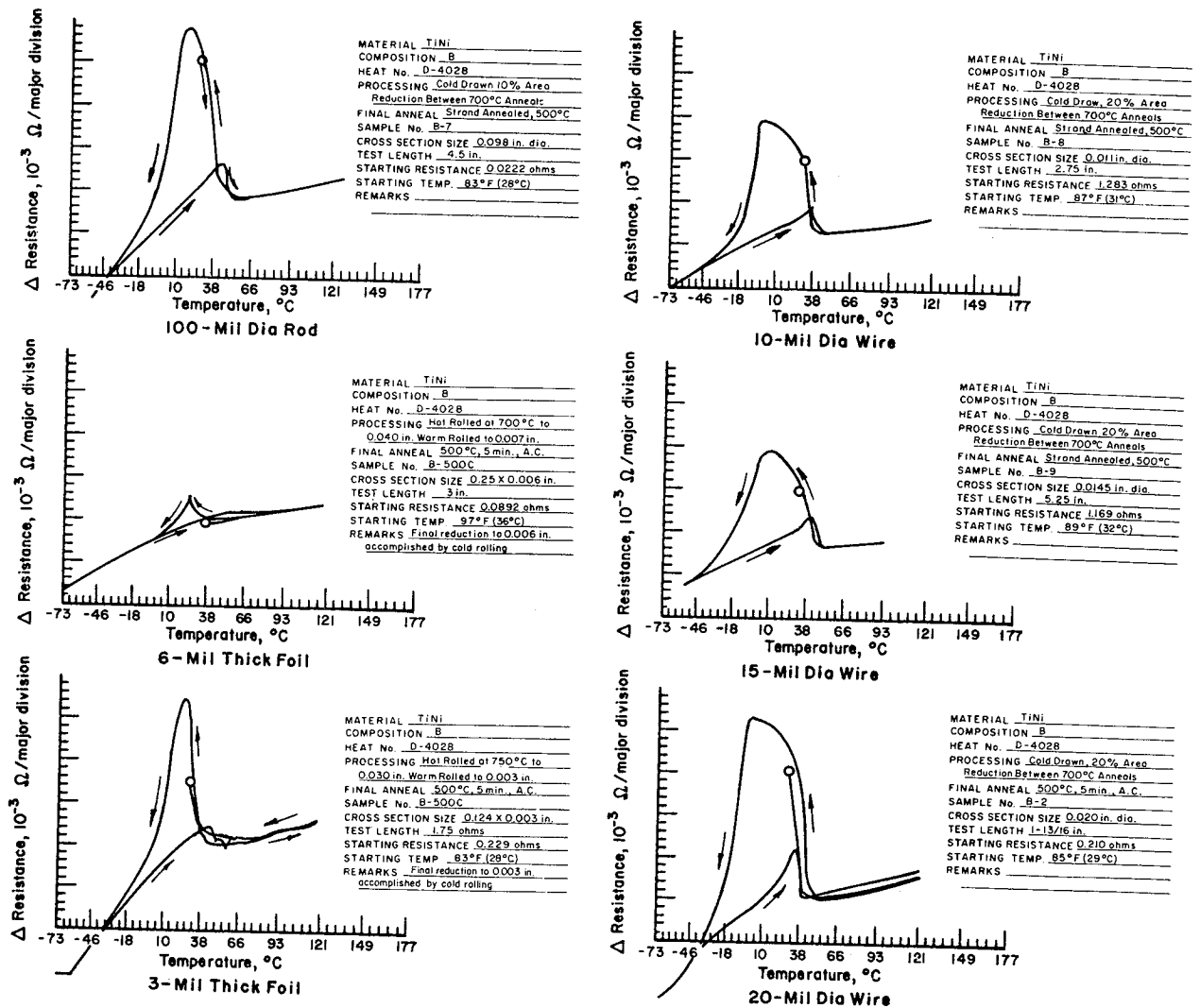


FIGURE 30.—Effect of temperature on the electrical resistance of composition-B materials.

Allgaier compared Hall coefficient data for TiFe, TiCo, and NiTi and rationalized the differences in terms of band theory (ref. 78). The results plotted as a function of the number of valence electrons per atom ( $N_{ve}$ ) are shown in figure 37. For NiTi at  $N_{ve}=7$ , the transport characteristics resemble those of the traditional two-band model of a transition metal: (1) a broad s-band that carries the current and (2) a narrow, low-mobility d-band that provides a high density of scattering sites.

### VELOCITY OF SOUND

Bradley investigated the velocity of sound in Nitinol as influenced by several variables (ref. 79). Three compositions were used for the experimental

work: 49.9, 50.3, and 50.8 atomic percent Ni, hereinafter referred to as NiTi 49.9, NiTi 50.3, and NiTi 50.8, respectively. Longitudinal sound velocities were measured over a temperature range of  $-50^{\circ}$  to  $+140^{\circ}$  C, and over a pressure range of atmospheric to 40 000 psi. The sound velocity was measured at a frequency of 5 MHz, using a pulse technique. The test specimens, in the form of rods 0.5 in. in diam and 2.5 in. long were arc cast, hot swaged, and machined to size. Then the material was annealed at  $400^{\circ}$  C for 2 hr in an inert atmosphere, and furnace cooled. To stabilize the specimens, they were cycled over the temperature range  $-30^{\circ}$  to  $200^{\circ}$  C until the sound velocity data over the range  $-10^{\circ}$  to  $+140^{\circ}$  C was repeatable.

The sound velocity of NiTi 49.9 in the stabilized

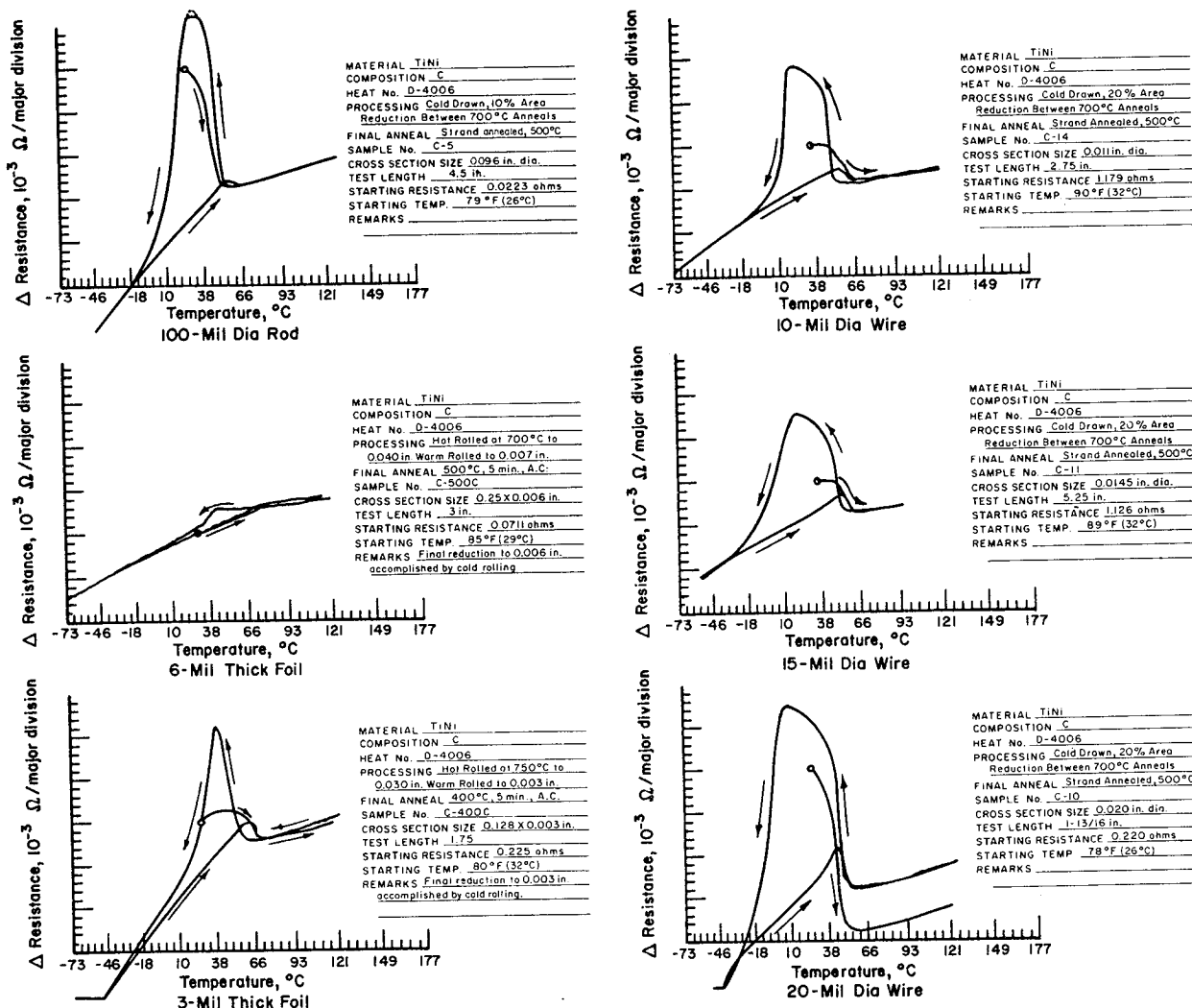


FIGURE 31.—Effect of temperature on the electrical resistance of composition-C materials.

condition is shown in figure 38 for one complete warming and cooling cycle. As the nickel content was increased, the temperature at which the sound-velocity minimum occurred was shifted to lower temperatures. The effect for the cooling half of the temperature cycle is shown in figure 39, but the same behavior was seen in the warming half. It was also observed that the minimum point shifts to higher temperature if the minimum exposure temperature is lowered. For example, the NiTi 50.8 sample showed a velocity minimum point of 56 $^{\circ}\text{C}$  when the lowest exposure temperature was +10 $^{\circ}\text{C}$  before proceeding with the warming cycle. When the lowest exposure temperature was -50 $^{\circ}\text{C}$ , however, the velocity minimum point had been raised to +63 $^{\circ}\text{C}$ .

The effect of annealing and stabilizing treatments on the sound velocity vs temperature is shown in figure 40 for the NiTi 49.9 alloy. The effect of pressure on the cooling half of the cycle is illustrated in figure 41. The change due to pressure is actually less than shown because no correction was made for dimensional changes in the specimen resulting from the compression, which would in itself cause a 10 m/sec increase.

Wang showed that the velocity vs temperature behavior changes, depending on whether the specimen undergoes complete or incomplete cycles (refs. 44 and 77). (See section on "Electrical Resistivity" for a description of incomplete and complete cycles.) The data shown in figure 42 (ref. 44) are for a

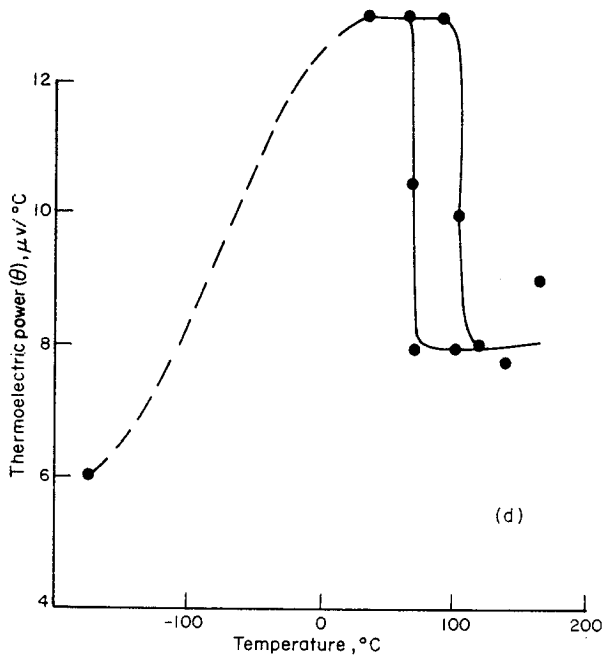


FIGURE 32.—Effect of temperature on the thermoelectric power of NiTi (50.6 atomic % Ti).

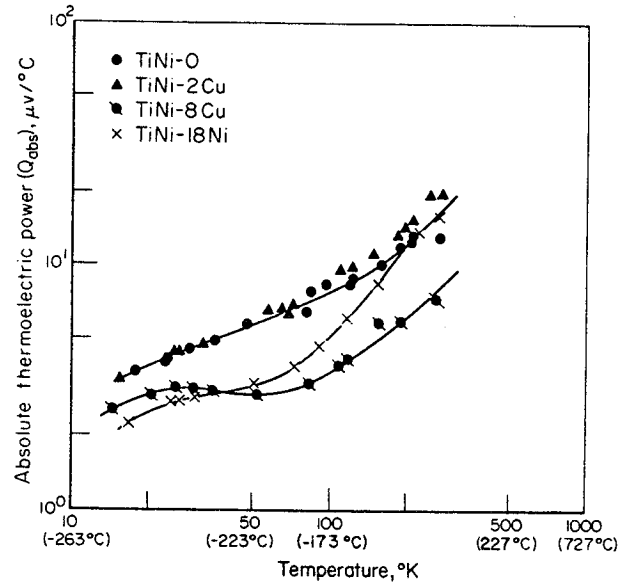


FIGURE 34.—The absolute thermoelectric power of selected NiTi-base alloys. ( $Q$  is positive.)

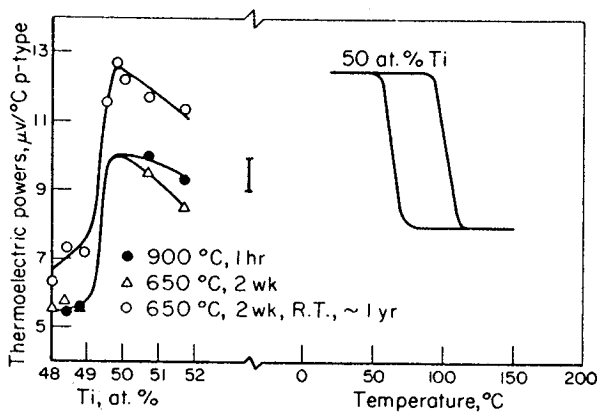


FIGURE 33.—(a) Thermoelectric power of NiTi alloys, measured at room temperature, as a function of chemical composition. (b) Effect of temperature on the thermoelectric power of NiTi (50 atomic % Ti).

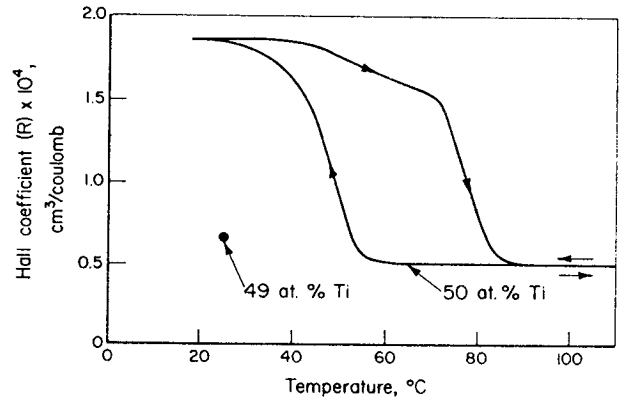


FIGURE 35.—Effect of temperature on the Hall coefficient of stoichiometric NiTi; Hall coefficient, at room temperature, of NiTi containing 49 atomic % Ti.

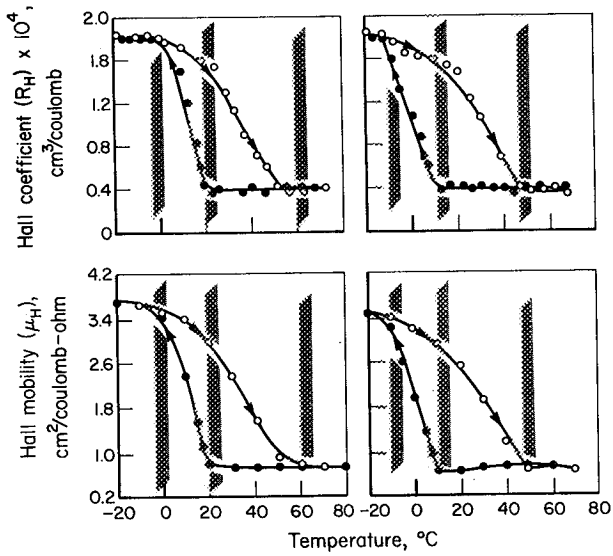


FIGURE 36.—The effect of temperature on the Hall coefficient and Hall mobility of stoichiometric NiTi containing 51 atomic % Ni. (The curves on the left are for a sample that had undergone complete cycles, while those on the right are for a sample that had undergone incomplete cycles.)

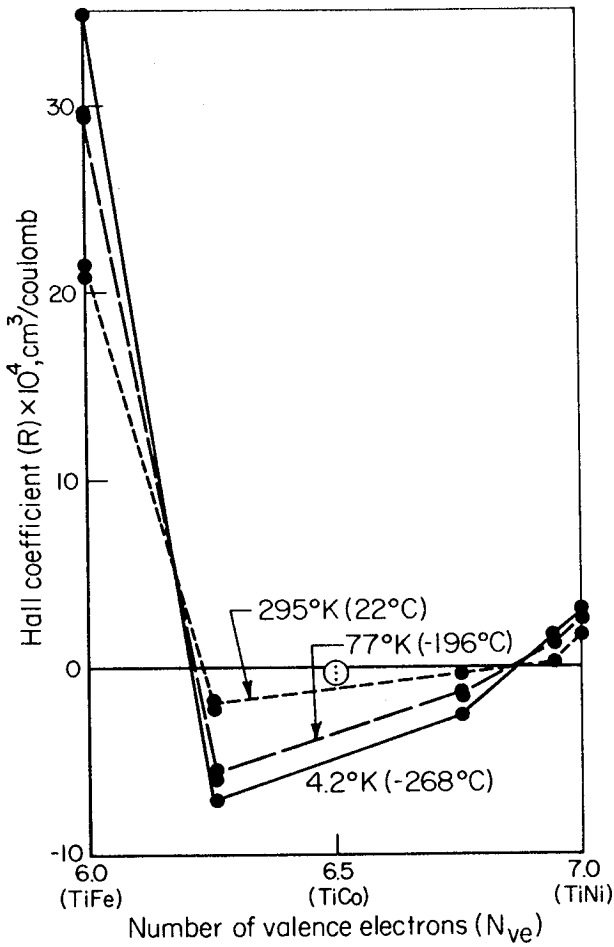


FIGURE 37.—The effect of the number of valence electrons,  $N_{ve}$  on Hall coefficient.

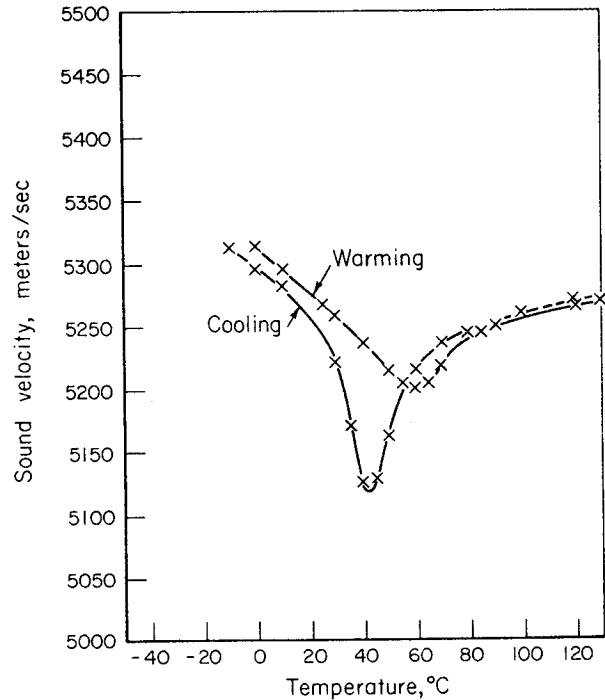


FIGURE 38.—The effect of temperature on the velocity of sound in NiTi containing 49.9 atomic % Ni. (The material was "stabilized" by temperature cycling between  $-30^{\circ}$  and  $+200^{\circ}$  C until repeatable results were obtained. The frequency of the sound was 5 MHz.)

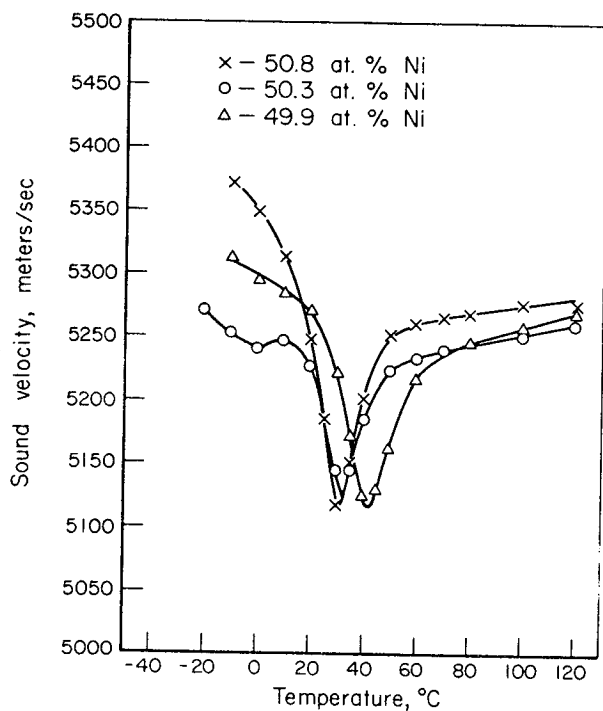


FIGURE 39.—The effect of chemical composition on the velocity of sound in NiTi. (Chemical compositions of specimens: x 50.8 atomic % Ni; o 50.3 atomic % Ni; Δ 49.9 atomic % Ni.) The measurements were made on the cooling half of the temperature cycle. The frequency of the sound was 5 MHz.

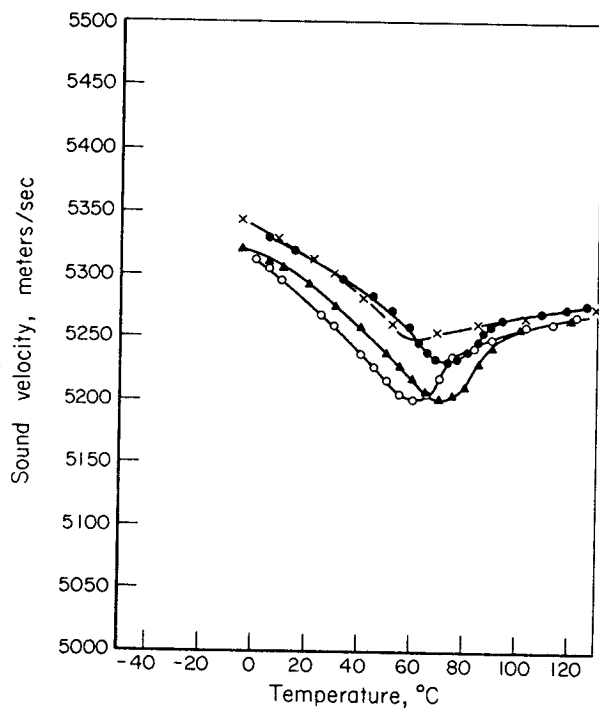


FIGURE 40.—The effect of heat treatment and stabilization on the velocity of sound in NiTi containing 49.9 atomic % Ni. (Specimen identification: x as-hot-swagged arc-cast material; · material was "stabilized" by temperature cycling between  $-30^{\circ}$  and  $+200^{\circ}$  C until repeatable results were; · material was heat treated at  $400^{\circ}$  C for 2 hr in an inert atmosphere and furnace cooled; Δ material was heat treated at  $300^{\circ}$  C (time, atmosphere, and cooling rate were not given.) All tests were carried out on the heating half of the temperature cycle. The frequency of the sound was 5 MHz.)

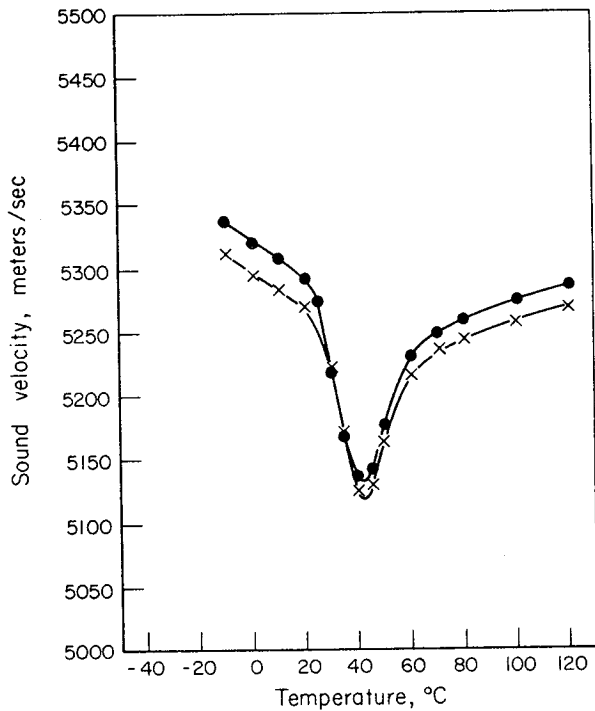


FIGURE 41.—The effect of pressure on the velocity of sound in NiTi containing 49.9 atomic % Ni. (Measurements were made on the cooling half of the temperature cycle at pressures of 14.7 psi (x data points) and 40 000 psi (• data points). In both cases, the frequency of the sound was 5 MHz.)

composition about 51 atomic percent Ni and a "transition temperature" ( $A_s$ ) near 60° C. Since the methods and procedures were the same as in Bradley's paper and, in fact, the experiments were carried out by Bradley, the results are comparable to the

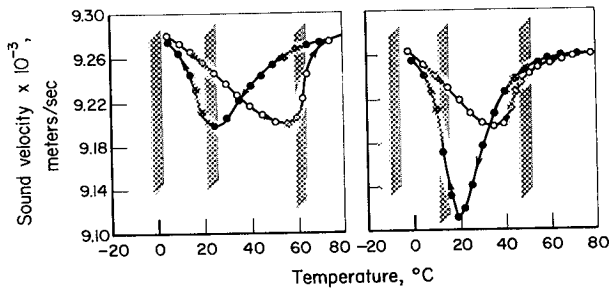


FIGURE 42.—The effect of temperature on the sound velocity in NiTi containing 51 atomic % Ni. (The curves on the left are for a sample that had undergone complete cycles, while those on the right are for a sample that had undergone incomplete cycles. The frequency of the sound was 5 MHz.)

earlier work (ref. 79). Particularly in the cooling half of the cycle, a great difference was noted between the complete and incomplete cycles.

**DAMPING, INTERNAL FRICTION, DYNAMIC MODULUS, AND POISSON'S RATIO**

Buehler and Wiley first noticed the unique mechanical-vibration-damping property of Nitinol by striking a bar\* of the material at room and elevated temperatures (refs. 11 and 12). At room temperature, a dead sound was produced by the blow, whereas at about 57° C the bar exhibited a metallic ring, which became more brilliant about 77° C. It was also observed that the phenomenon was dependent on composition. They investigated alloy compositions from 52.5 to 58 weight percent Ni, and found that arc-melted bars containing more or less nickel than 54.5 weight percent were unable to produce the high-damping-to-low-damping transition over such a narrow temperature range and at temperatures so close to room temperature. The results obtained are shown in figure 43 (ref. 12).

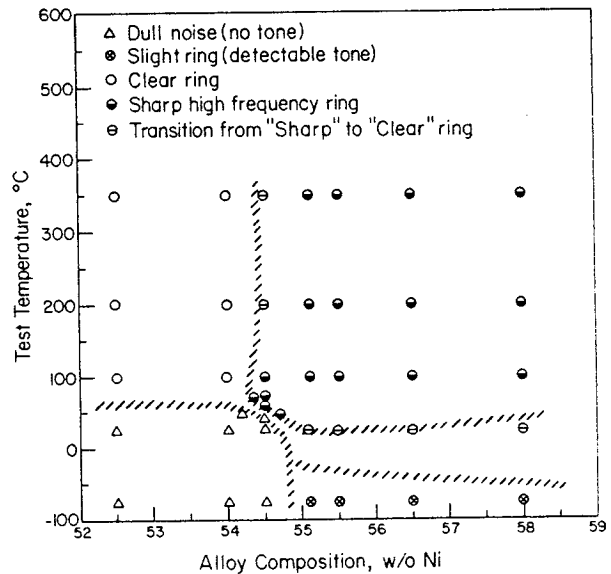


FIGURE 43.—The effect of temperature on the sound produced by striking suspended arc-cast bars (approximately 9/16 in. in diam by 4 in. long) of NiTi alloys. (Note sudden sound transition with temperature for alloys containing about 54.5 weight % Ni.)

\*Arc melted, containing about 54.5 weight percent Ni and 0.09 weight percent Fe.

Some of the same alloys—54, 54.5, and 55.1 weight percent Ni—were hot swaged at 900° C into uniform smaller diameter bars. When these were struck, the transition-temperature range from high- to low-damping was found to have widened, perhaps because of additional secondary phase(s) seen in the matrix of these worked bars (fig. 44) (ref. 12).

The purity of the titanium melting stock was important in determining the transition temperature. Thus, for 54.5 weight percent Ni, if the iron content was around 0.09 percent, the high-damping-to-low-damping transition was maintained around room temperature, as in figure 43. If higher-purity melts were made (without iron) the same behavior was shown by alloys containing 55.1 and 55.5 weight percent Ni (ref. 11).

Some hysteresis was noted qualitatively by Buehler and Wiley in arc-cast alloys with 54.7 and 54.8 weight percent Ni (ref. 12). They noted that the brilliant ring at room temperature could be completely eliminated by cooling to -15° C, but that when the bar was reheated to 25° C the brilliance was considerably lower than before. When the specimen was heated to 45° C, the brilliant ring was restored and persisted at room temperature. The time-dependent nature of the phenomenon was demonstrated by cooling a bar to -76° C and then warming it to room temperature; 92 hr later the "equilibrium-sound" behavior had been restored.

Buehler and Wiley made quantitative measurements of damping by the low-frequency (0.4 Hz) torsion-pendulum method, using 0.0206-in. and

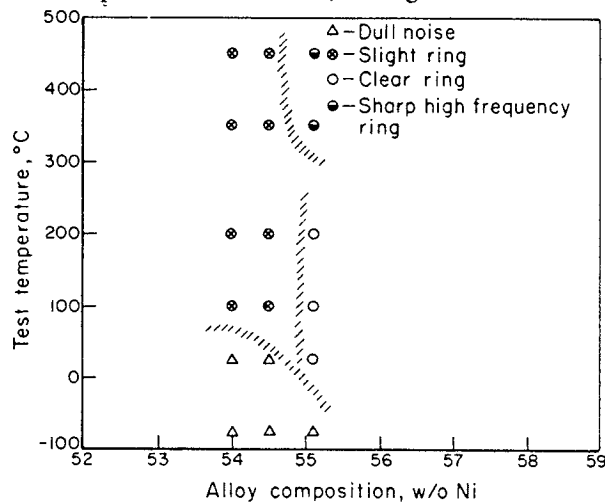


FIGURE 44.—The effect of temperature on the sound produced by striking suspended hot-swaged (900° C) bars (0.5 in. in diam by 5.5 in. long) of NiTi alloys.

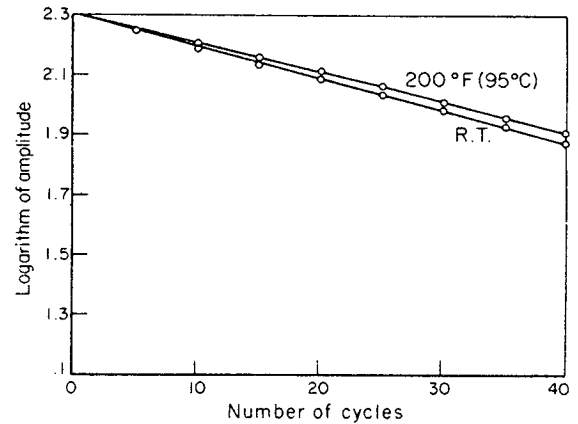


FIGURE 45.—The decay in torsional vibration as a function of number of cycles and temperature for 0.0206-in. diam NiTi wire containing 55.1 weight % Ni. (Average frequency = 0.408 Hz.)

0.0360-in.-diameter drawn wire as the specimens (ref. 12). Results for the 55.1 weight percent Ni alloy (with 0.09 percent Fe) are given in figure 45. This alloy showed little temperature sensitivity. On the other hand, the two wires of 54.5 weight percent Ni (fig. 46) showed a pronounced decrease in internal friction as the temperature was raised to 93° C. The change in damping as a function of temperature is shown in figure 47; it agrees with the acoustic data. Time at temperature was also important, as shown in figure 48. The damping transition seemed to require about 1 to 5 min to occur, and then stabilized after 10 min.

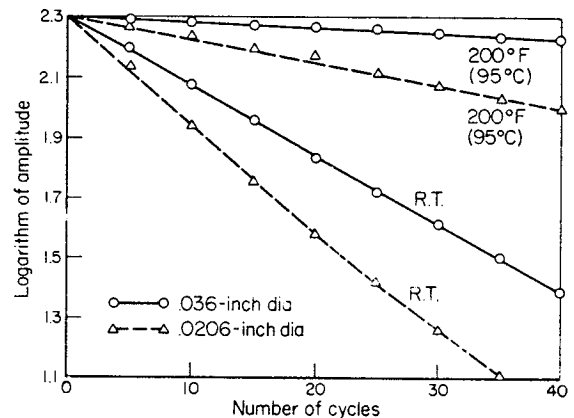


FIGURE 46.—The decay in torsional vibration as a function of number of cycles and temperature for NiTi containing 54.5 weight % Ni. (Average torsional frequency was 0.400 Hz for the 0.036-in.-diam wire and 0.440 Hz for the 0.0206-in.-diam wire.)

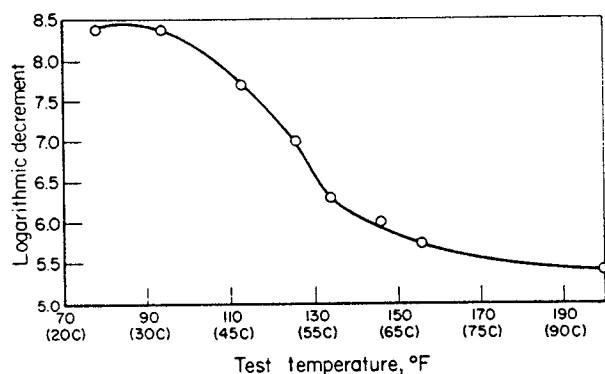


FIGURE 47.—The effect of temperature on the damping of NiTi wire containing 54.5 weight % Ni. (Average frequency of torsional vibration = 0.40 Hz.)

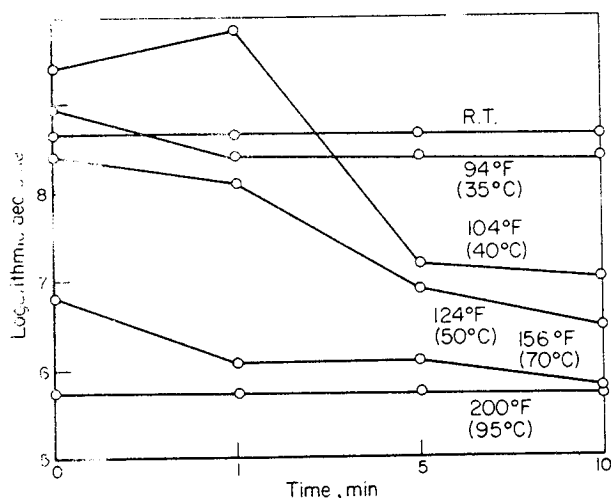


FIGURE 48.—The effect of time at temperature on the damping of NiTi containing 54.5 weight % Ni. (Wire diam = 0.036 in. Average frequency of torsional vibration = 0.40 Hz.)

Wasilewski investigated the dynamic elastic modulus and damping of stoichiometric NiTi (which contained less than 150 ppm oxygen, apparently associated with some second phase thought to be oxygen-bearing  $Ti_2Ni$  or possibly  $Ti_4Ni_2O$ ) (ref. 16). The material had been prepared by nonconsumable arc casting, extruding, and swaging to 3/8-in. bar. All test material was given a 650° C anneal for 1 hr, followed by overnight furnace cooling to minimize residual stresses.

Dynamic modulus measurements were made over the frequency range 600 Hz to 50 kHz. Fundamental resonance frequencies in the flexural mode were

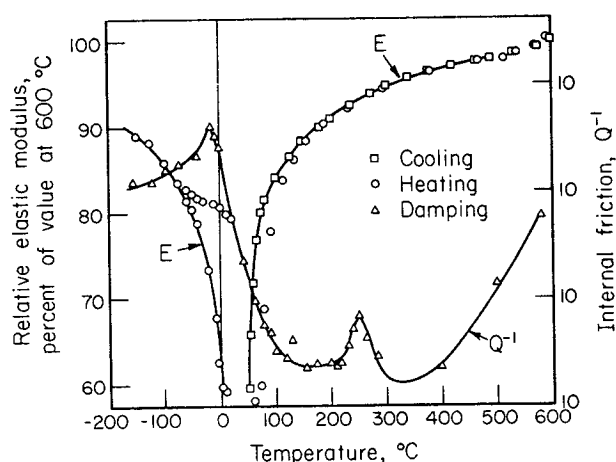


FIGURE 49.—Relative elastic modulus and internal friction of NiTi containing 50.0 atomic % Ti and 146 ppm oxygen. (Material was extruded, annealed for 1 hr at 650° C, and furnace cooled.)

determined on specimens approximately 0.32 in. in diameter by 4.8 in. long. Damping values are given as  $Q^{-1}$ . Relative values of the resonance frequency are accurate to 0.02 percent. The absolute accuracy of the modulus values could be in error by as much as 1.8 percent because of mode mixing in flexural vibration and because no correction was made for thermal expansion. Nevertheless, the relative accuracy of the data is high.

The relative elastic modulus and damping of stoichiometric NiTi, taking the elastic modulus at 600° C as 100 percent, is shown in figure 49 (ref. 16). The transition temperature  $T_c$  was arbitrarily defined as the temperature at which the modulus was 50 percent of its value at 600° C, by extrapolation of the  $E$  vs  $T$  plot on cooling. Table 4 shows the values for various TiNi compositions on either side of the stoichiometric composition (ref. 16).

At the heating and cooling rates used (1 to 2° C/min) the resonance frequency and damping values observed were highly reproducible when the specimen temperature was above  $T_c$ . In the temperature range of -100° to +50° C, however, some ambiguity was observed, as the resonance peak split into two distinct, gradually separating resonances as illustrated in figure 50 (ref. 16) for a specimen heated from liquid nitrogen temperature. On continued heating the higher frequency peak gradually diminished and the lower frequency one decreased, finally appearing as a single, sharp resonance above the transformation range.

TABLE 4.—Variation in the Elastic Behavior of NiTi With Composition

Ti, atomic %	50.5	50.0	<sup>a</sup> 50.0	49.8	49.5	(49.3)
O <sub>2</sub> , ppm	160	146	170	150	158	480
$E_{600^\circ\text{C}} \times 10^{-6}$ psi	ND	15.40	15.55	15.11	ND	14.4
$E_{150^\circ\text{C}} \times 10^{-6}$ psi	12.32	12.48	12.87	12.37	12.54	13.28
$E_{\text{min}} \times 10^{-6}$ psi	11.50	11.10	11.50	8.99	10.12	8.67
$Q^{-1}$	$\gg 10^{-3}$	$\gg 10^{-3}$	$> 10^{-3}$	$8 \times 10^{-3}$	$2 \times 10^{-3}$	$2 \times 10^{-3}$
$T_c$ , cooling, °C	90	70	69	54	27	7
Hysteresis, °C	35	25	34	15	30	$b > 85$

<sup>a</sup>This specimen was repeatedly zone-melted *in vacuo* in an unsuccessful attempt to produce a single crystal.

<sup>b</sup>Transformation on heating should occur below 57° C, but was incomplete at 92° C—presumably due to O<sub>2</sub> content.

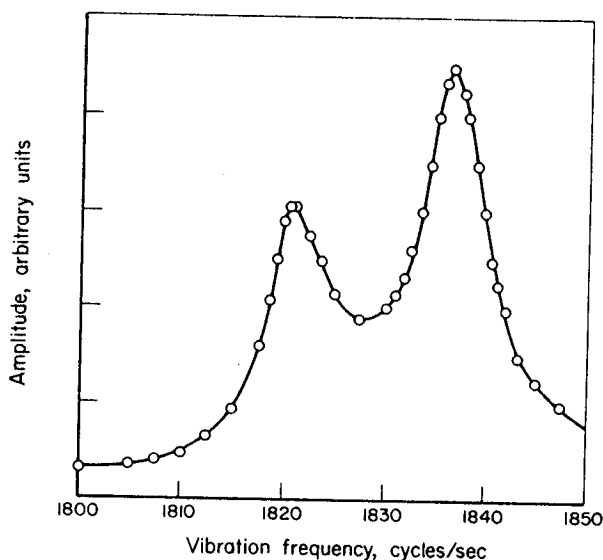


FIGURE 50.—Resonance-peak splitting in stoichiometric NiTi at  $-67^\circ\text{C}$ .

In general, high damping was associated with the transformation of NiTi on cooling, the high damping persisting at low temperatures. Low damping was observed from 125° to  $\sim 400^\circ\text{C}$ , with possibly minor peaks, but as the temperature was further increased the damping rose again, probably because of grain-boundary damping.

Spinner and Rozner have made a more exhaustive study of the elastic modulus and internal friction of NiTi, using nonconsumable-arc-cast material prepared from high-purity carbonyl nickel and sponge titanium (refs. 80 and 81). The cast billets were canned in steel and hot swaged at 800° C to about 0.75-in. diameter. As reported in other investigations, all of the melts contained a small amount of finely dispersed second phase which, according to reference 26, was associated with oxygen- and nitrogen-bearing phases tentatively identified as  $\text{Ti}_4\text{Ni}_2\text{O}$  and  $\text{Ti}_4\text{Ni}_2\text{N}$ . The

oxygen and nitrogen levels were, respectively, about 250 and 150 ppm. Table 5 shows the specimens used in the investigation. The effect of cold working was also studied; the specimens were cooled in liquid nitrogen and worked at about  $-180^\circ\text{C}$ .

Measurements of elastic moduli were made by a resonance technique using an audio oscillator at frequencies from 60 Hz to perhaps 20 kHz (refs. 85 to 86). Table 6 contains the room-temperature values of Young's modulus,  $Y_0$ , and the shear modulus,  $G_0$ . A standard deviation of 11 kbar around the average value of  $Y = 694$  kbar for all specimens, or a coefficient of variation of 1.5 percent, was obtained. This was considered unexpectedly favorable because the resonance peaks were broad, and because

TABLE 5.—Preparation of the Specimens

Specimen*	Preparation	Heat treatment
A	Hot swaged and hot rolled at 800° C. Rolling was accomplished in longitudinal direction.	1 hr anneal <i>in vacuo</i> $10^{-6}$ mm Hg at 800° C and furnace cooling.
B	Hot swaged and hot rolled at 800° C. Rolling was accomplished in transverse direction.	As above.
C	Hot swaged at 800° C.	As above.
D	As in specimen A plus 10 percent cold rolled at about $-180^\circ\text{C}$ .	None
E	As in specimen A plus 20 percent cold rolled at about $-180^\circ\text{C}$ .	None

\*Specimen C was cylindrical in shape; length, 13.45 cm; diameter, 0.637 cm. Specimens A, B, D, and E were rectangular bars about 14 cm by 1.27 cm by 0.205 cm (ref. 82).

TABLE 6—Room-Temperature Values of Elastic Moduli of NiTi

Specimen	Young's Modulus, $Y_0$ , kbar	Shear Modulus, $G_0$ , kbar	Poisson's ratio
A	681	256	0.33
B	698	235	0.485
C	$Y_1 = 695$ $Y_2 = 702\ 700^*$ $Y_3 = 703$	---	---
D	706	270	0.31
E	684	280	0.22
	Av. 694		

\* $Y_1$ —Young's modulus from fundamental frequency;  $Y_2$ —Young's modulus from the first overtone; and  $Y_3$ —Young's modulus from the second overtone.

the specimen was perhaps not as homogeneous and isotropic as would be required by the theory. Poisson's ratio was computed from

$$\mu = (Y/2G) - 1$$

The accuracy of  $\mu$  is reduced from the accuracy of  $Y$  and  $G$  by an order of magnitude. Hence, the accuracy of Poisson's ratio in table 6 is about 15 percent.

The relative-modulus vs temperature relationships are shown in figures 51 through 55 for all specimens

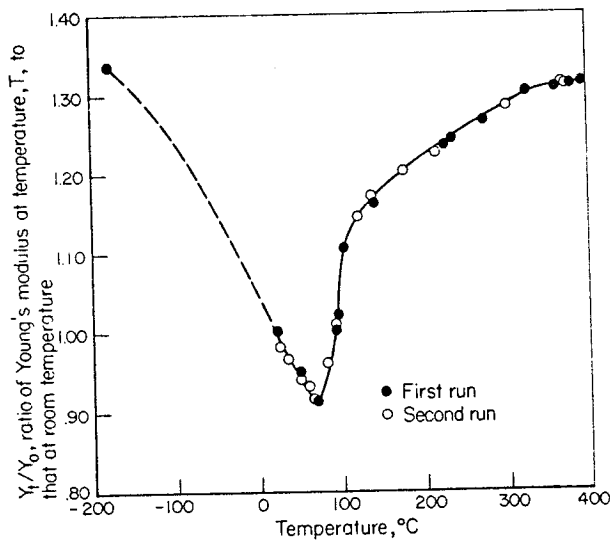


FIGURE 51.—Ratio of Young's modulus to Young's modulus at room temperature, as a function of temperature for annealed stoichiometric NiTi. (Specimen C, the preparation and heat treatment of which are described in table 5, was used in this experiment.)

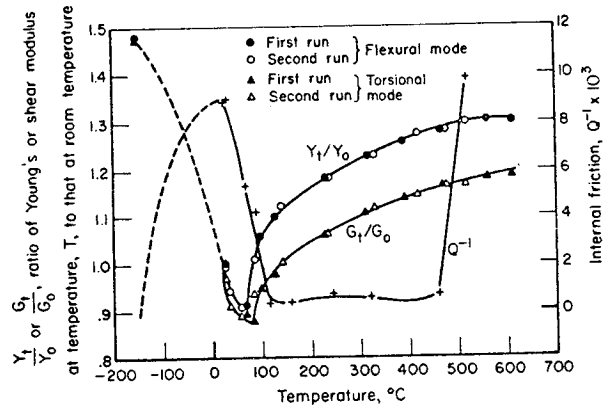


FIGURE 52.—Modulus ratio and internal friction as a function of temperature for annealed stoichiometric NiTi. (Specimen A, the preparation and heat treatment of which are described in table 5, was used in these experiments.)

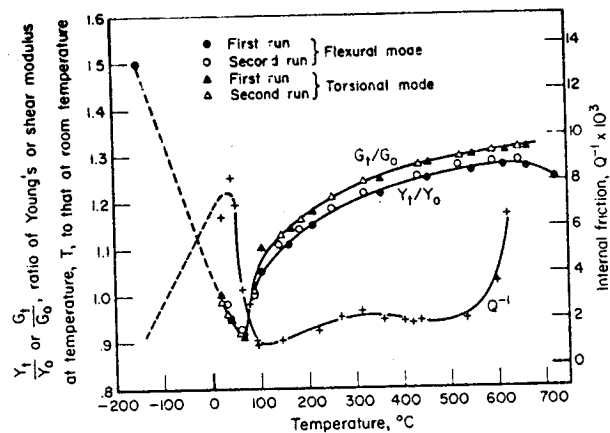


FIGURE 53.—Modulus ratios and internal friction as a function of temperature for annealed stoichiometric NiTi. (Specimen B, the preparation and heat treatment of which are described in table 5, was used in these experiments.)

(ref. 80). In general, a minimum appeared between 70° and 140° C, depending on the particular specimen. Immediately above and below the minimum the values rose rapidly, in qualitative agreement with Wasilewski's data (ref. 16).

If the sound velocity is computed, the value  $V = 3800$  m/sec at room temperature is obtained. This is not in good agreement with Bradley's value of 5250 m/sec (ref. 79). Spinner and Rozner attributed the difference partly to a difference in the specimens, and possibly also to the fact that Bradley used a frequency of 5 MHz, several orders of magnitude higher than used in their measurements.

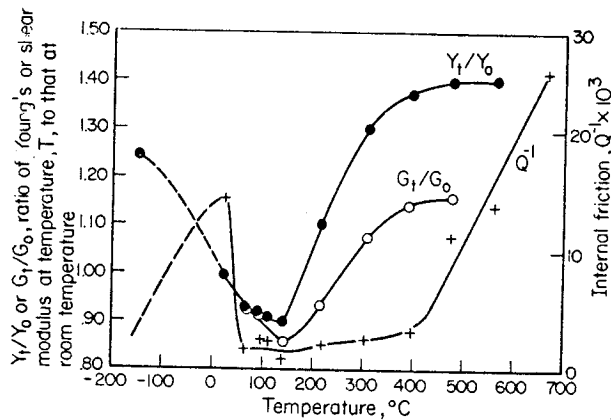


FIGURE 54.—Modulus ratios and internal friction as a function of temperature for cold-rolled stoichiometric NiTi. (Specimen *D*, the preparation and cold rolling of which are described in table 5, was used in these experiments.)

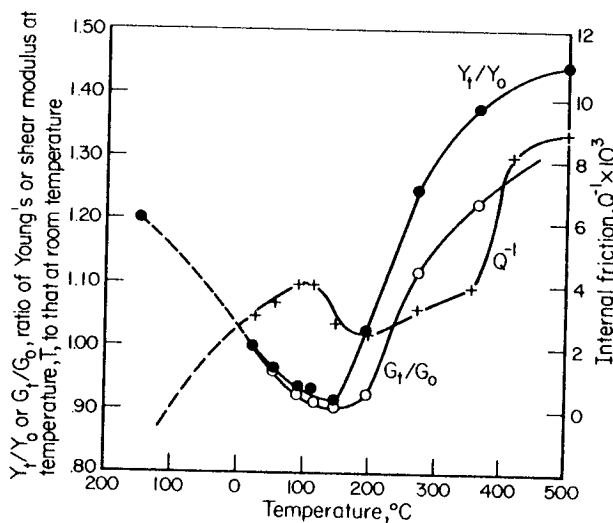


FIGURE 55.—Modulus ratios and internal friction as a function of temperature for cold-rolled stoichiometric NiTi. (Specimen *E*, the preparation and cold rolling of which are described in table 5, was used in these experiments.)

Note that the maximum of  $Q^{-1}$  occurs about  $50^{\circ}\text{C}$  lower than the minimum for the elastic moduli. No explanation was offered, but apparently this is not unusual materials behavior.

Hasiguti and Iwasaki measured internal friction with a torsion pendulum (ref. 82). The wire specimens were prepared by Wang, and were 51 atomic percent nickel and 49 atomic percent Ti (ref. 17). The titanium sponge used for alloying contained about 0.07 weight percent iron and 0.15 weight percent (max.) of other impurities. The  $M_s$  of the alloy was

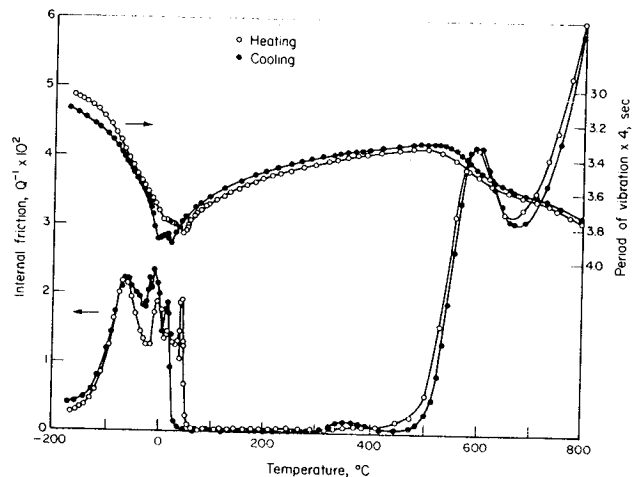


FIGURE 56.—Internal friction and period of vibration of NiTi containing 51 atomic % Ni, as a function of temperature (ref. 82). (The specimen was annealed at  $800^{\circ}\text{C}$  for 2 hr and furnace cooled prior to testing. Shear modulus is inversely proportional to the square of the period of vibration.)

about  $40^{\circ}\text{C}$ . Typical curves of internal friction and period of vibration (times 4) over the range  $-170^{\circ}\text{C}$  to  $+800^{\circ}\text{C}$  are shown in figure 56. (The shear modulus  $G$  is proportional to  $1/T^2$ , where  $T$  is the period of vibration.) Two well defined peaks occurred in the internal friction curves, one at about  $-70^{\circ}\text{C}$  and the other at about  $+600^{\circ}\text{C}$ . In addition, a small peak was observed at  $350^{\circ}\text{C}$  and a group of several sharp peaks, or an irregular serration, was noticed in the temperature range from the  $M_s$  temperature ( $+40^{\circ}\text{C}$ ) to about  $-50^{\circ}\text{C}$ . These irregular serrations are referred to as "fine structure" by the authors. Above  $40^{\circ}\text{C}$ , which is said to correspond to the  $M_s$  temperature, the internal friction drops abruptly; this is said to reflect a structural change from NiTi III to NiTi II on heating. Corresponding but less abrupt changes in the shear modulus were noted. The positive-temperature coefficient of modulus in the  $40^{\circ}$  to  $520^{\circ}\text{C}$  region is quite unusual.

The temperature intervals between measurements by Hasiguti and Iwasaki were much smaller than in the experiments reported by Wasilewski (ref. 16), Bradley (ref. 79), or Spinner and Rozner (ref. 81). Accordingly, the fine structure reported here was not resolved by the other investigators and was reported by them as single peaks.

When the specimen was annealed for 2 hr at  $600^{\circ}\text{C}$  and furnace cooled, the peak previously seen at  $-70^{\circ}\text{C}$  disappeared, along with the fine structure. This is illustrated in figure 57. Nevertheless, the  $-70^{\circ}$

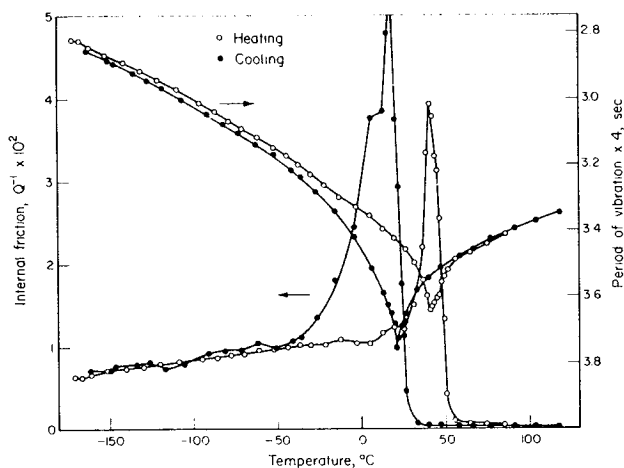


FIGURE 57.—Internal friction and period of vibration of NiTi containing 51 atomic % Ni, as a function of temperature (ref. 82). (The specimen was heated at 600° C for 2 hr and furnace cooled prior to testing. Shear modulus is inversely proportional to the square of the period of vibration.)

C peak and the fine structure are believed not to be related because the  $-70^{\circ}$  C peak shows a temperature shift when the frequency is changed, but the fine structure does not.

The  $-70^{\circ}$  C peak and the fine structure were said to be quite reproducible, in the same specimen, if the lowest temperature in the cooling cycle was not changed (which is reminiscent of Bradley's (ref. 79) findings regarding his sound velocity experiments, as noted earlier), and if the upper temperature did not exceed about 200° C. A difference of about 20° C was noted in what was believed to be the transition from NiTi II to NiTi III, between the cooling and heating cycles. No such difference was observed in the high-temperature transition.

When the specimen was elongated 5 percent at 80° C (following a 2-hr anneal at 800° C and furnace cooling), the changes of internal friction at the  $M_s$  temperature became sluggish. Elastic modulus, on the other hand, continued to show sharp transitions. In addition, considerable scatter in the internal friction curves resulted from shifting the lowest temperature in the cycle. No shift in the  $M_s$  temperature resulted from plastic deformation, and all the other effects noted were eliminated when the specimen was re-annealed above the deformation temperature.

The movement of the zero point of the torsion pendulum is shown in figure 58; the zero point is reproduced unless the specimen is heated above 200° C. The slight change in the second cooling run was

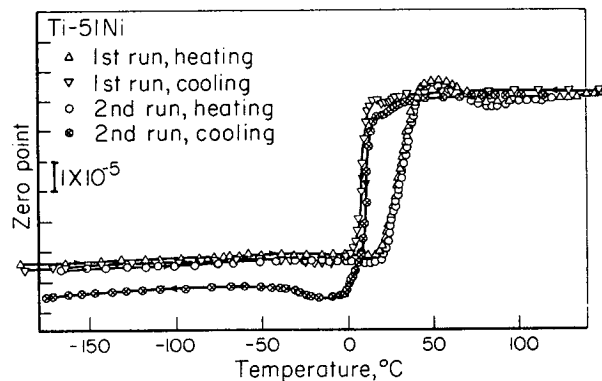


FIGURE 58.—Zero-point movements of the torsion pendulum for an as-received NiTi specimen containing 51 atomic % Ni (ref. 82). (The scale of the ordinate shows the surface-shear strain of the specimen, which corresponds to the zero-point movement.)

the result of an accidental displacement of the optical lever system.

Hasiguti and Iwasaki explained their observations in terms of Wang's model that the NiTi II–NiTi III transition is caused by a martensitic-shear movement of atoms. This is discussed in detail in the section titled "Crystal Structure," but, briefly, it is believed that the atoms move rather freely in the temperature region from  $M_s$  to  $M_f$ ; this means that there is a large amount of nonelastic strain due to the shear movement of atoms, and a correspondingly high internal friction. The fine structure is rationalized in terms of metastable intermediate atom positions between the initial and final positions. In the NiTi II region, the atoms are believed to be strongly bound as in a covalent crystal; therefore, the internal friction would be expected to be low. Similar arguments were advanced for the observed behavior.

Further studies of internal friction in relation to the effect of plastic deformation were reported by Hasiguti and Iwasaki (ref. 83). Figure 59 shows the internal friction and elastic moduli for a specimen (same as used in the previous work) deformed 10 percent after a 600° C anneal. As shown in the figure, plastic deformation has caused the changes of internal friction around the  $M_s$  to become sluggish. Heating at 400° C for 2 hr has restored the initial sharp transitions. Fast cooling from a 1000° C anneal had an effect similar to that of deformation (fig. 60); namely, the transitions have become more sluggish. In figure 61, however, annealing of the fast-cooled specimen at 400° C has restored the sharp transitions in the internal friction properties. These investigators,

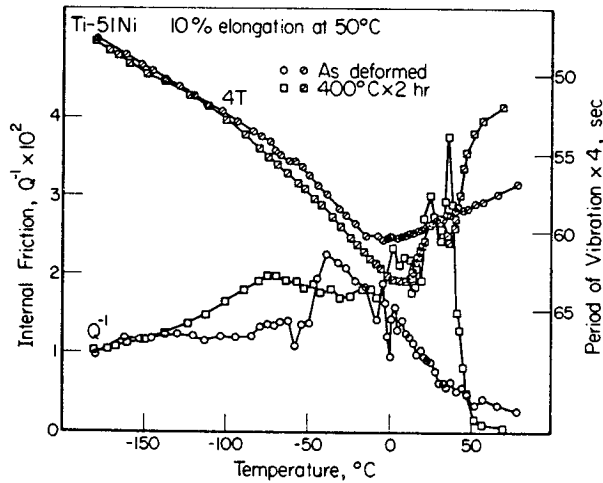


FIGURE 59.—The effect of deformation on the internal friction and period of vibration of NiTi containing 51 atomic % Ni, as a function of temperature. (The specimen was first annealed at 600° C. It was then deformed 10 percent at 50° C and tested. After testing, it was heated at 400° C for 2 hr and retested. Shear modulus is inversely proportional to the square of the period of vibration.)

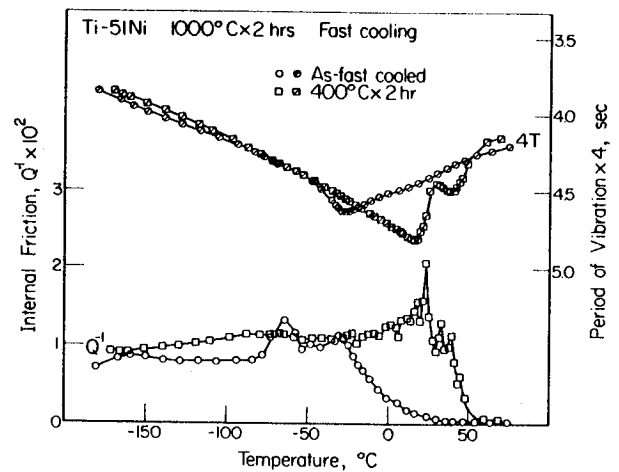


FIGURE 61.—The effect of annealing on the internal friction and period of vibration of NiTi containing 51 atomic % Ni. (Specimen had been heated at 1000° C for 2 hr and fast cooled prior to being annealed at 400° C for 2 hr. Shear modulus is inversely proportional to the square of the period of vibration.)

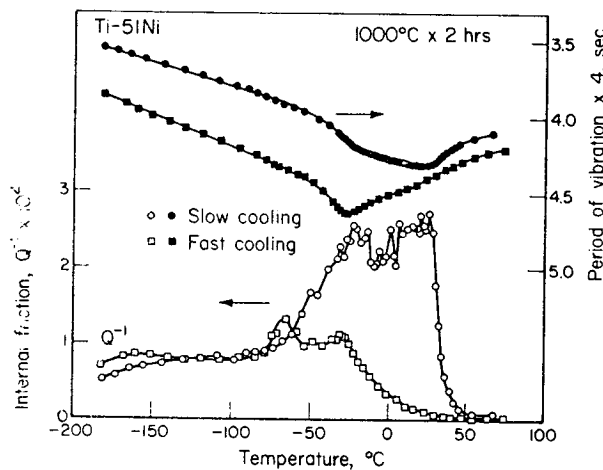


FIGURE 60.—The effect of cooling rate from 1000° C on the internal friction and period of vibration of NiTi containing 51 atomic % Ni. (The specimens were heated at 1000° C for 2 hr prior to cooling. Shear modulus is inversely proportional to the square of the period of vibration.)

proposed that the behavior could be explained by assuming that deformation in the NiTi II phase occurred by means of  $1/2 [\bar{1}\bar{1}1]$  dislocations in  $(\bar{1}\bar{1}\bar{2})$ ,  $(\bar{1}\bar{2}1)$ , and  $(211)$  planes. Then, the NiTi II phase partially transforms to NiTi I by the passage of dislocations.

#### HEAT CAPACITY AND LATENT HEAT OF TRANSFORMATION

The diffusionless transition of the *B2* structure to the martensitic structure,\* and the reverse transition, have attracted considerable attention, especially since they are connected with the shape-memory phenomenon and the attendant high forces in the return to the memory shape.

Wang, Buehler, and Pickart carried out differential thermal analysis (DTA) experiments on NiTi containing 51 atomic percent Ni, which had a damping transition at a temperature of about 40° C (ref. 17). They found that the 40° C transition is endothermic in a heating cycle and exothermic in a cooling cycle. From the heat capacity of the alloy ( $0.077 \text{ cal deg}^{-1} \text{ g}^{-1}$ ), Wang et al. estimated the latent heat of the 40° C transition to be 5.78 cal/g, or about 307 cal/gram atom.

Wasilewski, Butler, and Hanlon made a calorimetric study of a 50.2 atomic percent Ti alloy containing <150 ppm oxygen (wt) (ref. 21). Selected heat content values are given in table 7 and the corresponding specific heat variation with temperature is shown graphically in figure 62. A sharp peak in

\*NiTi II to NiTi III, using the nomenclature of Wang and Buehler.

TABLE 7.—Heat-Content Values,  $\Delta H_T - \Delta H_{25^\circ \text{C}}$  (cal/g-mole), of NiTi Containing 50.2 Atomic Percent Ti (150 ppm oxygen)

Temperature, °C	$\Delta H$	Temperature, °C	$\Delta H$
-196	-1120	100	822.6
-79	-610	122.5	978.7
0	-160	226	1626
50	153	327	2310
70	267.1	427	2990
82.5	571.2	527	3665
93	774.8		

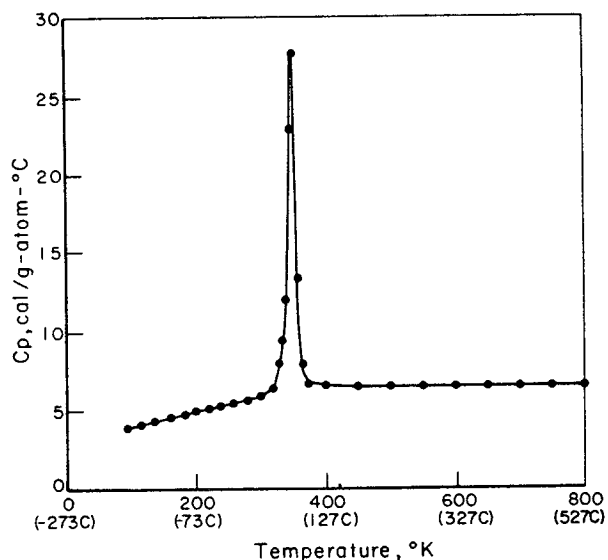


FIGURE 62.—Specific heat of NiTi containing 50.2 atomic % Ti. (Transformation temperature (heating):  $90^\circ \text{C}$   $\Delta H = 370 \pm 20$  cal/g-mole.)

$C_p$  is seen to occur at  $90^\circ \text{C}$  ( $363^\circ \text{K}$ ). The enthalpy  $\Delta H$  was calculated to be about  $370 \pm 20$  cal/g-mole, and the best estimate of the entropy  $\Delta S = 1.01 \pm 0.05$  cal/deg K at  $90^\circ \text{C}$ .

Wasilewski further studied the transformations by DTA against an annealed-copper standard. The results are presented in figure 63; the  $92^\circ \text{C}$  endothermic peak on heating and a double exothermic peak on cooling, the larger being at  $55^\circ \text{C}$ , are shown in the figure.

Another calorimetric study of the phase transition was made by Dautovich et al (ref. 40). Their sample was prepared by arc-melting spectroscopic-standard nickel and iodide titanium in a gettered argon atmosphere; the alloy contained 51 atomic percent

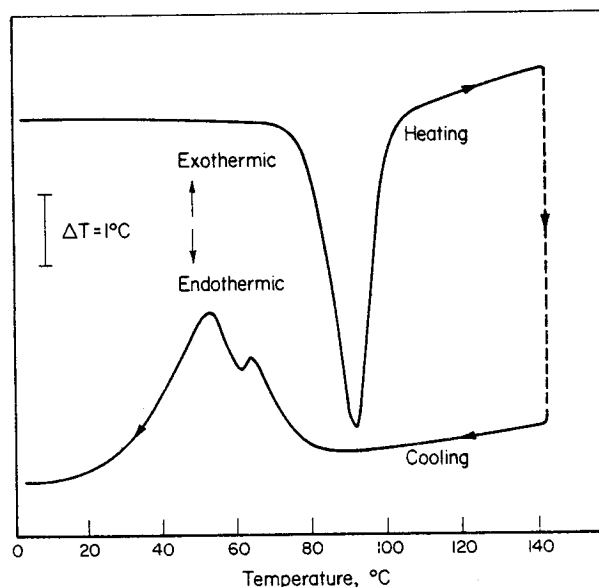


FIGURE 63.—Differential thermal analysis results for NiTi containing 50.2 atomic % Ti vs annealed nickel standard. (Transformation temperature: heating,  $92^\circ \text{C}$ ; cooling,  $55^\circ \text{C}$ . Note apparent two-step transformation on cooling.)

Ni. After being hot forged and machined to 0.5-in. diameter by 1 in. long, the specimen was sealed in an evacuated silica capsule, and annealed for 2 days at  $700^\circ \text{C}$ , followed by 6 days at  $400^\circ \text{C}$ , and then quenched to room temperature. Typically, material prepared this way contained less than 200 ppm oxygen, and this particular sample contained 112 ppm oxygen after the heat treatment. This heat treatment was said to have suppressed the martensitic transformation in the temperature range studied, and thereby allowed the heat effects accompanying reversion of an "intermediate" transition phase between the transformation of the parent phase to martensite to be examined. Longer treatments at  $400^\circ \text{C}$  were found to limit the temperature range of existence of the transition phase, which transformed completely to martensite at or near room temperature. The sample was placed in the heating coil of an evacuable adiabatic calorimeter and cycled to increasingly lower temperatures (to  $-196^\circ \text{C}$ ). The specific heat of a sample heated from  $43^\circ \text{C}$ ,  $0^\circ \text{C}$  and  $-196^\circ \text{C}$  is shown in figure 64. Also shown in the figure are resistivity data for the same sample.

Dautovich stated that the calorimetric data can only give a lower limit for the heat of transformation of the martensite, since the transformation of these samples was not complete even at the lowest temperatures used in the experiments. The heat of transfor-

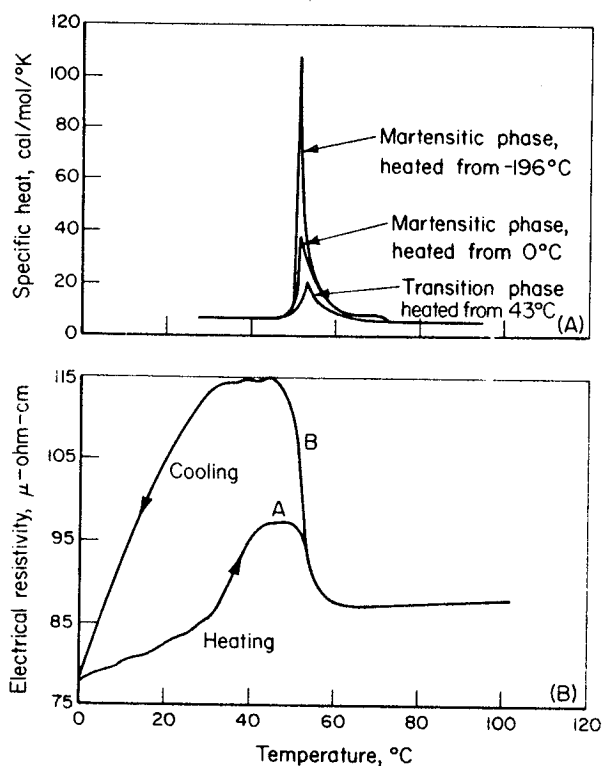


FIGURE 64.—Calorimetric and electrical resistivity data for NiTi containing 51 atomic % Ni. ((a) Calorimetric data obtained upon heating a single sample from  $-196^{\circ}$ ,  $0^{\circ}$ , and  $43^{\circ}$  C, in three separate runs. (b) Electrical resistivity vs temperature for the same sample cycled between  $0^{\circ}$  and  $100^{\circ}$  C.)

mation was more than 310 cal/g-mole, which is consistent with the work of Wang, Pickert, and Buehler (ref. 17) and Wasilewski (ref. 21).

Other calorimetric data obtained by Dautovich (ref. 40) are presented in figure 65. This shows the results of heating from progressively lower temperatures, and shows more detail than figure 64. The specific heat increase at  $70^{\circ}$  C was said to be associated with the reversion of martensite, rather than the transition phase. While not well understood, it was speculated that the reversion of martensite formed first on cooling.

Specific heat measurements in the  $25^{\circ}$  to  $218^{\circ}$  C range were made by Berman, West, and Rozner on an arc-cast 50 atomic percent Ni specimen that had been hot swaged and vacuum ( $10^{-6}$  torr) annealed for 2 hr at  $800^{\circ}$  C (ref. 84). The sample contained fine precipitates thought to be  $Ti_4Ni_2O$  and  $Ti_4Ni_2N$ ; the oxygen content was 250 ppm and the nitrogen content 80 ppm. The method consisted of determining the amount of energy required to raise the

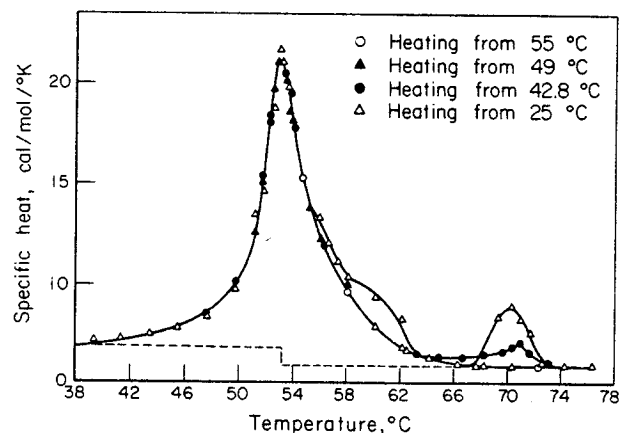


FIGURE 65.—Calorimetric data obtained during heating from the temperatures indicated. (Each heating run was preceded by heating the sample to  $95^{\circ}$  C or above. The broken line indicates the base values used in the graphical integration.)

temperature by a small amount, usually less than  $10^{\circ}$  C, but as little as  $0.8^{\circ}$  C in the transition region. The difference between the heat capacity of the calorimeter itself and that obtained during runs with the specimen is the heat capacity of the sample. Three series of experiments and a single run were made as follows:

*First series*— $128^{\circ}$  C to  $218^{\circ}$  C; cooled to room temperature.

*Second series*— $25^{\circ}$  C to  $82^{\circ}$  C; cooled to room temperature, then  $80^{\circ}$  C to  $154^{\circ}$  C; cooled to room temperature.

*Single run*— $35^{\circ}$  C to  $151^{\circ}$  C to obtain overall heat of transition; cooled to room temperature.

*Third series*— $40^{\circ}$  C to  $179^{\circ}$  C without intermediate cooling to room temperature.

In figure 66, the data obtained are shown for the second and third series. Noticeably different results were obtained in each of these runs. The heat of transition was taken as the area under the heat capacity curve (fig. 66); the area used was that which lies above the extrapolation of the heat capacity curves from  $50^{\circ}$  C and  $113^{\circ}$  C to the temperature of the peak. The results were

	Heat of transition		Uncertainty J/mole
	J/g mole	cal/g-atom	
Second series	4150	496	$\sim 10$
Single experiment	3831	458	7
Third series	3375	403	$\sim 10$

Berman et al. expressed their results as follows (ref. 84):

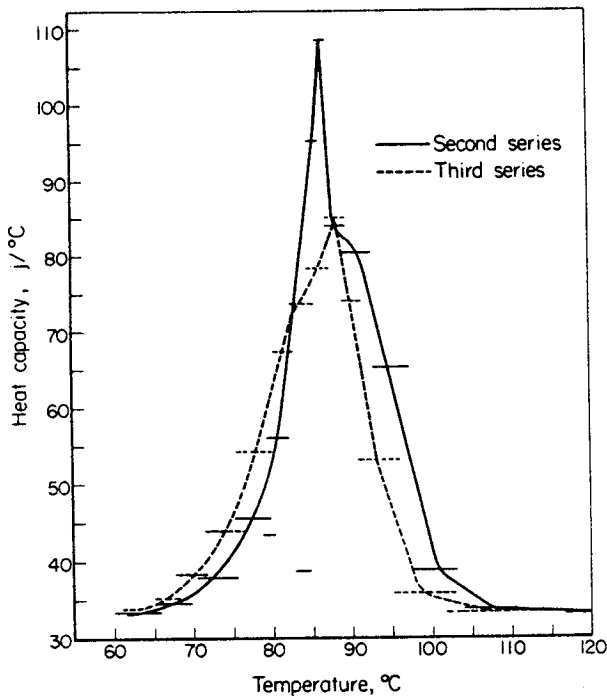


FIGURE 66.—The effect of temperature on the heat capacity of stoichiometric NiTi (ref. 80). (Curves constructed on the basis of two series of measurements are shown.)

(1) From 24° to 61° C,

$$C_p = 48.211 + 0.075797 t,$$

where  $C_p$  is in J/deg mole NiTi and  $t$  is in °C. In this temperature range no structural changes occurred, and the results adhered well to the Kopp-Neuman rule; i.e., the molar heat capacity of the compound is the sum of the molar heat capacities of nickel and titanium.

(2) From 61° to 113° C there is said to be a higher order transition,\* with a maximum heat capacity at about 87° C.

(3) From 113° to 145° C,

$$C_p = 47.406 + 0.019667 t$$

(4) From 145° to 218° C,

$$C_p = 64.437 - 0.168509 t + 0.00048679 t^2.$$

In the 113° to 218° C range the specific heat is nearly a linear function of temperature, but slightly below the sum of the molar heat capacities of nickel and titanium. Thus, at 127° C the calculated value (Kopp-Neuman rule) is 54.8 J/deg mole, while 49.90 was observed.

\*Wasilewski calls it a first-order transition (ref. 21).

These investigators confirmed that the thermal history of the sample has an important influence on the thermal properties. Their values for heat of transition were appreciably higher than found by Wang (ref. 17), Dautovich (ref. 40), or Wasilewski (ref. 21). The gradual reduction in the three series run by Berman indicates, perhaps, that equilibrium was being approached, and that the values reported by the other investigators are perhaps more nearly equilibrium values. No two-step transitions of the type reported by Dautovich (ref. 40) were observed by Berman.

In a subsequent paper, Wang et al. showed that the DTA results were identical for the incomplete cycles and complete cycles (ref. 44). The anomalous heat-capacity change that is associated with the two irreversible paths  $M_s - M_s$  on cooling, and  $M_s' - A_s$  on heating, and that no such change occurs within the reversible  $A_s - M_s$  range is shown in figure 67. Wang interpreted the results to mean that electrons are the major cause for the heat capacity changes observed. He considered changes from covalent transformation to conduction-electronic transformation, and calculated the energy involved in the transformation, based on the theory of Bragg and Williams on cooperative phenomena in which an order-disorder parameter is involved (refs. 85 and 86). Wang's calculated value of the energy of transition was 4161 J/mole (498 cal/g-atom), which is in surprisingly good agreement with the maximum value observed by Berman (ref. 84).

To characterize Nitinol for the purpose of developing structural-mechanical applications, Schuerch performed DTA of Nitinol wire (ref. 67). For one of the tests he used a specimen of 0.026-in.-diameter wire containing 44.6 weight percent Ti, 0.07 weight percent C, balance Ni that had been vacuum-heat treated, reaching 522° C in 29 sec, held for 7 sec, and cooled. DTA results from -48° to 437° C were as follows:

Temperature, °C	Specific Heat, cal/g deg
-48	0.110
-23	0.109
+77	0.109
+97	0.111
+437	0.113

These values, when converted to cal/g-mole-deg, range from 5.86 to 6.03, which are in agreement with

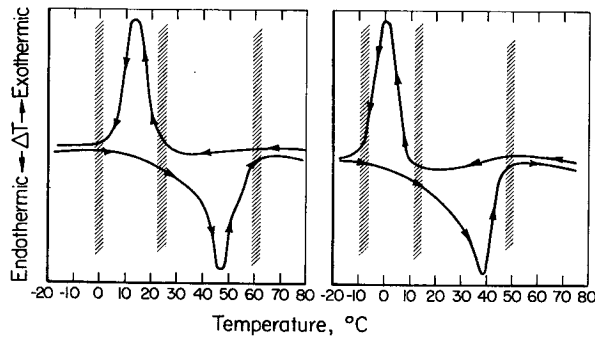


FIGURE 67.—Differential thermal analysis results obtained after complete and incomplete cycles. (Complete cycles are on the left and incomplete cycles are on the right.)

the results of other investigators, except that the anomalous change associated with the transition was missed. Additional thermal cycling within the range  $-80^{\circ}$  to  $+500^{\circ}$  C showed that latent heat peaks occurred between  $-40^{\circ}$  and  $+54^{\circ}$  C. Two endothermic peaks, one at  $47^{\circ}$  C and one at  $54^{\circ}$  C were observed on heating, and up to three exothermic peaks were observed on cooling. All of these values were sensitive to the thermal history of the specimen, as shown in table 8 (ref. 67).

TABLE 8.—Differential Thermal Data on 55-Nitinol Wire

	Heat effect	Peak shape	Temperature, °C	$\Delta H$	
				cal/g	cal/g-atom
<u>NiTi containing 44.6 weight percent Ti and 0.07 weight percent C</u>					
Heat treat in vacuum at $522^{\circ}$ C for 7.3 sec					
Store 4 months at room temperature					
Cool from $+25$ to $-80^{\circ}$ C	exo	broad	$-40$	1.26	68
Heat from $-80^{\circ}$ to $+140^{\circ}$ C	endo	sharp	$+47$	---	---
		very sharp	$+54$		
<u>Niti containing about 45.4 weight percent Ti and 0.06 weight percent C</u>					
Heat treat in vacuum at $522^{\circ}$ C for 7.3 sec					
Store 4 months at room temperature					
Heat from $20^{\circ}$ to $161^{\circ}$ C	endo	sharp	$\sim +54$	---	---
Cool from $161^{\circ}$ to $15^{\circ}$ C	exo	sharp	$+45$	---	---
Heat from $15^{\circ}$ to $80^{\circ}$ C	endo	sharp	$+54$	1.53	82
Cool from $+95^{\circ}$ to $-80^{\circ}$ C	exo	sharp	$+44$	2.08	112
	exo	broad	$-40$	2.14	115
Heat from $-80^{\circ}$ to $+160^{\circ}$ C	endo	sharp	$+47$	4.74	254
		very sharp	$+54$		
Heat to $300^{\circ}$ C					
Cool from $+100^{\circ}$ to $-80^{\circ}$ C	exo	sharp	$+47$	$>2.08$	$>112$
	exo	broad	$-40$	$\sim 2.14$	$\sim 115$
Heat from $-80^{\circ}$ to $+100^{\circ}$ C	endo	sharp	$+47$	$>4.74$	$>254$
		very sharp	$+54$		
Heat from $100^{\circ}$ to $500^{\circ}$ C					
Cool from $+100^{\circ}$ to $-60^{\circ}$ C	exo	sharp	$+39$	2.21	119
	exo	medium	$-2$	3.29	117
	exo	medium	$-8$		
Heat from $-60^{\circ}$ to $+100^{\circ}$ C	endo	sharp	$+54$	5.56	299

MAGNETIC SUSCEPTIBILITY

Cloud, as reported by Wasilewski et al. found a marked increase in the magnetic susceptibility of Nitinol (50.6 atomic percent Ti) at about 100° C (fig. 68), which was associated with the martensitic transformation (ref. 21).

Hanlon et al. measured the magnetic susceptibility of two compositions from -190° to +150° C and found that the 50.7 atomic percent titanium alloy showed a sharp increase in magnetic susceptibility (from about 2.5 to 3.8×10<sup>-6</sup> emu/g) at about 75° C. The 48.8 atomic percent titanium alloy however, did not show any sharp change (fig. 69). The behavior of the 50.7 titanium alloy was also characterized by differences in values taken during the heating and cooling cycles. (See ref. 59.)

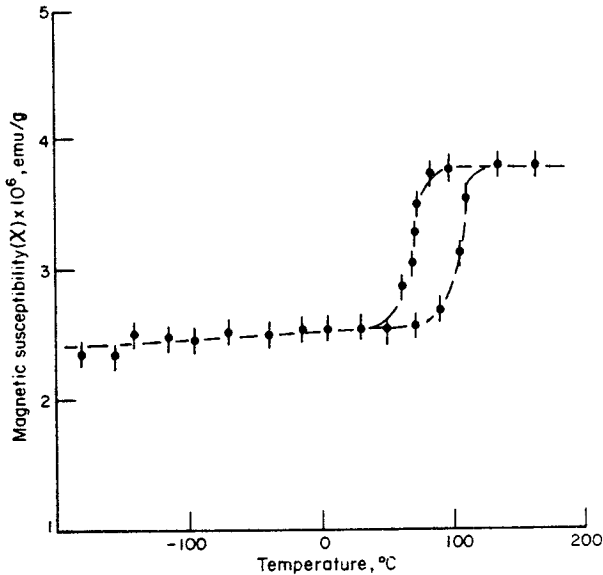


FIGURE 68.—Magnetic susceptibility of NiTi (50.6 atomic % Ti), as a function of temperature (after W. H. Cloud).

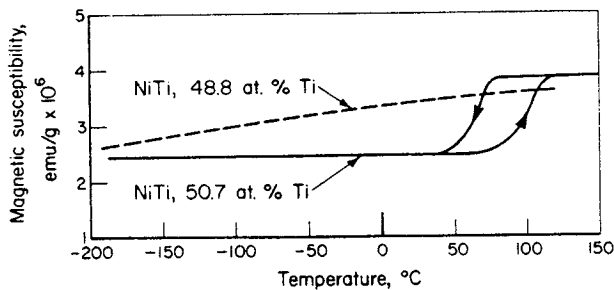


FIGURE 69.—Magnetic susceptibility of NiTi (48.8 and 50.7 atomic % Ti).

Wang et al. studied the magnetic susceptibility of NiTi (51 atomic percent nickel) over the temperature range from -20° to +75° C (ref. 44). The behavior of material that had been given complete cycles was compared with that which had been given incomplete cycles. As shown in figure 70, no difference (within

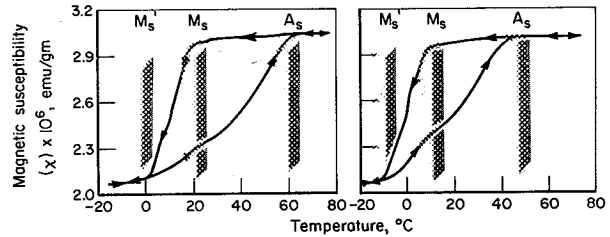


FIGURE 70.—Magnetic susceptibility obtained after complete and incomplete cycles: complete cycles on the left and incomplete cycles on the right (ref. 44).

the limits of experimental error) was found in the magnetic susceptibility of material given the two types of treatments. The curves have the same general shape as those reported by Wasilewski et al. (ref. 21) and Hanlon et al. (ref. 59).

THERMAL CONDUCTIVITY

The thermal conductivity of NiTi and alloys of NiTi with copper or nickel was measured by Goff (ref. 75). The chemical compositions of Goff's alloys were given in table 2. Plots of the measured thermal conductivities as a function of temperature are shown in figure 71. In general, the thermal conductivity *K* is the sum of a lattice component *Kg* and an electronic component, *Ke*. Thus,

$$K = Kg + Ke.$$

*Ke* is related to the electrical resistivity  $\rho$  by the Lorenz number *L*:  $L = Ke/\rho T$ , where *T* is the absolute temperature. When only elastic scattering processes are present, *L* has the Sommerfeld value of  $2.44 \times 10^{-8}$  W-ohms/(°K)<sup>2</sup>. Inelastic processes cause the heat flux to diminish more than the charge flux, and as a consequence *L* is decreased. On the other hand, when *Kg*, the lattice component, is not negligible, the measured *L* values will exceed the Sommerfeld value.

The Lorenz number vs temperature for the various NiTi alloys is given in figure 72. Since *L* exceeds the Sommerfeld value, *Kg* is not negligible at any

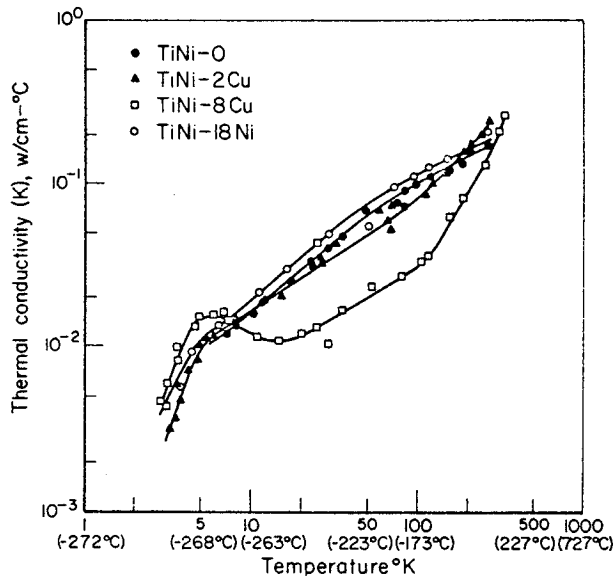


FIGURE 71.—The thermal conductivity of selected NiTi-base alloys.

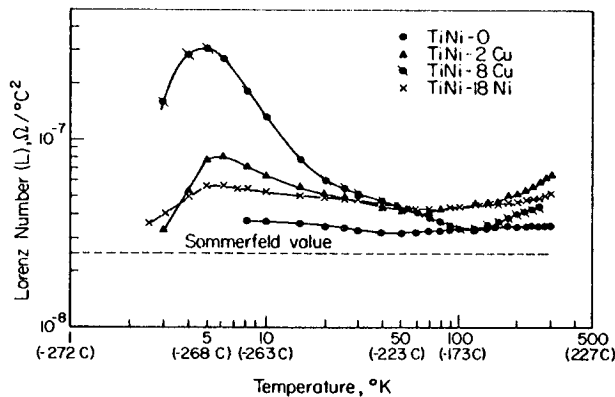


FIGURE 72.—The Lorenz number vs temperature for selected NiTi-base alloys (ref. 75).

temperature. Calculated values for  $Kg$  are shown in figure 73. The sharp difference between the TiNi-8Cu sample and the others was attributed to changes in structure that take place between  $10^\circ$  and  $100^\circ$  K. Also,  $Kg$  values of the alloyed samples seemed to increase more rapidly above  $100^\circ$  K than did that of the unalloyed sample. For an overview of the transport properties of NiTi in comparison with those of other TiX compounds, see reference 87.

### THERMAL EXPANSION EFFECTS AND SHAPE MEMORY

The shape-memory characteristic of Nitinol is so interwoven with ordinary thermal-expansion effects

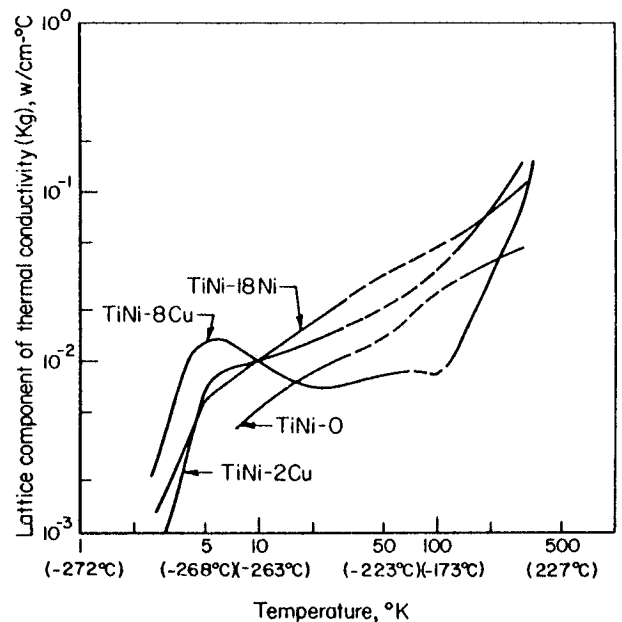


FIGURE 73.—The lattice component of the thermal conductivity of selected NiTi-base alloys (ref. 75). (The dashed lines indicate temperature ranges where the separation is only approximate.)

that it is difficult to discuss them separately. Shape memory is, after all, a thermal expansion or contraction of a special sort. Perhaps, in order to make the discussion easier to follow, these points should be kept in mind:

- (1) Thermal expansion usually means linear expansion and contraction.
- (2) Thermal expansion is usually reversible, although the heating path and cooling path might not coincide over the entire temperature range.
- (3) Shape-memory effects are usually irreversible, but some part of the change might be reversible. For some applications complete reversibility is desired; for others none is wanted.

The unusual thermal expansion and contraction behavior of Nitinol was not recognized at first. In fact, Buehler and Wiley reported in 1961, that the linear thermal-expansion coefficient is  $10.4 \times 10^{-6}/^\circ\text{C}$  between  $24^\circ$  and  $900^\circ$  C (ref. 12).

Other data presented by Spinner and Rozner, and attributed to Wiley and Heintzelman of the Naval Ordnance Laboratory, are shown in figure 74 (ref. 81). The relationship of  $\Delta l/l$  vs temperature is almost linear from  $100^\circ$  to  $300^\circ$  C, with a slope of about  $10 \times 10^{-6}/^\circ\text{C}$ . Between about  $25^\circ$  and  $100^\circ$  C, however, there is a hint of a slight hysteresis, but because the observations were taken at relatively large

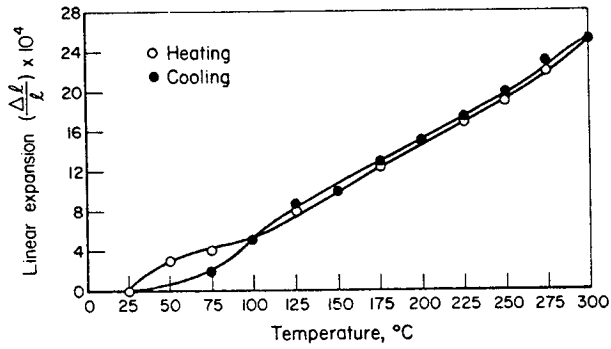


FIGURE 74.—Thermal expansion of stoichiometric NiTi. (o:heating; ●:cooling.)

temperature intervals, the effect is not well defined.

Wasilewski, Butler, and Hanlon, in nearly stoichiometric NiTi that had been warm worked at temperatures between 600° and 300° C, reported the results shown in figure 75 (ref. 21). These results give an indication of the presence of low- and high-temperature structures with linear expansion coefficients of  $6.6 \times 10^{-6}$  and  $11 \times 10^{-6} / ^\circ\text{C}$ , respectively. The latter value agrees with the earlier work by Buehler and Wiley (ref. 12). Most significant, however, is the linear contraction on heating through the transformation range, which averaged  $18 \times 10^{-4} / ^\circ\text{C}$ , which corresponds to a volume change  $\Delta V = -0.54$  percent.

Irreversible as well as reversible shape changes were first mentioned by Buehler in 1963 (ref. 68). In discussing the martensitic transformations taking

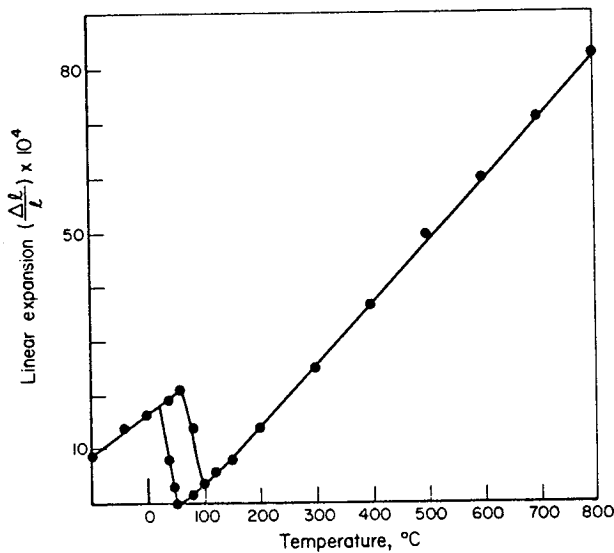


FIGURE 75.—Linear expansion of NiTi containing 50.2% Ti between  $-100^\circ$  and  $+800^\circ$  C. (Courtesy J. L. Youngblood.)

place in Nitinol, he presented evidence that Knopp-hardness indentations would almost completely disappear after a sample had been heated to 100° C and cooled to room temperature several times. Irreversible shape recovery was also demonstrated with 20-mil-diameter Nitinol wire which had been heat treated after cold drawing. When coiled into a tight helix and dipped into water about 65° C, the wire straightened itself out practically instantaneously.

To show contraction and expansion effects, both reversible and irreversible, Buehler et al. performed dilational studies on hot-swaged rod (refs. 62, 68 and 72). A hot-swaged rod was divided into two lengths. One was cold worked by swaging to introduce about 8 percent reduction of area by a compressive metalworking process. The other length was cold worked the same amount by drawing through a die.

When these two rods were machined to standard 50-mm-long dilational specimens and heated, they showed drastically different behavior. When the cold-drawn specimen was heated for the first time, a "very large" irreversible contraction was observed (ref. 72). Conversely, when the swaged specimen was heated for the first time it expanded irreversibly. Subsequent heating and cooling produced reversible expansion and contraction, the direction depending on the mode of deformation of the original rod (fig. 76).

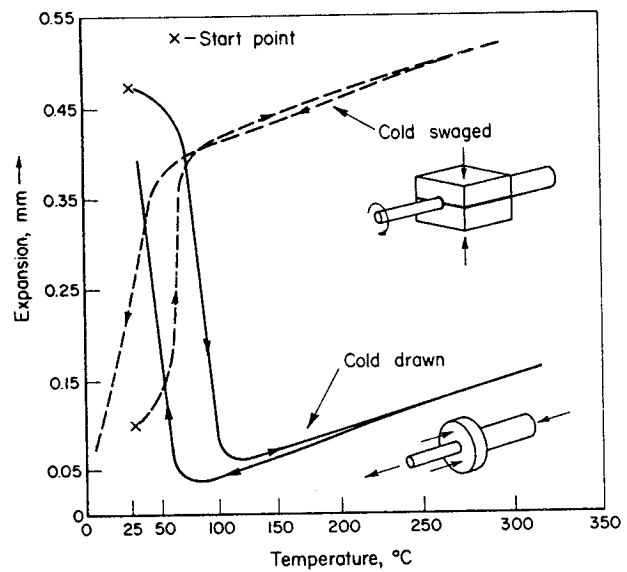


FIGURE 76.—Dilatation curves of stoichiometric NiTi following initial heating, showing reversible expansion and contraction depending on straining method (ref. 11).

Some expansion and contraction characteristics of Nitinol wire under load were proposed by Schuerch, who was obtaining design information to develop various devices (ref. 67). The Nitinol wire was heated and cooled while under a constant preload. In a typical test the procedure was to preload the sample and set the axial strain scale to about zero at ambient temperature (20° C). The sample was then cooled to -50° C, recording the axial strain at intervals of 5 to 10 degrees. The sample was then heated to 150° C, or higher if necessary, to reach the transition temperature range. The sample was then cooled to ambient temperature. Preloads of 1, 5, 10, 20, 30, and 40 lb were used. Some of the results obtained are shown in figure 77 (ref. 67). The heating and cooling transition temperatures increased as the constant load was increased. The approximate transition temperatures as functions of the constant load are given in figure 78 (ref. 67).

NASA-Langley sponsored a comprehensive investigation of the shape-memory characteristics of Nitinol (refs. 55, 63, and 70). In this work, a great deal of data were obtained on the factors influencing the shape-recovery vs temperature characteristics: chemical composition, processing, wire size, amount of

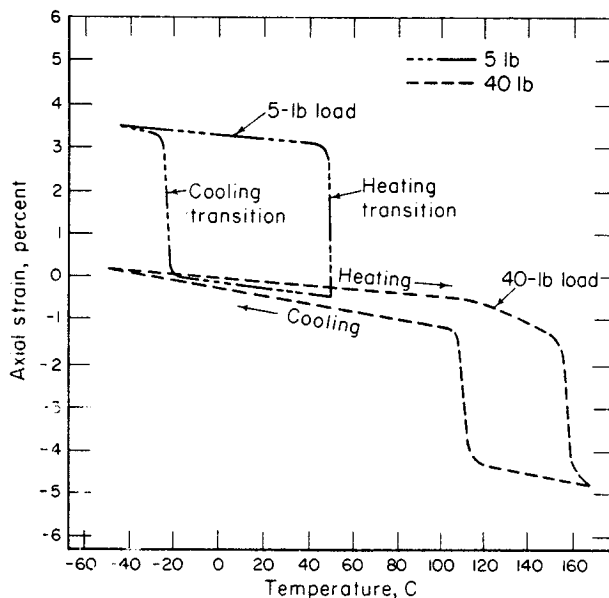


FIGURE 77.—Strain-temperature curves for 0.026-in.-diameter 55-Nitinol wire containing 44.6 weight % Ti and 0.07 weight % C while under two constant applied loads. (The wire was preloaded with the indicated load, which caused the wire to extend. The zero point for the axial strain measurements was the extended length, at about 20° C.)

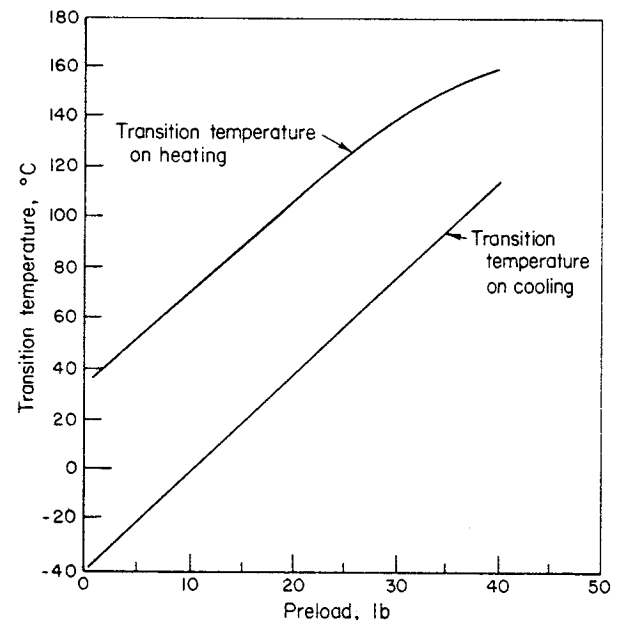


FIGURE 78.—The effect of preload weight on the transition temperature observed for 0.026-in.-diameter 55-Nitinol wire containing 44.6 weight % Ti and 0.07 weight % C.

strain, and other factors. Three alloys with different compositions and different transition temperatures were investigated. The compositions and transition temperatures are given in table 3; in this table the  $M_s$  is defined as the temperature at which the electrical resistance curve reaches a maximum on cooling. The implication is that it represents the temperature at which the martensitic transformation starts.

The detailed processing procedures are discussed in chapter 3. For the purposes of the present discussion it is important to note that foil and wire do not behave the same way, and that the foil thickness and wire diameter have an important effect on the shape-recovery characteristics.

Drennen, Jackson, and Wagner showed that temperature of the final heat treatment—the so-called “memory heat treatment”—was extremely influential in determining the efficiency of shape recovery (ref. 71). The shape of the electrical resistivity vs temperature curves (given in the “Electrical Resistivity” section) was shown by Cross, Kariotis, and Stimler to correlate well with the efficiency of shape recovery (ref. 63).

The influence of the final heat-treatment temperature on the reversible-thermal-expansion characteristics of the annealed material is shown in figures 79 and 80. In compositions *B* and *C* annealing at 700° C resulted in no hysteresis over the temperature range

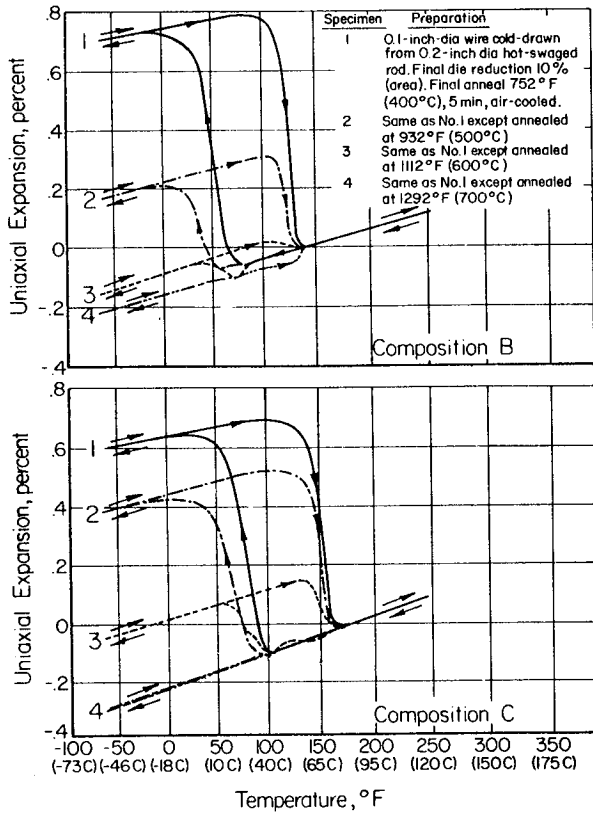


FIGURE 79.—The effect of temperature on the longitudinal dimension of 0.100-in.-diameter composition-B and -C rods (ref. 63).

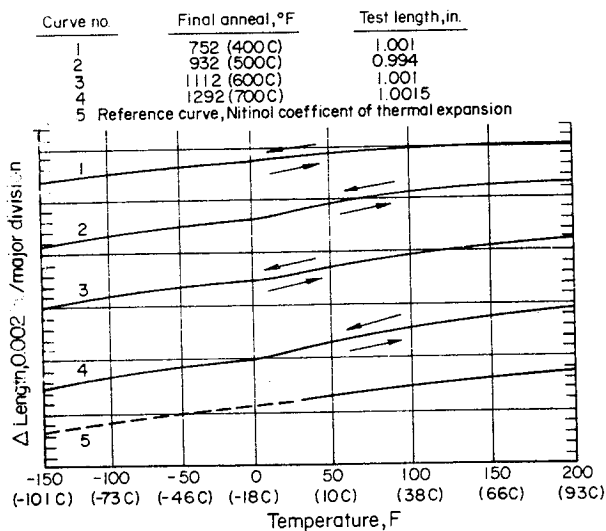


FIGURE 80.—The effect of temperature on the longitudinal dimension of 0.100-in.-diameter composition-A rods (ref. 63).

in which the various metallurgical transitions occur, whereas with lower annealing temperatures large hysteresis loops could be observed. Composition A, which was said to have an  $M_s$  temperature of  $-51^\circ\text{C}$ , failed to show any hysteresis. No interpretation of this behavior was given.

Tensile recovery tests on the A, B, and C compositions consisted in uniaxially elongating the specimen to a predetermined strain, removing the load and recording the elastic spring-back, and then applying heat to restore the wire to its original length (ref. 63). Deformation was carried out near what was said to be the  $M_s$  temperature of the materials, i.e., at  $24^\circ\text{C}$  for compositions B and C, and at  $-54^\circ\text{C}$  for composition A. The results are summarized in figures 81, 82, and 83. For most of the compositions and sizes, 100 percent recovery could be obtained if the strain did not exceed 6 to 8 percent. Variations did occur, however, particularly between the 6-mil foil and the various wire specimens. Compressive loading of compositions B and C rods indicated that perhaps the recovery limit is about 4 percent, though only a few tests were run in this deformation mode (ref. 63).

Bend-recovery tests were performed by bending the specimens around mandrels of various sizes to give different amounts of outer fiber strain. All

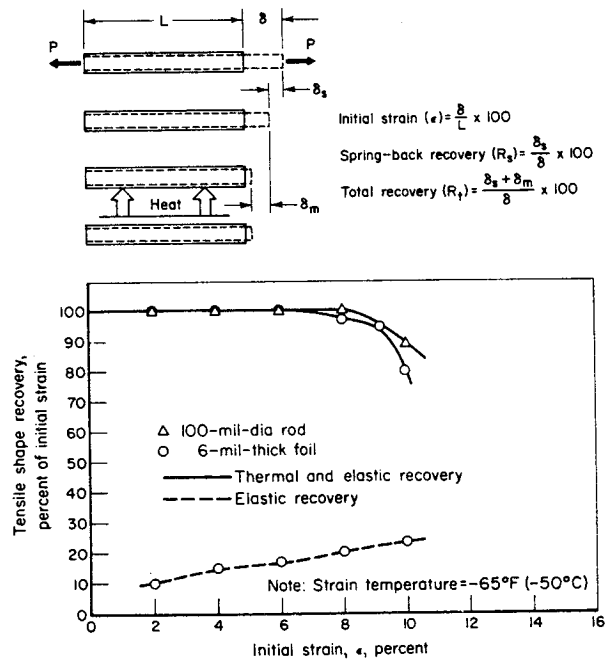


FIGURE 81.—The effect of initial strain on the tensile-shape recovery of composition-A materials.

specimens had been given a "straight" memory anneal at the temperature considered to be optimum for shape recovery efficiency. As before, composition *A* was bent at  $-54^{\circ}\text{C}$ , and compositions *B* and *C* at  $24^{\circ}$

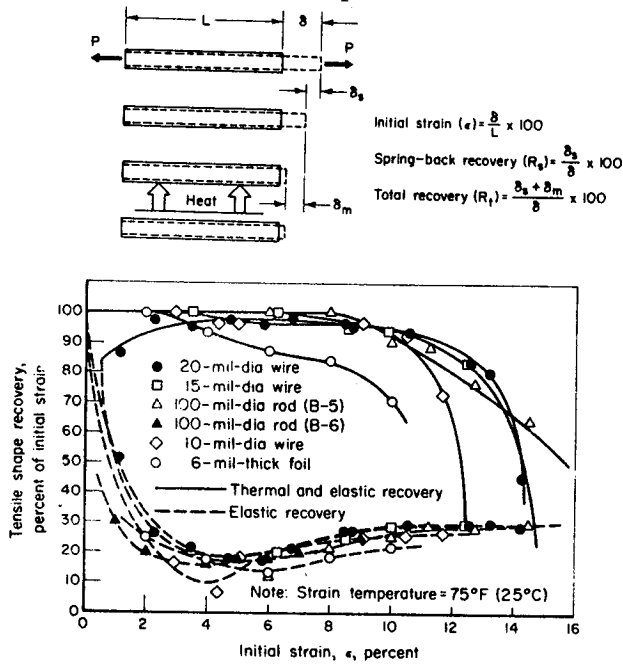


FIGURE 82.—The effect of initial strain on the tensile-shape recovery of composition-*B* materials.

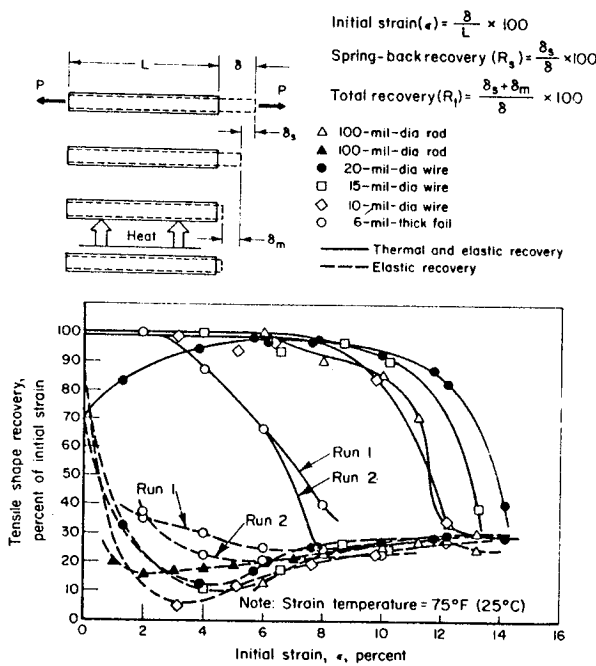


FIGURE 83.—The effect of initial strain on the tensile-shape recovery of composition-*C* materials.

*C*. The results obtained are shown in figures 84, 85, and 86. Important features of these curves are:

(1) The complete recovery limit was between 6 and 10 percent. Summary curves showing the completeness of recovery are shown in figures 87, 88, and 89.

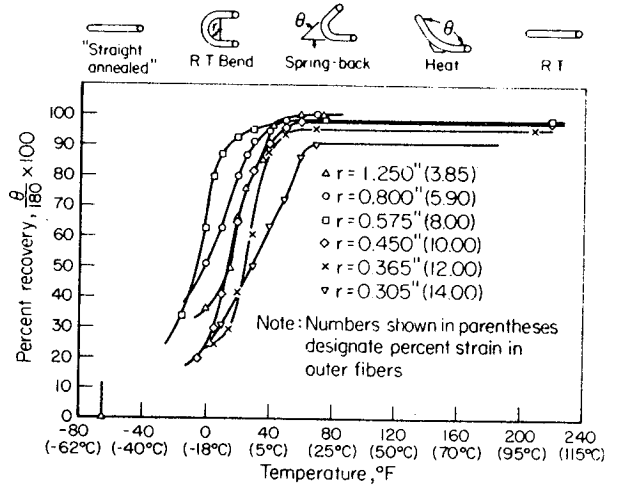


FIGURE 84.—The effect of temperature on the bend-shape recovery of 0.100-in.-diameter composition-*A* rods (ref. 63).

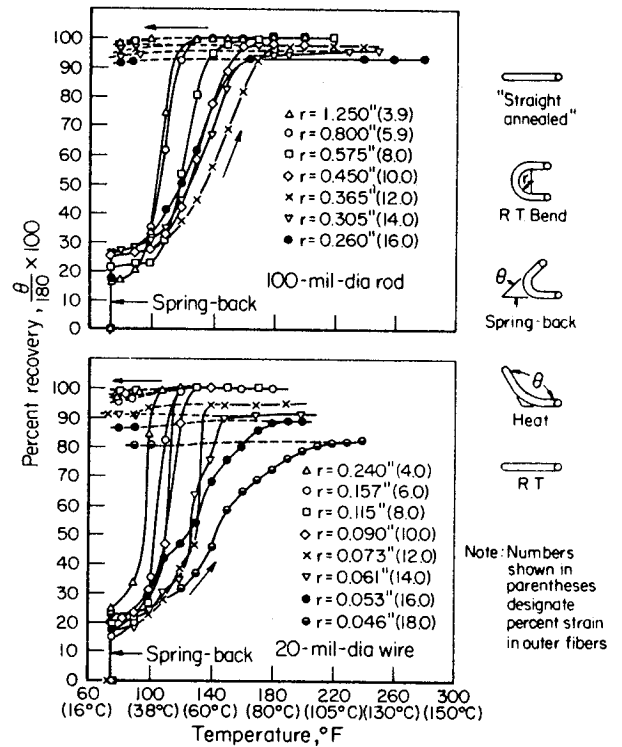


FIGURE 85.—The effect of temperature on the bend-shape recovery of composition-*B* materials (ref. 63).

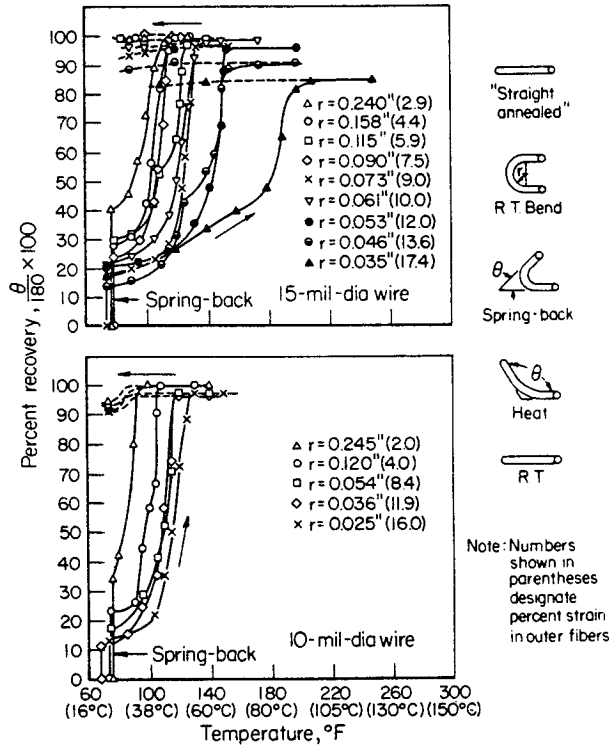


FIGURE 85.—The effect of temperature on the bend-shape recovery of composition-B materials—Continued.

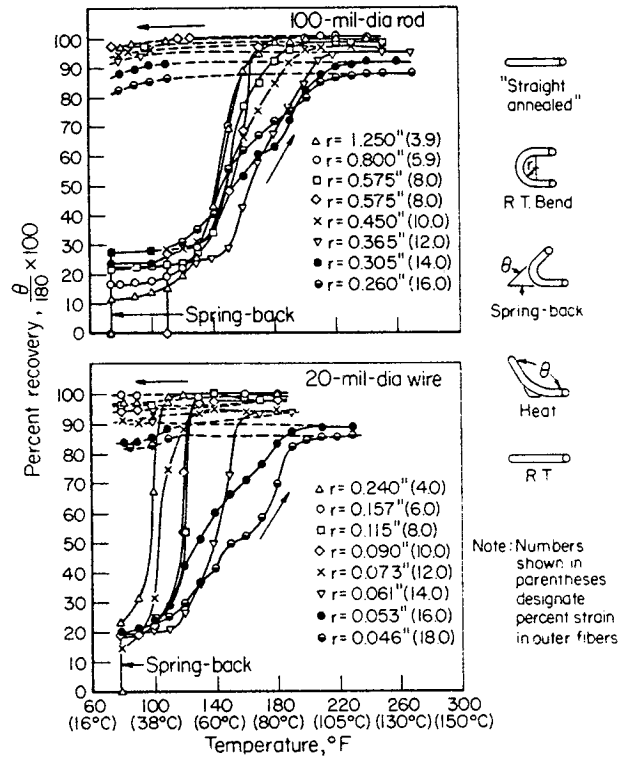


FIGURE 86.—The effect of temperature on the bend-shape recovery of composition-C materials (ref. 63).

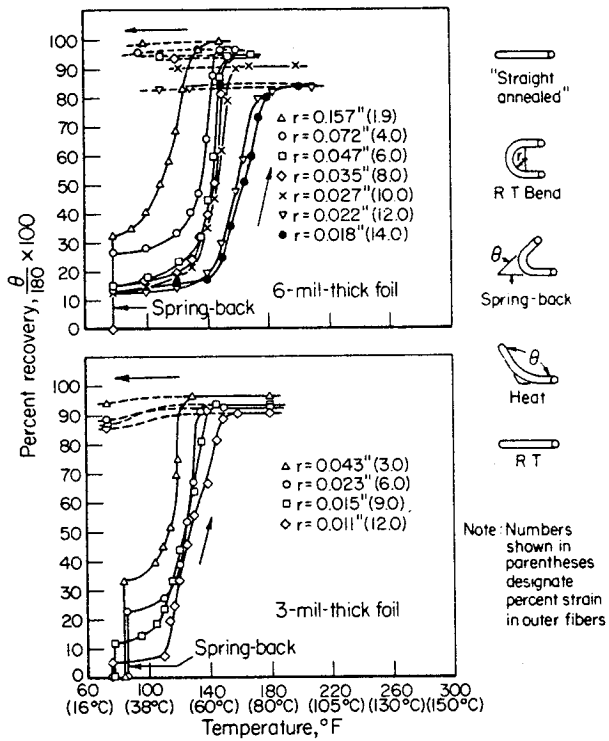


FIGURE 85.—The effect of temperature on the bend-shape recovery of composition-B materials—Concluded.

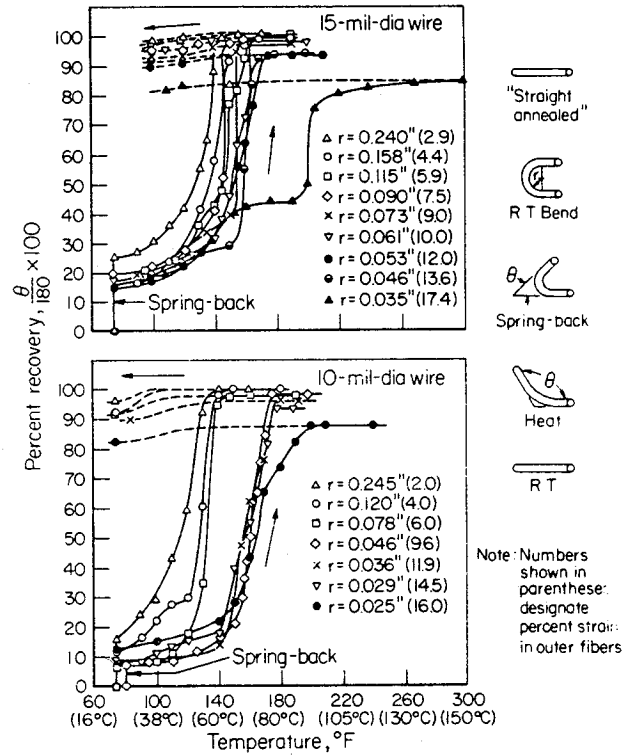


FIGURE 86.—The effect of temperature on the bend-shape recovery of composition-C materials—Continued.

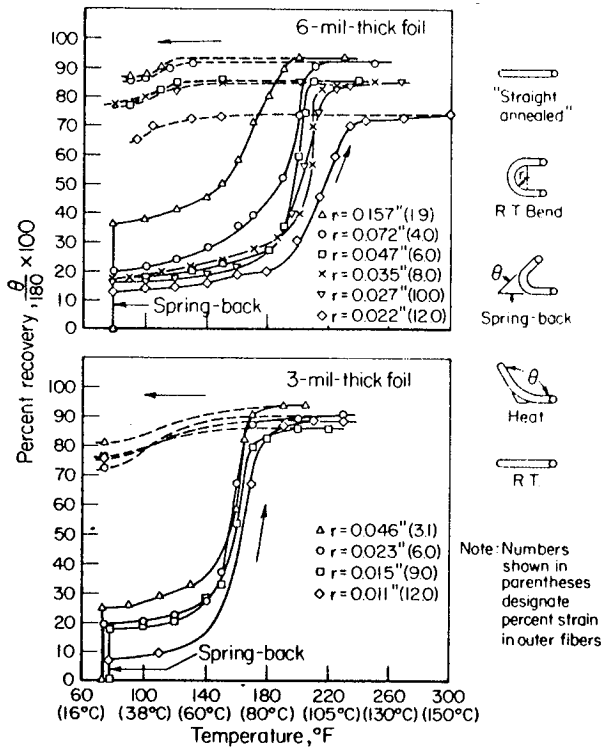


FIGURE 86.—The effect of temperature on the bend-shape recovery of composition-C materials—Concluded.

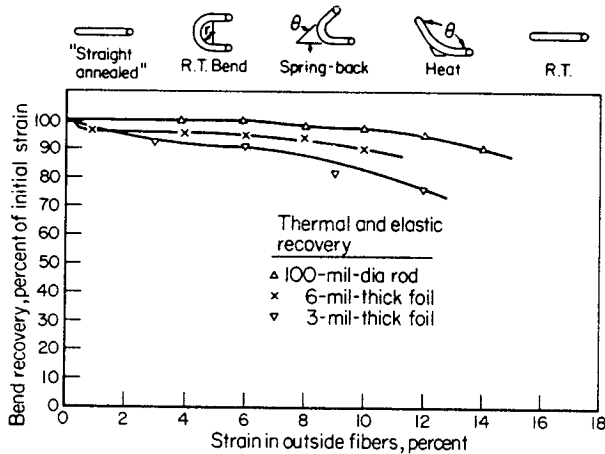


FIGURE 87.—The effect of initial strain on the bend-shape recovery of composition-A materials (ref. 63).

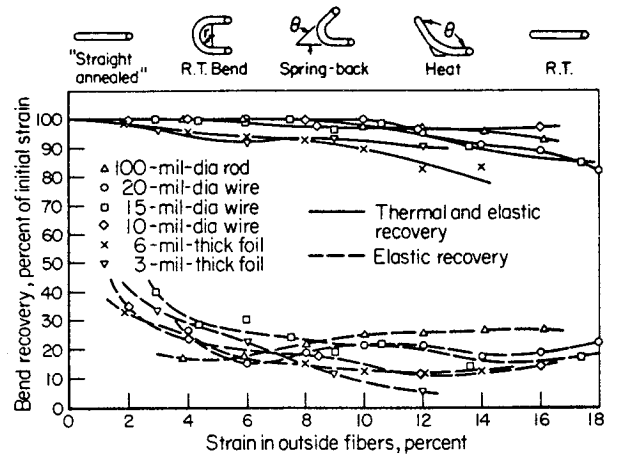


FIGURE 88.—The effect of initial strain on the bend-shape recovery of composition-B materials (ref. 63).

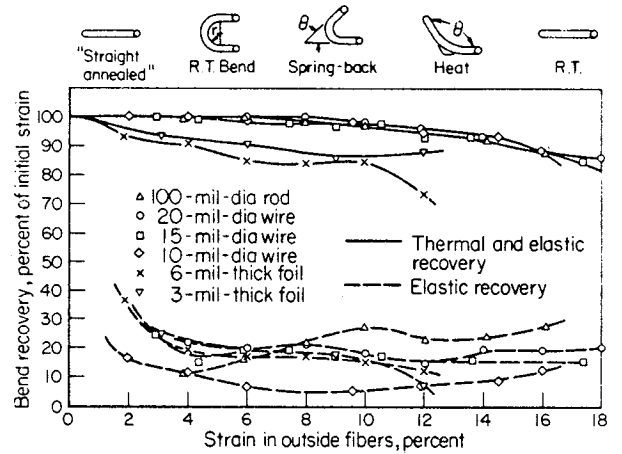


FIGURE 89.—The effect of initial strain on the bend-shape recovery of composition-C materials (ref. 63).

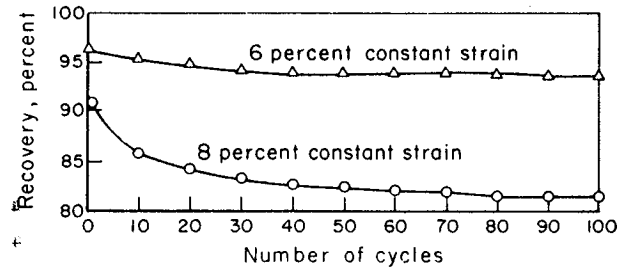


FIGURE 90.—The effect of successive strain-heat-cool cycles on the tensile-shape recovery of 0.020-in.-diameter composition-B wire (ref. 63).

(2) The temperature at which the rate of recovery is a maximum (the nearly vertical part of the curve) increased with increasing amounts of prior strain.

(3) A slight amount of "reversion", i.e., return to the bent shape, occurred in all specimens.

#### *Shape Recovery Fatigue*

Cross et al. also studied the extent to which the shape recovery phenomenon was repeatable (ref. 63). In these experiments, they subjected 0.020-in.-diameter composition *B*\* wire to 100 strain-heat-cool (SHC) cycles. Each SHC cycle consisted of straining the wire in tension by 6 percent of the original gage length, heating the wire to effect shape recovery, and cooling it to room temperature. As may be seen in

figure 90, the first time the wire was heated it recovered about 96 percent of the 6 percent strain. During subsequent SHC cycles, the recovery upon heating decreased slightly. It reached about 94 percent after about 40 cycles and remained essentially constant during the remaining 60 SHC cycles.

A companion specimen was also given 100 SHC cycles, but this time the strain each cycle was 8 percent of the original gage length. The results of these tests, also shown in figure 90, indicate that the use of this higher amount of strain resulted in a much greater decrease in degree of recovery. After 40 cycles, the recovery was down to 83 percent; after 100 cycles, it was 82 percent.

\*The chemical composition is given in table 3.



## Mechanical Properties

Because of the transformations that occur in them, Nitinol alloys undergo unique changes in mechanical properties with temperature. Furthermore, the properties of the alloys are very sensitive to prior processing.

### STRESS-STRAIN CHARACTERISTICS

#### Tensile Properties

While in the early work at NOL (ref. 12) some unusual aspects of Nitinol were noted, the tensile properties were found to be more or less conventional in value. Ultimate tensile strength was between 110 000 and 140 000 psi, yield strength varied with heat treatment and composition between 33 000 and 81 400 psi, and elongation had values of up to 15.5 percent. Somewhat later, it was reported that annealed cold-drawn wire had a tensile strength of 177 000 psi and 25-percent elongation, while cold-drawn wire had a tensile strength of 271 000 psi and an elongation of 6 percent (ref. 68). Considerably later, more attention was paid to the tensile properties and their variation with temperature. A related property, "recovery force," was investigated in 1967 through 1969 (refs. 63 and 67) in projects supported by NASA. Also related to recovery force is the work that Nitinol can do while recovering its prior shape. These topics are covered in a later discussion in this report.

The early interest in NiTi was as an intermetallic compound, although the transformations that occurred in it and caused unusual behavior aroused some interest. Rozner and Waselewski (ref. 19), in a paper submitted for publication in 1965, indicated that the tensile properties were of interest in developing methods for hot working intermetallic compounds. Arc-cast and hot-extruded rods were annealed for 1 hr at 600° C and furnace cooled.

Load-elongation plots were obtained at temperatures from -196° to 700° C on polycrystalline samples at a strain rate of about  $10^{-3}$  in./in./sec. Three distinct temperature ranges within which the behavior was different could be distinguished:

(1) At -196° to +70° C: the stress-strain plots shown in figure 91 are characterized by a well-defined, though rounded, yield point and a small

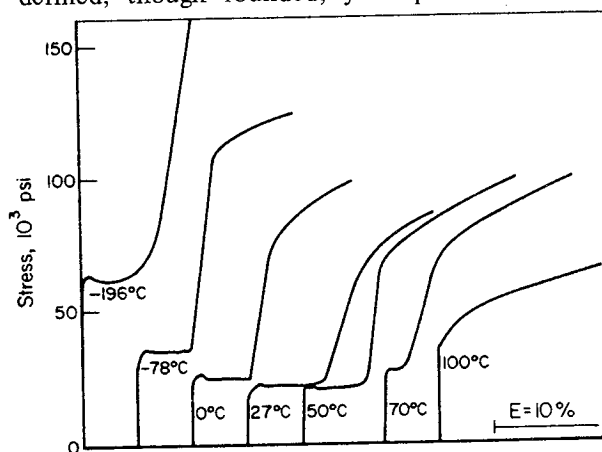


FIGURE 91.—Stress-strain curves for polycrystalline "normalized" NiTi from -196° to +100° C. (Discontinuous yield and large Luders strains are present below the transformation temperature (75° C).

yield drop. Luders strains of 4 to 7 percent took place before strain hardening began, but then the work-hardening rate was exceptionally high. Elongations between 15 and 40 percent were reported. As shown in figure 91, (ref. 19) an abrupt change in yielding behavior occurred between 70° and 100° C. This change was observed in repeated tests. The martensitic transformation in this alloy occurred at 75° C.

(2) At 100° to 400° C: smooth yielding occurred, with a decreasing work-hardening rate with increasing temperature, as shown in figure 92 (ref. 19).

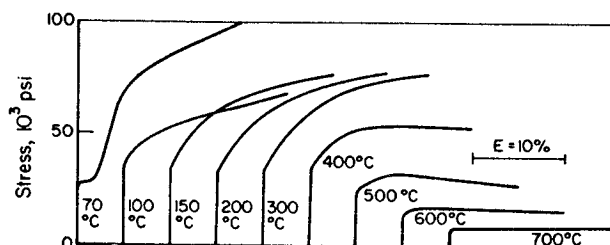


FIGURE 92.—Stress-strain curves for polycrystalline “normalized” NiTi above the transformation temperature.

(3) Above 400° C: the yielding was continuous, with large uniform elongation before fracture.

Figure 93 (ref. 19) shows the yield strength, ultimate tensile stress, and elongation as functions of temperature. Perhaps the most striking characteristic is the temperature-independent behavior of the yield strength between 100° and 400° C, where the yield strength remains at about 35 000 psi.

The upper- and lower-yield stress between -196° and 70° C could be expressed by the exponential relationship

$$\sigma_y = A \exp(-\alpha T),$$

where

$A = 92$ ,  $\alpha = 4.35 \times 10^{-3}$  for the upper-yield stress

$A = 84$ ,  $\alpha = 4.78 \times 10^{-3}$  for the lower-yield stress

$\sigma_y$  = the yield stress, psi  $\times 10^3$

$T$  = absolute temperature, °K.

The true-stress true-strain relationship is plotted in figure 94 (ref. 19), with the strain-hardening exponent  $n$  corresponding to

$$\sigma = \sigma(T) \delta^n,$$

where  $\sigma(T)$  is the flow stress at unit strain at a given temperature  $T$ ;  $\delta = \ln(1 + \Delta l/l)$  is the natural strain;  $\sigma$  is the flow stress at strain  $\delta$ .

Rozner and Buehler (refs. 73 and 88) reported on the effect of cold working on the tensile properties of NiTi. Arc-cast and hot-swaged (at 800° C) specimens were annealed at 800° C for 1 hr and furnace cooled. The cold working was done by swaging, wire drawing, and rolling. The  $M_s$  temperature of this alloy specimen was 70° C; consequently, for ease of cold working, the specimen was soaked in liquid nitrogen prior to deformation, and in the case of wire drawing,

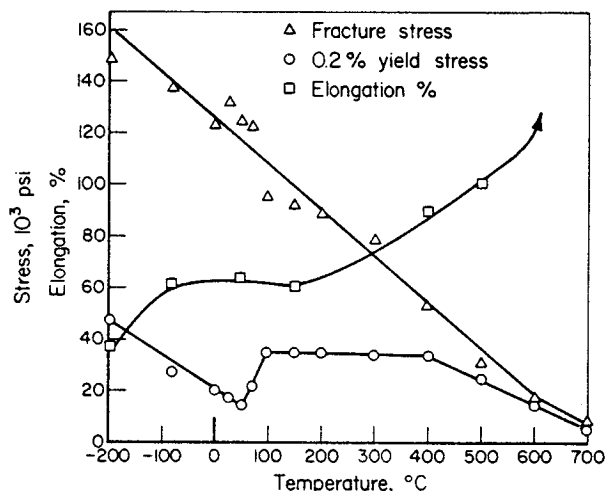


FIGURE 93.—Temperature-dependence of the mechanical properties of polycrystalline “normalized” NiTi between -196° and +700° C.

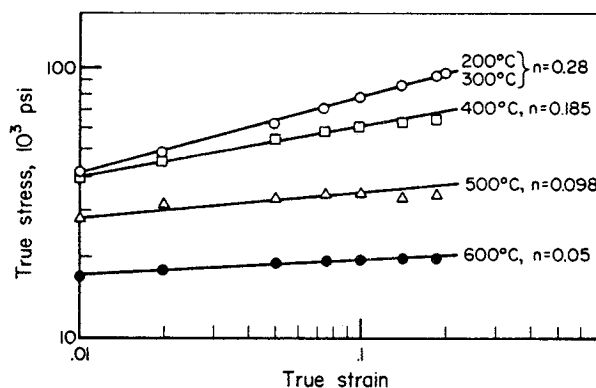


FIGURE 94.—True-stress-natural-strain plots for polycrystalline NiTi.

the dies were chilled in a mixture of dry ice and acetone.

Samples deformed an equivalent amount by swaging, rolling, and wire drawing produced essentially the same results. Load-elongation plots were obtained at room temperature at strain rates of about  $10^{-3}$  in./in./sec. Typical curves of engineering stress vs strain are shown in figure 95 (ref. 73). The annealed specimen had a well-defined yield point and Luders strain of about 7 percent before the onset of strain hardening; the cold-worked material exhibited continuous yielding and nonlinear strain hardening. Elongation was more than 60 percent in the annealed material, 25 percent at 8 percent reduction of area, and 14 to 15 percent for the other specimens.

In figure 96, the tensile properties as a function of the degree of deformation by rolling, drawing, or

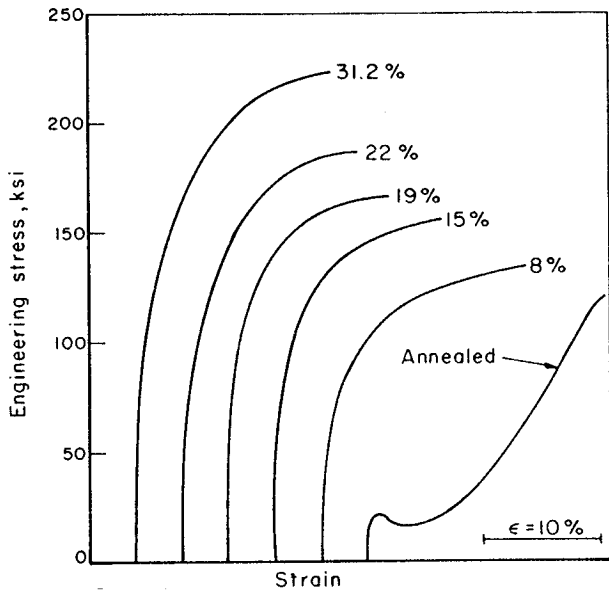


FIGURE 95.—Engineering stress vs strain curves of cold-worked and annealed NiTi.

swaging are presented (ref. 73). The tensile strength data plotted on semilog paper fall on a straight line whose equation is

$$\sigma_u = 120\,000 \exp 1.9r$$

where  $\sigma_u$  is the ultimate tensile strength in psi and  $r$  is the reduction in area by working

$$r = A_i - A_f / A_i$$

$A_i$  and  $A_f$  are, respectively, the initial and final cross-sectional areas of the workpiece.

It is instructive to examine these data from a purely mechanical viewpoint. Thus, if ultimate strength is the maximum load in the tensile test divided by the specimen's cross section, we can visualize a tensile test in which the specimen is loaded to a certain permanent elongation, which can be calculated as a reduction in area on the basis of volume constancy; then the specimen is unloaded. Considering this as a new specimen, and reloading it, the new specimen has a cross-sectional area  $A_2$  which is less than the initial area  $A_1$ . Accordingly, since the maximum load remains the same as if the initial specimen were tested to failure:

$$\sigma_{u1} = L_{\max} / A_1 ; \sigma_{u2} = L_{\max} / A_2$$

or

$$\sigma_{u2} = \sigma_{u1} / (1-r)$$

where

$$r = A_1 - A_2 / A_1$$

Taking the observed value of 125 000 psi as the ultimate tensile strength of the annealed NiTi, the equation for the ultimate strength as a function of area reduction would be

$$\sigma_u = 125\,000 / (1-r)$$

The above equation and Rozner's exponential function are plotted in figure 97 along with the observed values. It is clear that the observed values, except for the 8-percent reduction, are higher than expected from the relationship derived from the tensile-test curve. It is not likely that the discrepancy arises from the mode of deformation, since Rozner indicated that the results obtained from swaging, rolling, and drawing were the same. Furthermore, the deformation was quite uniform in each

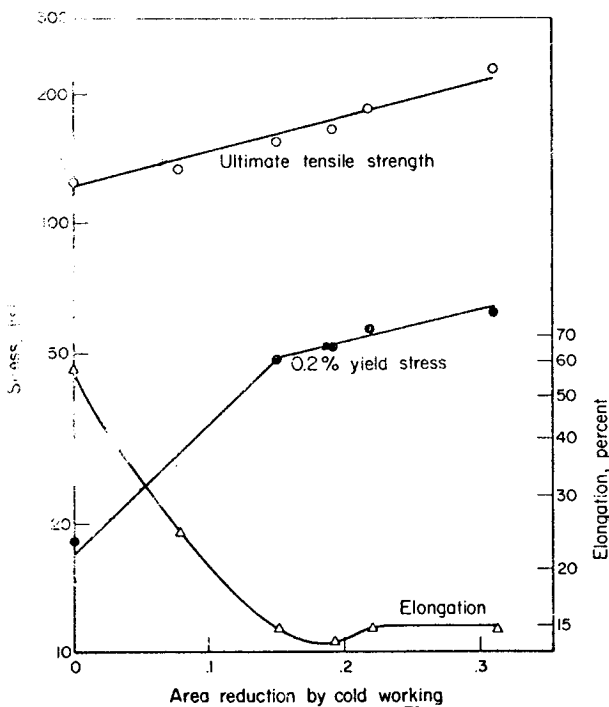


FIGURE 96.—The effect of cold work on yield strength, ultimate tensile strength, and elongation of stoichiometric NiTi.

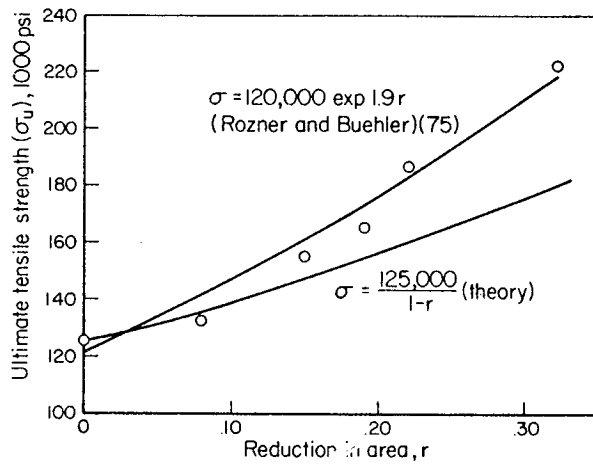


FIGURE 97.—Ultimate tensile strength of 55-Nitinol as a function of degree of deformation, showing theoretical and observed dependency.

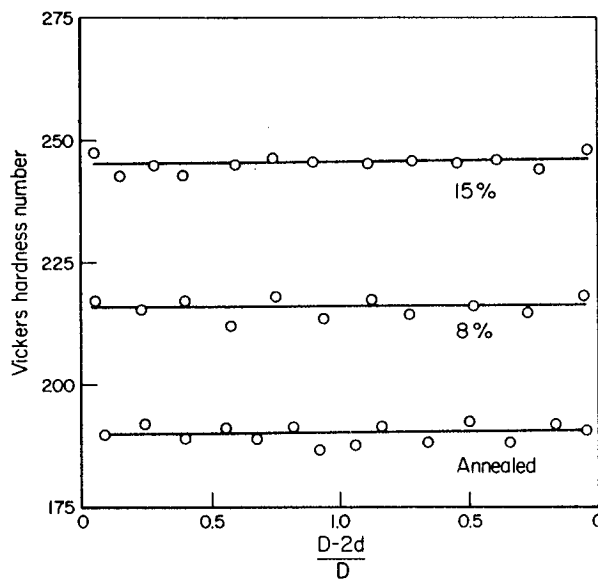


FIGURE 98.—Distribution of microhardness across the section of annealed and cold-worked stoichiometric NiTi rods. ( $D$  = diam of the specimen;  $d$  = distance of the hardness indentation from the center of the specimen.)

case, as illustrated by the microhardness traverses (fig. 98) (ref. 73). It must be concluded, therefore, that the higher ultimate strength was the result of the deformation at cryogenic temperatures, whereas the annealed value and the tensile tests run on all specimens were at room temperature. It is likely that more martensite formed during the low-temperature deformation. This agrees with Rozner and Buehler's

conclusion that stress applied at temperatures below the transition temperature helps to complete the transformation in NiTi alloys (ref. 73).

The yield strength in the Rozner and Buehler papers (refs. 73 and 88) is shown in two distinct ranges, one below 15-percent reduction of area, and one from 15 to 31 percent. The flow stress was determined and expressed in terms of a true-stress true-strain relationship

$$\sigma = \sigma_0 \epsilon^n,$$

where  $\sigma$  = flow stress at a given strain, psi;  $\sigma_0$  = flow stress at unit strain, psi,  $\epsilon = \ln(1 + \Delta l/l)$ ;  $n$  = strain-hardening exponent. These plots are shown in figure 99 (ref. 73). They indicate that the strain-hardening exponent is essentially constant for a given amount of cold work.

Tensile tests were run by Schuerch (ref. 67) on 0.026-in.-diam wire (55.4Ni-44.6Ti-0.07C by weight) that had been vacuum heat treated at 522° C. In these tests, the results of which are shown in figure 100, the specimen was loaded to a certain level, unloaded, and then reloaded. After six such cycles, the material had about 5 percent residual strain. It

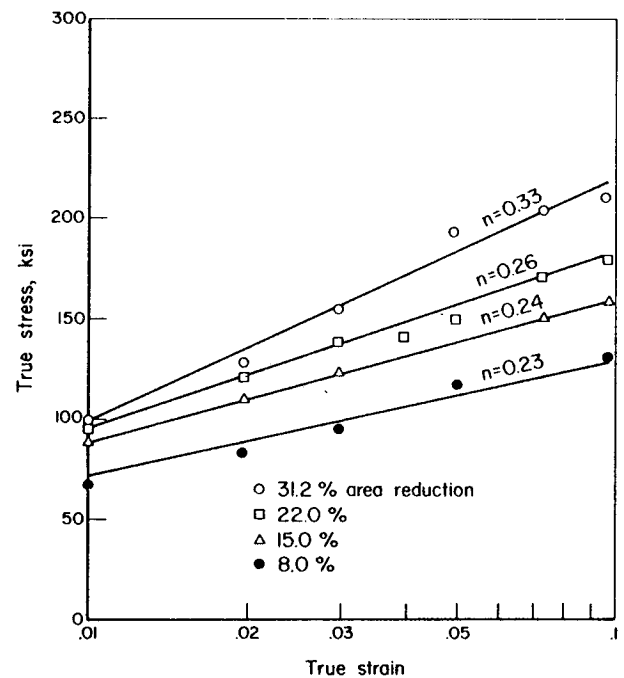


FIGURE 99.—True-stress vs true-strain curves for cold-worked stoichiometric NiTi.

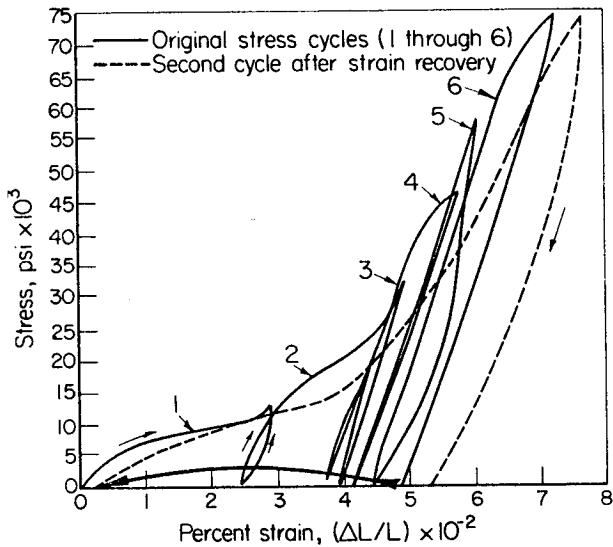


FIGURE 100.—Tensile stress-strain curves for 55-Nitinol containing 44.6 weight % Ti and 0.07 weight % C.

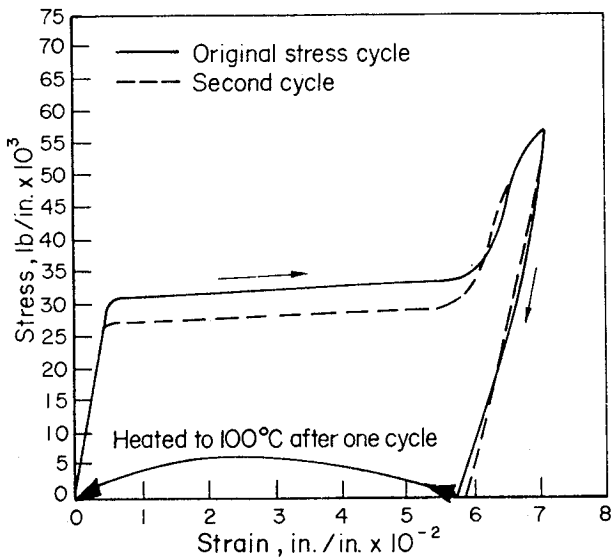


FIGURE 101.—Tensile stress-strain curve for 55-Nitinol containing 44.6 weight % Ti and 0.07 weight % C. (Wire was tested after storage for 1 year.)

was then heated to recover almost all of this strain and retested to the same stress level. As indicated in the figure, the stress-strain curve of the recovered material was almost the same as that of the material loaded and unloaded through six cycles, although it

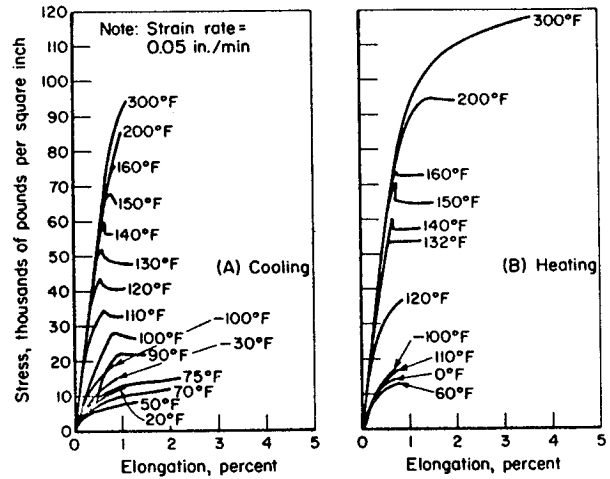


FIGURE 102.—Stress-vs-elongation curves for 0.100-in.-diam composition-B rods during cooling and heating cycles.

was displaced slightly on the strain axis. The same wire was stored for about 12 months under normal laboratory conditions. When retested it was found that the yield strength had increased sharply. This is illustrated in figure 101. It was believed that this increase was caused by small temperature variations of room temperature.

Goodyear's research provided a great deal more information about the tensile properties of Nitinol (refs. 55, 63, and 70). Stress versus-elongation curves were obtained at various temperatures above and below the transformation range. Two typical sets of stress-strain curves are given in figure 102 (ref. 63) for 100-mil-diam wire of composition-B material (55.0Ni, 0.07C, balance Ti;  $M_s$  temperature around 18° C). The "cooling" notation means that the measurements were made when cooling from 149° C; "heating" is the reverse direction. These are not complete curves. They merely show the behavior in the vicinity of the elastic region and yield point. Graphs of the elastic modulus and yield stress from these curves are presented in figure 103 (ref. 63).

In figure 104, the stress-strain behavior of 20-mil wire of composition B is shown, with the same test temperature approached during heating and during cooling as that used for the 100-mil wire. It is clear that the yield behavior changes drastically when the transition temperature is reached. This behavior was found to be typical of all the compositions and forms tested. (See ref. 63.)

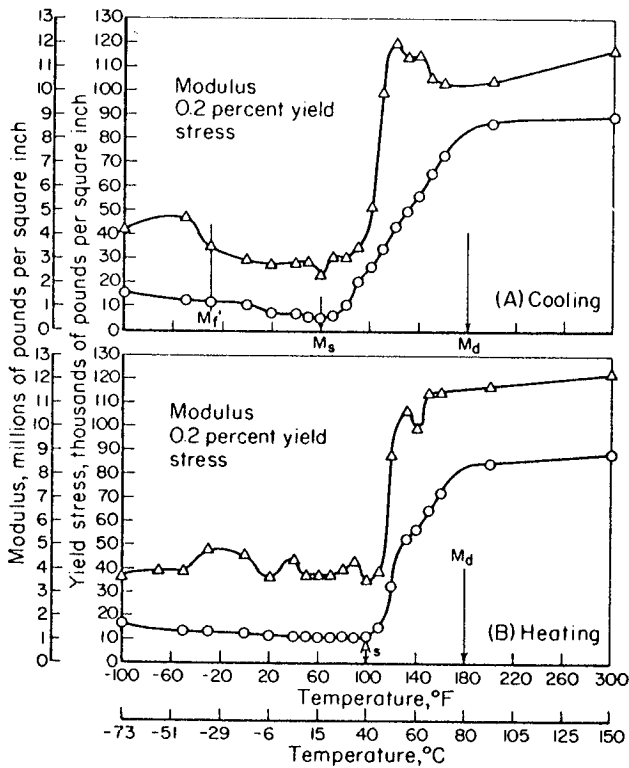


FIGURE 103.—The effect of temperature on the yield stress and modulus of elasticity of 0.100-in.-diam composition-B rods during cooling and heating cycles.

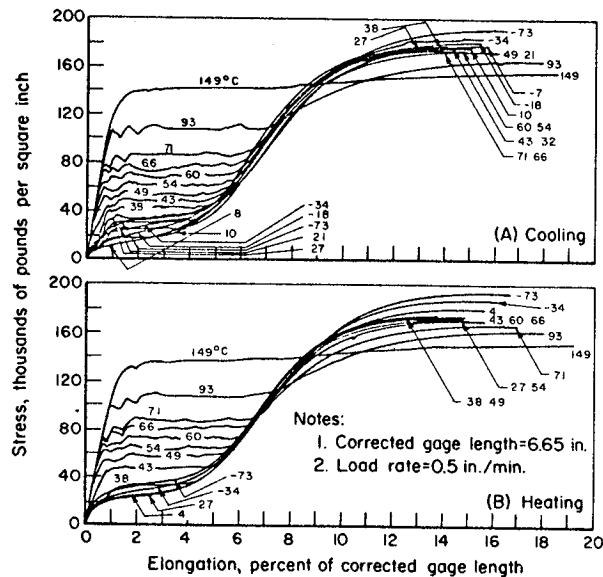


FIGURE 104.—Stress-vs-elongation curves for 0.020-in.-diam composition-B wire during cooling and heating cycles.

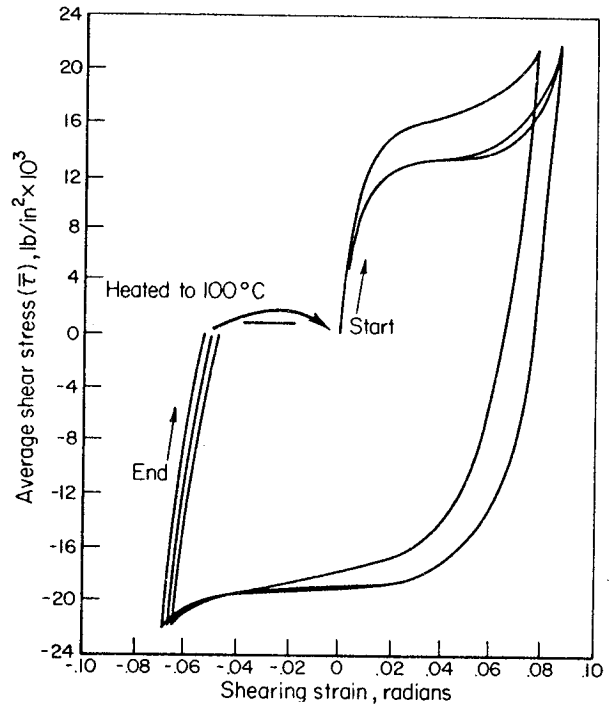


FIGURE 105.—Torsional stress-strain curves for 55-Nitinol containing 44.6 weight % Ti and 0.07 weight % C. (Strain was recovered after each stress cycle.)

*Torsion Properties*

Figures 105 and 106 give the torsional stress-strain curves for 55.4Ni-44.6Ti-0.07C wire obtained in the NASA-Astro research program (ref. 67). In these curves the effective average shear stress was defined as

$$\bar{\tau} = 12M_T/d^3\pi$$

where

$$M_T = \text{applied torque, in.-lb.}$$

$$d = \text{wire diameter,}$$

This equation assumes a fully plastic distribution of uniform circumferential shearing stress throughout the wire cross section. The shearing strain,  $\gamma_{max}$ , at the surface of the wire is defined by

$$\gamma_{max} = \theta \frac{d}{2\ell}$$

where

- $\theta$  = relative angle of rotation at bench-marked sections, rad
- $\ell$  = length of the test specimen between bench marks, in.

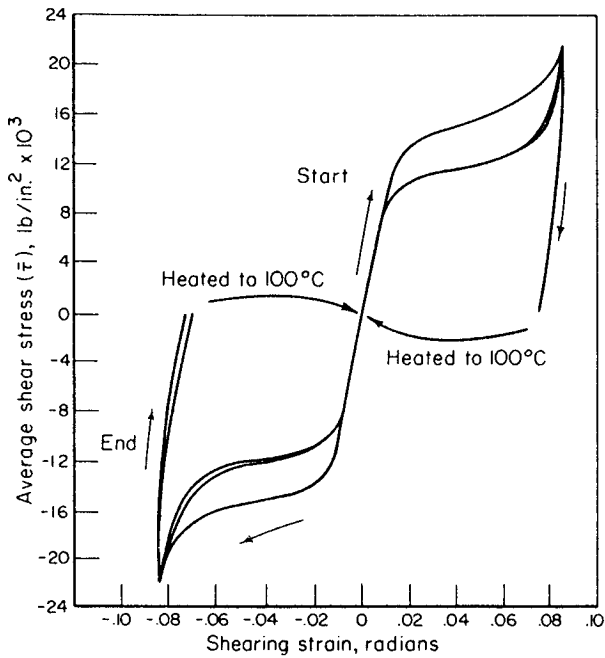


FIGURE 106.—Torsional stress-strain curves for 55-Nitinol containing 44.6 weight % Ti and 0.07 weight % C. (Strain was recovered before each stress reversal.)

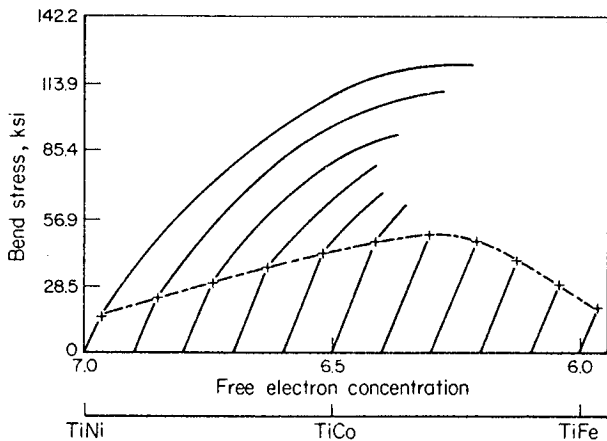


FIGURE 107.—Bend stress-strain curves on the Ti-Ni-Co and Ti-Co-Fe ternary alloys with the CsCl-type structure (ref. 89). (The measurements were made at room temperature on a Baldwin Universal Tester, using 0.64 cm/min loading rate. All samples were in the arc-cast condition and given a stress-relief anneal at 800° C for 1 hr prior to testing.)

Figure 105 contains the data obtained by applying the load, reversing it, and returning to zero load. The residual strain was then recovered by heating the specimen to 100° C. In figure 106, the residual strain

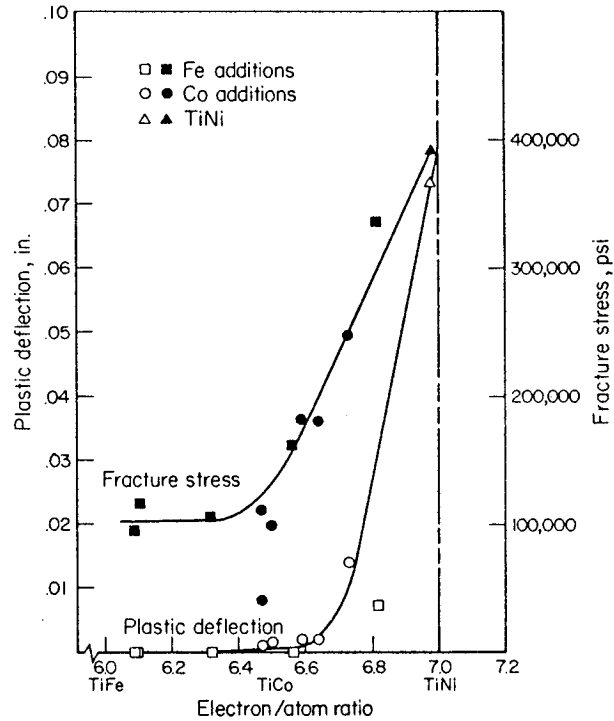


FIGURE 108.—The effect of electron/atom ratio on the plastic-beam deflection and fracture stress of TiX compounds (ref. 90).

was returned to zero in each half cycle by heating the specimen to 100° C.

**Bending Properties**

Wang has investigated the bending properties of NiTi in connection with a general study of the ductilities of TiFe, TiCo, and NiTi (refs. 89 and 90). He presented a correlation of the bending fracture stress and ductility with the electron/atom ratio of these compounds (figs. 107 and 108). The results obtained were qualitatively similar, showing greater ductility in NiTi than in the other compounds. However, the fracture stress in one case was about 400 000 psi, and in the other, about 120 000 psi. The difference might be the result of either composition, treatment, bending rate, or other variables.

**THERMOMECHANICAL RECOVERY FORCE AND WORK**

**Recovery Force**

In the section dealing with shape recovery and thermal expansion effects, we discussed the shape

changes that occur when Nitinol is heated while it is under a sustained load.

In Goodyear's NASA research program, there was a need to gain a better understanding of the forces associated with the shape recovery process (ref. 63). Accordingly, each specimen was elongated a predetermined amount by loading it in tension. Each wire specimen was then heated, and the force required to prevent recovery was recorded as a function of temperature. Tensile-"recovery"-stress curves for the 100-mil-diam composition-B wire are given in figure 109. They show the stress exerted as the wire attempts to return to its original length after being strained to the extent indicated. These curves are typical of all three alloys investigated. Characteristically the return (cooling) curve showed some hysteresis. The maximum recovery stress increased with increasing strain up to a maximum of about 8 percent. Also, the "transition"-temperature range (defined here as the temperature range over which the stress rises rapidly) increased with increasing amounts of prior strain. Figures 110, 111, and 112 summarize the maximum recovery stress as a function of initial strain for the various compositions, sizes, and forms of Nitinol. The chemical compositions of the three alloys were given in table 3.

Beuhning, Jackson, and Wagner examined the shape of the recovery-stress-vs-temperature curve during both heating and cooling (ref. 64). The test specimens were 0.089-in.-diameter wire (45.9 weight percent

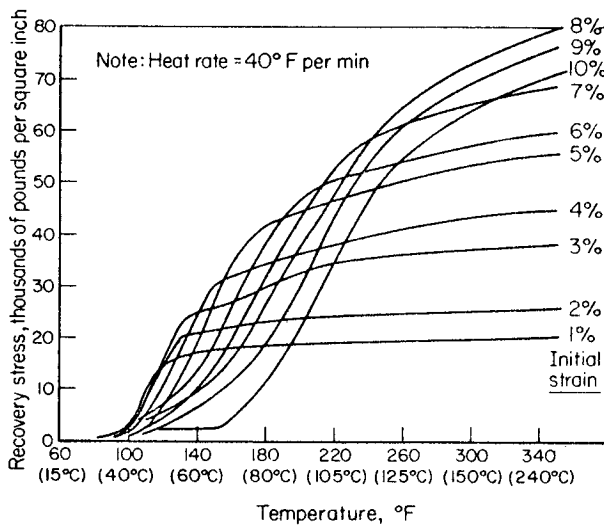


FIGURE 109.—Tensile-recovery-stress-vs-temperature curves for J.100-in.-diam composition-B rods at various strain levels.

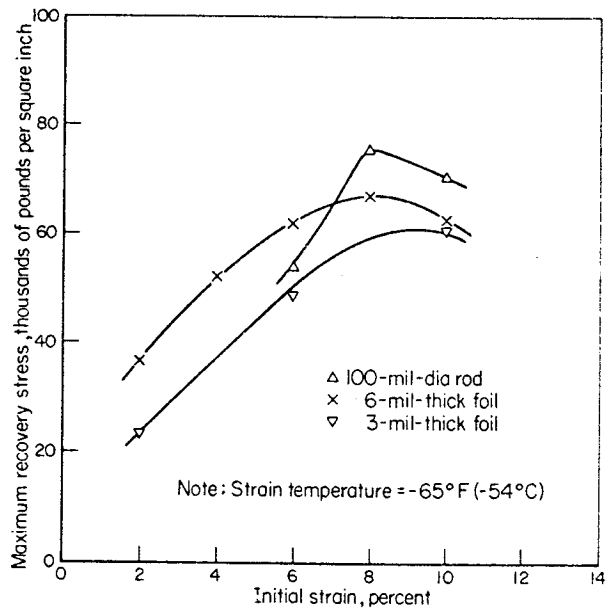


FIGURE 110.—The relationship between maximum recovery stress and initial strain for composition-A materials.

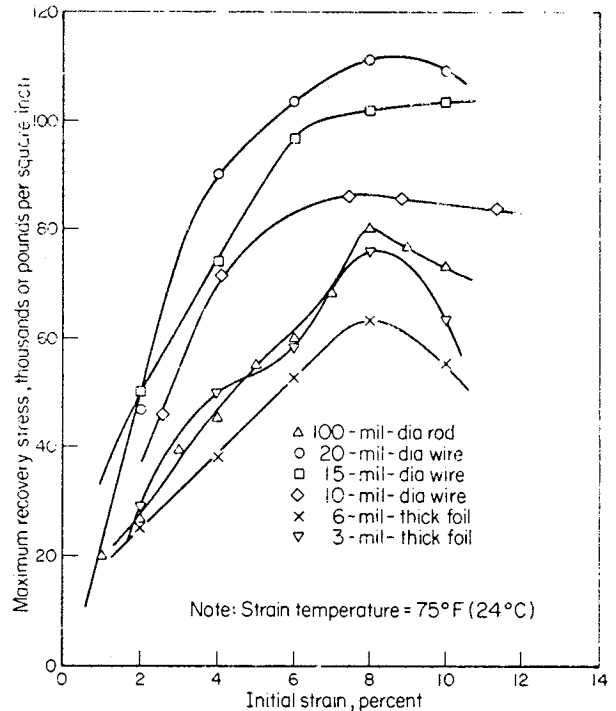


FIGURE 111.—The relationship between maximum recovery stress and initial strain for composition-B materials.

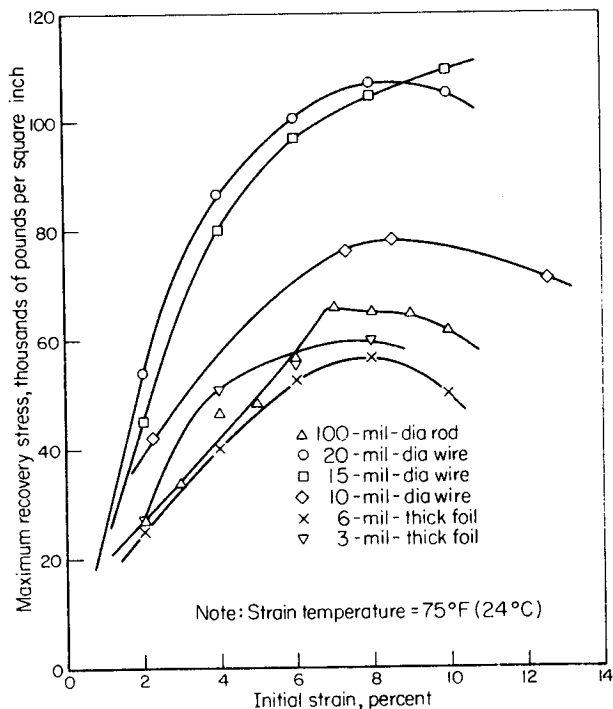


FIGURE 112.—The relationship between maximum recovery stress and initial strain for composition-C materials.

Ti), which had been heat treated for memory at 930° F for 20 min while under a tension of 5 lb. The specimens were then given “stabilization” treatments consisting of SHC cycles. These SHC cycles were carried out according to the following schedule:

(1) Strain in tension an amount equal to 6 percent of the original gage length, release the load, and remove the specimen.

(2) Heat above the transition-temperature range of the alloy, i.e., to about 205° C.

(3) Cool to room temperature.

Recovery-stress-vs-temperature curves were determined for specimens of the material that had been given selected numbers of SHC cycles. The experimental procedure consisted of straining a wire specimen by 6 percent in tension and then heating it while constraining it to prevent shape recovery. The force required to prevent recovery was recorded as a function of temperature. It was found that material given 5 SHC cycles had reproducible recovery-stress-vs-temperature curves. A typical curve is given in figure 113 (ref. 64).

Early exploratory work at NOL on the phenomenon of recovery stress revealed that significant stresses could be generated even when the

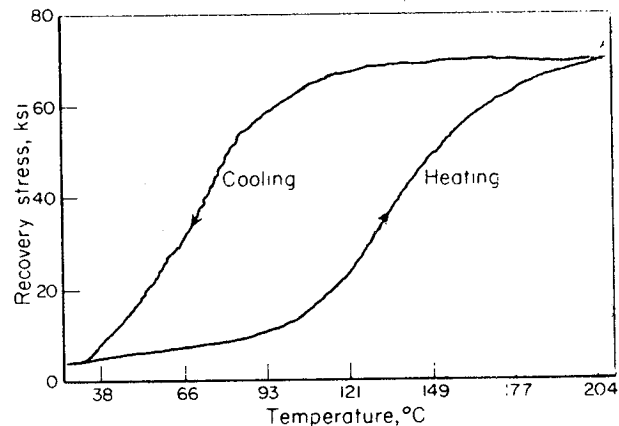


FIGURE 113.—Typical recovery-force curve of “stabilized” and strained 55-Nitinol (45.9 weight % Ti).

memory-annealing temperature was not optimum (ref. 69). In this work, wire was drawn to 0.020-in. diameter and annealed at 800° C, which is now considered to be about 300° C higher than optimum. After the annealing, the wire was reduced various amounts by drawing to diameters as small as 0.012 in. The wire was gripped in a tensile machine, and the load recorded as separate wire samples were heated electrically to different temperatures. After the test temperature was reached, the current was turned off, and the wire specimen returned to room temperature quickly. The maximum stress increased with test temperature up to about 220° C where it reached values in the neighborhood of 50 000 psi; between 220° and 320° C (the highest temperature examined) the maximum stress increased only slightly.

A residual stress was exerted by the wire after cooling to room temperature. An important observation is that, for severely drawn wire, the stress reached by heating was maintained to a much higher degree at room temperature than it was for lightly drawn wire.

#### Work

The ability of Nitinol to do work while being restored to its memory shape is of great practical significance. Essentially, Nitinol acts as a transducer, converting thermal energy or electrical energy to mechanical energy. For example, Nitinol is the basis of a method patented by Buehler and Goldstein for converting heat energy to mechanical energy (ref. 91). Figure 114, taken from the patent, illustrates the principle. A strip of Nitinol is deflected at room

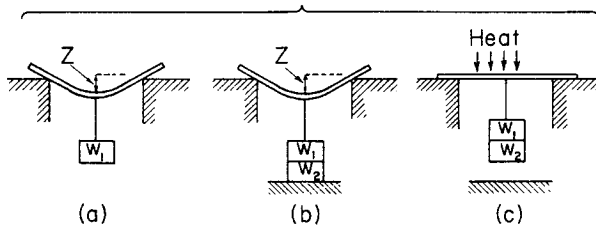


FIGURE 114.—Schematic diagram illustrating the conversion of heat energy to mechanical energy using 55-Nitinol.

temperature by an amount  $Z$  by a weight  $W_1$ . A second weight  $W_2$  is added while the deflection  $Z$  is maintained constant. When the Nitinol is heated through its transition-temperature range, the Nitinol returns to its approximately zero-deflection position. The amount of useful work performed ( $W_1Z + W_2Z$ ) is greater than the work expended ( $W_1Z$ ) in producing the deformation, and thus the Nitinol bar converts heat energy to mechanical energy.

The work capacity of Nitinol was measured in the NASA-Goodyear research program in terms of the ability of the wire to lift a weight a certain height when the wire was heated (ref. 63). The experimental technique involved hanging a weight on the Nitinol wire (or using a pneumatic actuator), thus stretching the wire by an amount depending on the weight, and then heating the wire with the weight attached. The recovered strain was measured as a function of temperature for both the heating and cooling cycles.

Mechanical work was calculated by the following equation (ref. 70):

$$W = \frac{F \Delta \ell}{A \ell}$$

where

$W$  = mechanical work, in.-lb/in<sup>3</sup>

$F$  = weight applied to specimen, lb

$\Delta \ell$  = change in length of a certain gage length, in.

$\ell$  = gage length, in.

$A$  = cross sectional area of the specimen, in<sup>2</sup>

Figures 115, 116, and 117 illustrate the behavior of the various compositions for 100-mil wire strained by different amounts (ref. 63). Notice that, on the cooling cycle, the work drops to zero abruptly. This is because, when the specimen was cooled under load, it would elongate plastically under load beyond the starting length if a stop were not provided; that is, the weight would have done work on the specimen. The

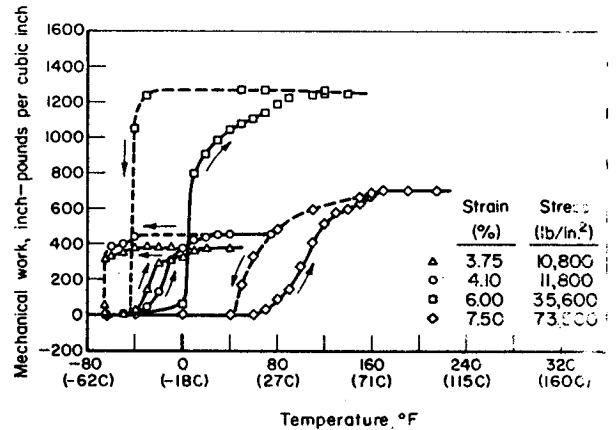


FIGURE 115.—Mechanical-work vs temperature curves for 0.100-in.-diameter composition-A rods.

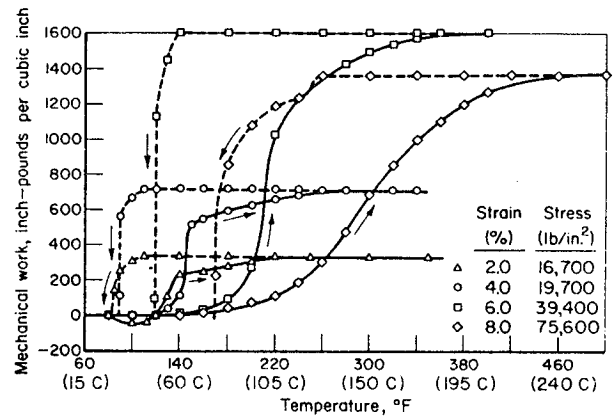


FIGURE 116.—Mechanical-work vs temperature curves for 0.100-in.-diameter composition-B rods.

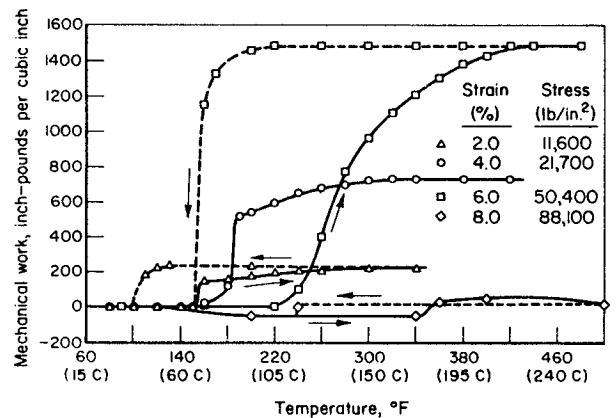


FIGURE 117.—Mechanical-work vs temperature curves for 0.100-in.-diameter composition-C rods.

maximum mechanical work output was observed at about the 7-percent strain level. This behavior is seen more clearly in figures 118, 119, and 120 (ref. 63), which summarize the data for all forms, sizes, and compositions. A great deal of difference was found among the test materials; the maximum work output was seen in the 20-mil composition-C wire. Foils were capable of the least amount of work, perhaps because of the manner in which they were processed rather than the inherent characteristic of the specimen's shape.

In another study, Marks of Harry Diamond Laboratories investigated the efficiency of converting electrical energy (ref. 92). A dc source was used to heat the Nitinol wire. The electrical energy input was the product of voltage by current by time. The mechanical work done was the product of the weight by displaced height. Drawn wire of unspecified chemical composition was reduced in area by 20 to 24 percent before it was given the memory-annealing treatment of 500° to 530° C for 3 min. The transition-temperature range was 54° to 64° C. In this experiment, the weight was attached to the wire and remained

attached during the entire heating and cooling cycle. Figure 121 shows the efficiency for repeated trials. Various voltages were used for 20-mil and 25-mil wire. In general, preliminary results indicated that 6 volts produced better results than 1.5 or 3 volts, probably reflecting the efficiency of heating rather than the transformation efficiency.

The effect of strain on efficiency is shown in figure 122. At 6-percent strain the efficiency was highest. In this particular test, the samples that were strained 7 and 8 percent failed to recover more than 3- to 5-percent strain. Under some conditions, the efficiency was about 25 percent, and values of 15 to 20 percent were quite frequently observed.

A variation of the energy conversion experiments was reported by Scheurch (ref. 67). In these experiments, a 13.3-in.-long Nitinol wire measuring 0.026 in. in diam was first loaded with 30 lb at room temperature and heated above the transition-temperature range. After the wire had contracted, the load was reduced to 10 lb causing some additional strain recovery at constant temperature. Then the wire was cooled to room temperature. As the temperature

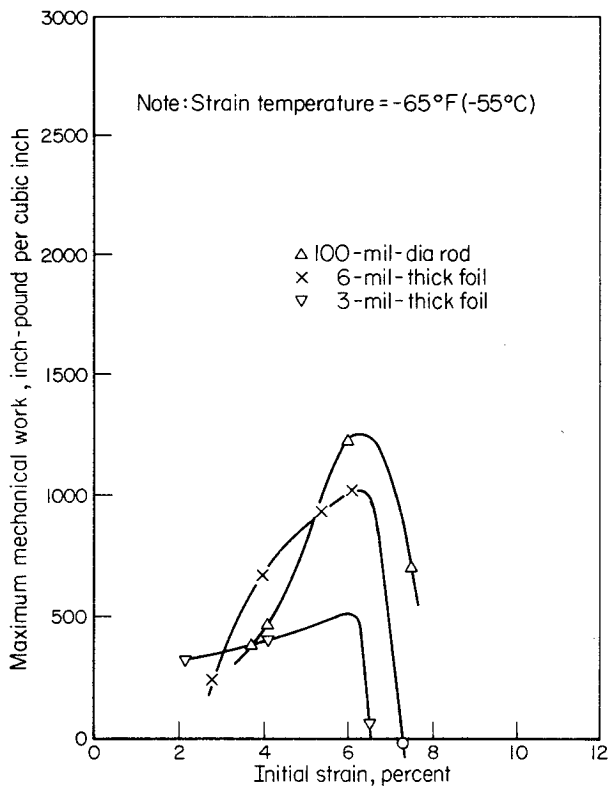


FIGURE 118.—The effect of initial strain on the maximum mechanical work for composition-A materials.

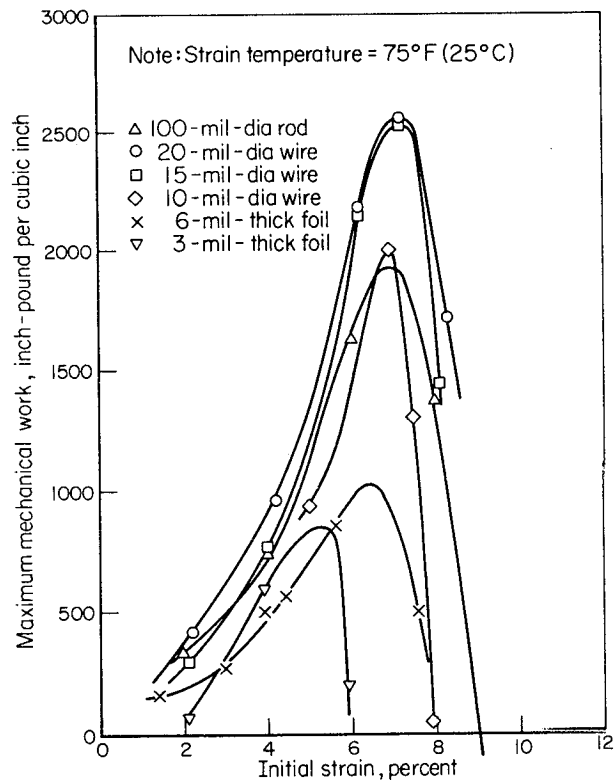


FIGURE 119.—The effect of initial strain on the maximum mechanical work for composition-B materials.

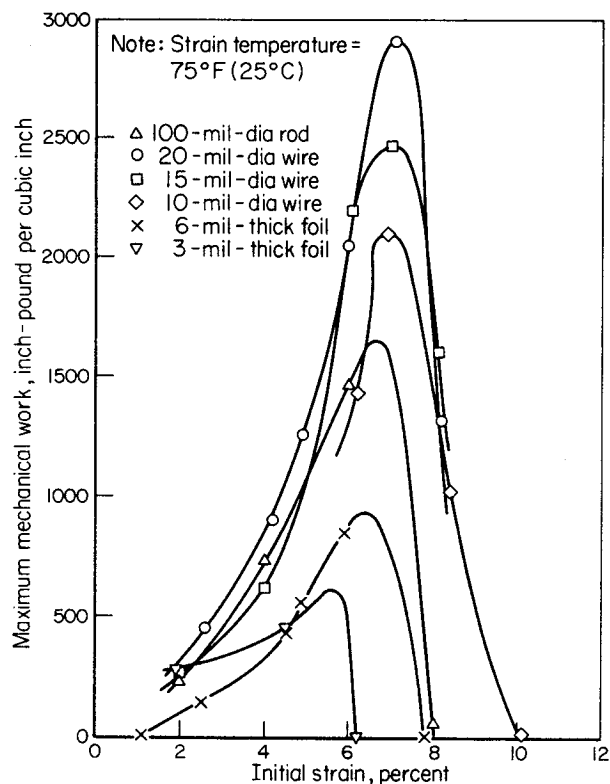


FIGURE 120.—The effect of initial strain on the maximum mechanical work for composition-C materials.

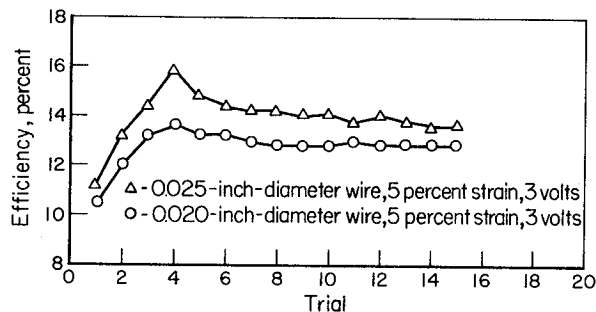


FIGURE 121.—The variation of the efficiency of 55-Nitinol during repeated trials. (The chemical composition of the alloy was not given. Efficiency was defined as the ratio of the mechanical energy expended by a Nitinol wire in lifting a weight half the distance that the wire was originally strained to the electrical energy put into the wire while the weight was lifted this distance.)

passed through the 40° C region, elongation at constant stress occurred. Finally, the 30-lb preload was restored, and the wire was brought back to its original condition of load and elongation. Figure 123 (ref. 67) shows the load-elongation-temperature behavior for two duplicate runs. Because of the lower

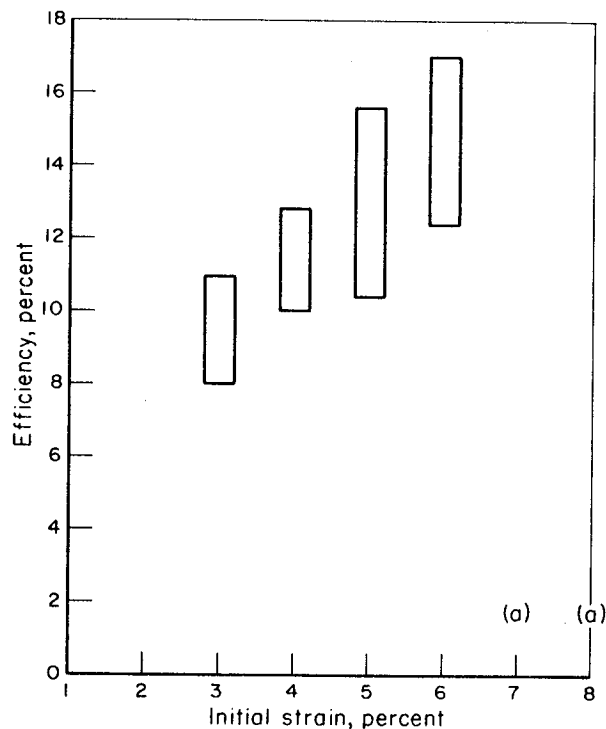


FIGURE 122.—The effect of initial strain on the efficiency of 55-Nitinol. (The chemical composition of the alloy was not given. Efficiency was defined as the ratio of the mechanical energy expended by a Nitinol wire in lifting a weight half the distance that the wire was originally strained to the electrical energy put into the wire while the weight was lifted this distance.)

load during cooling, the wire did not stretch beyond the zero point; that is, no negative work, such as that occurring in the Goodyear experiments, was done. For the two runs, the work done was reported to be 11.0 and 10.8 in.-lb. By converting these results to the same units as those used by Goodyear, the following expression can be derived:

$$\frac{11.0 \text{ in.-lb}}{13.3 \text{ in.} \times \frac{\pi}{4} (0.026)^2 \text{ in}^2} = 1560 \text{ in.-lb/in}^3$$

Considering the differences in the experiment, and the differences in the wire used, the work done is remarkably close to that found in the Goodyear experiments for 0.020-in. wire strained 6 percent, which was a maximum of about 2000 in.-lb/in<sup>3</sup> for the composition-B and -C materials.

## HARDNESS

A test for hardness has always been one of the first

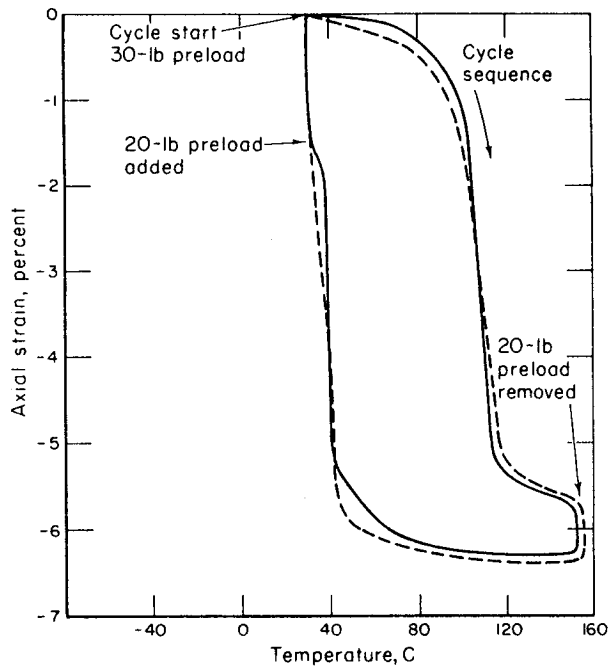


FIGURE 123.—Temperature-elongation relationship for discontinuously loaded 55-Nitinol containing 44.6 weight % Ti and 0.07 weight % C.

tests made on new materials. Such tests provide a simple way of assessing the strength of a material. The hardness of Nitinol was covered in detail in the early reports on NiTi (refs. 11 and 74). Hardness measurements in Buehler and Wiley's first report for NOL were made at temperatures ranging from  $-75^{\circ}$  to  $+982^{\circ}$  C for various compositions. At room temperature the following hardnesses were obtained for an arc-cast 55.1 weight percent Ni composition:

Condition	Hardness, $R_C$
Arc-cast	30-31
Hot-rolled from $600^{\circ}$ C, rapidly cooled	38
Hot-rolled from $700^{\circ}$ C, rapidly cooled	38
Hot-rolled from $950^{\circ}$ C, rapidly cooled	32-34
Hot-rolled from $1000^{\circ}$ C, rapidly cooled	39
Hot-rolled from $1100^{\circ}$ C, rapidly cooled	39-41

The hardness as a function of composition and cooling rate from high temperature is shown in figure 124. These variations in hardness were attributed to the presence of varying amounts of  $Ni_3Ti$  in the NiTi matrix. Additional data for the 54.5 weight percent Ni composition are given in figures 125 and 126. The graph of figure 125 shows how hardness is affected

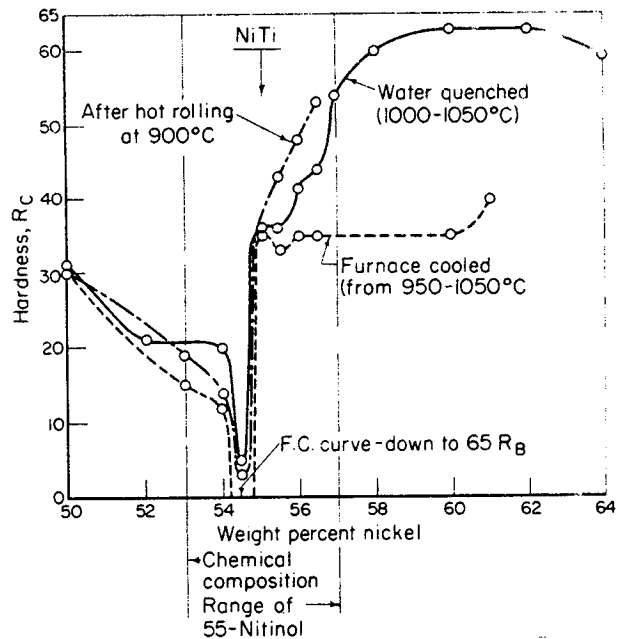


FIGURE 124.—The effect of chemical composition and heat treatment on the hardness of NiTi alloys (ref. 74).

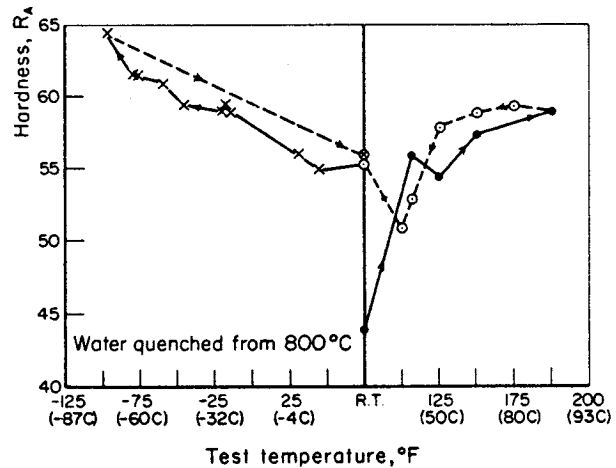
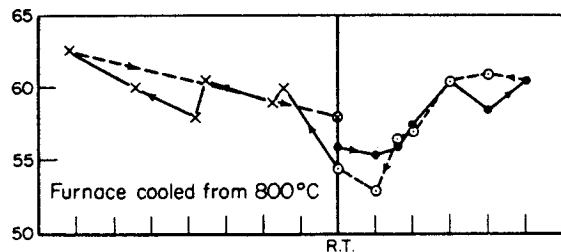


FIGURE 125.—The effect of temperature on the hardness of NiTi (54.5 weight % Ni) cooled from  $800^{\circ}$  C at two different rates (ref. 74).

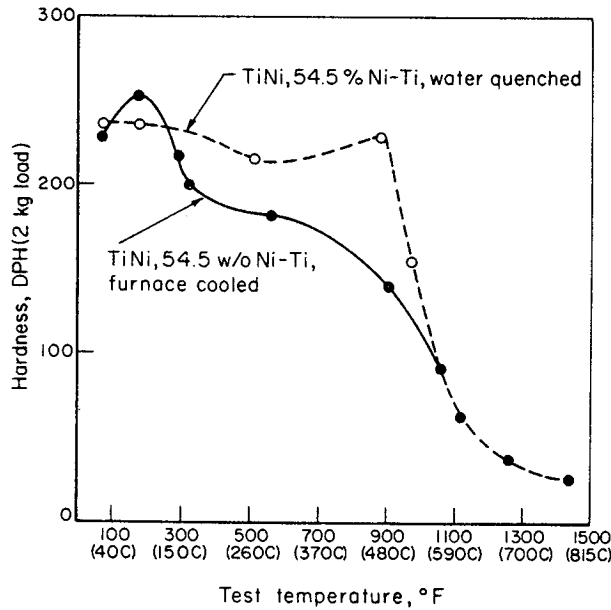


FIGURE 126.—Effect of temperature on the hardness of NiTi (54.5 weight % Ni) cooled from 800° C at two different rates (ref. 74).

by temperature and cooling rate, and also suggests that some hysteresis has occurred. Figure 126 illustrates how cooling rate influenced the hardness of the 54.5 weight percent Ni alloy at elevated temperatures, and figure 127 contains similar data for the 55.1 weight percent Ni composition. The microhardness of annealed and worked rod of the 55.1 percent Ni alloy was shown in figure 98 (ref. 73).

#### EFFECTS OF ALLOYING

Efforts have been made to increase the strength of NiTi alloys by introducing a third substitutional-type element into the binary system. Alloys were prepared by arc casting and hot working at 900° C (ref. 93). The alloying additions were made to the 55.1 weight percent Ni base. Figures 128 through 130 give the room-temperature hardness of the alloys prepared; it can be seen that chromium, aluminum, and iron had the greatest effect on the hardness, each producing over 300 DPH ( $\sim R_C$  30) with a 2 weight percent addition. No information was reported on the influence of alloying additions on memory properties.

Hot hardness was also of interest as an indication of high-temperature strength. The data are summarized in figures 131 through 136 (ref. 93). The Nitinol control alloy is shown in the top graph in figure

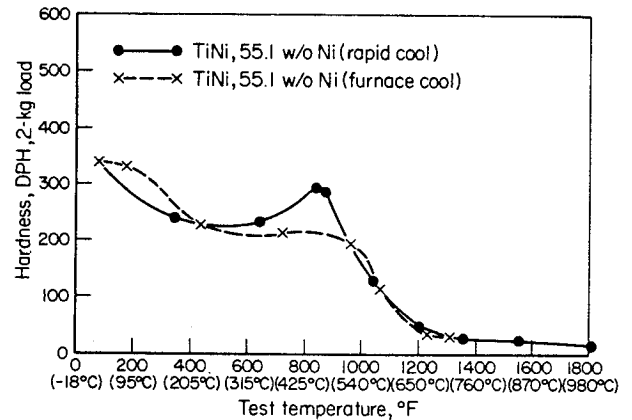


FIGURE 127.—The effect of temperature on the hardness of NiTi (55.1 weight % Ni) cooled from 800° C at two different rates (ref. 74).

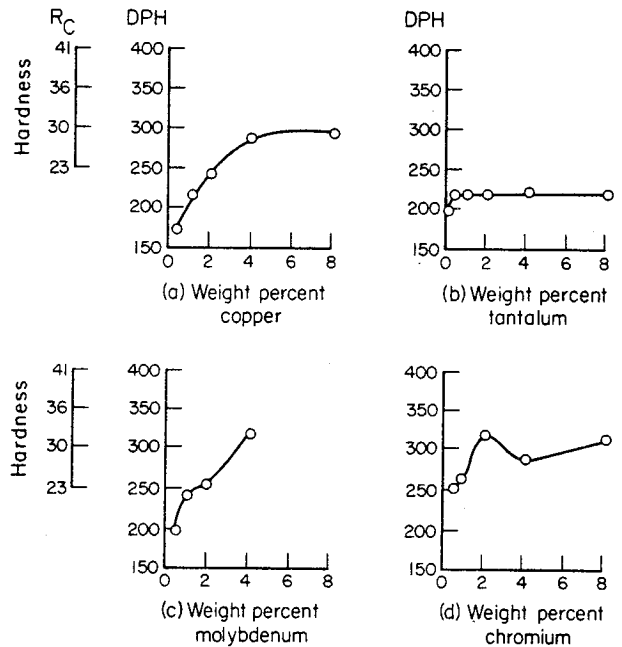


FIGURE 128.—The effect of chemical composition on the hardness of Nitinol alloys at room temperature. (Base alloy contained 55.1 weight % Ni. Specimens were tested in the hot-wrought condition.)

131, and the triangular point from this graph is reproduced for comparison in the other figures. In general, it appears that the alloys are limited to service below 538° C.

The effects of the interstitials oxygen, nitrogen, and hydrogen have also been investigated by NOL (ref. 26). Arc-melted buttons of the NiTi composition

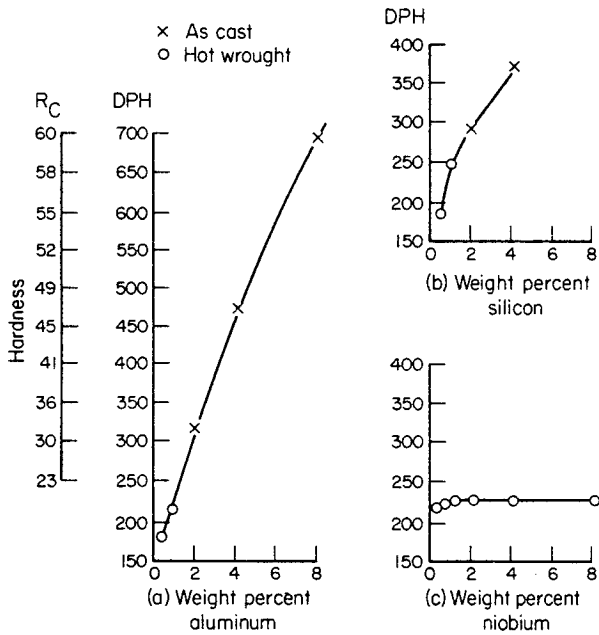


FIGURE 129.—The effect of chemical composition on the hardness of Nitinol alloys at room temperature. (Base alloy contained 55.1 weight % Ni. Data points indicated by “o” refer to tests on hot wrought alloys. Data points indicated by “x” refer to tests on as-cast alloys.)

were prepared in an argon atmosphere and then remelted in the presence of about 0.06 atmosphere of either O<sub>2</sub>, N<sub>2</sub>, or H<sub>2</sub>. Microhardness measurements were made on the matrix and on the secondary phase particles of all samples. The data are given in table 9.

Hot-working trials on these materials indicated that the nitrogen-containing alloy was ductile even though the matrix had a relatively high hardness. On the other hand, the oxygen-containing specimen was reported to have cracked severely when rolling at 900° C was attempted.

In a paper by Wang, it was indicated that the absorption of 150 ppm of hydrogen in NiTi strip

TABLE 9.—Microhardness Data on NiTi With Controlled Interstitial Contaminants.

Melting atmosphere	Knopp microhardness, 50-g load*	
	Matrix	Secondary phases
Argon	211	211
Hydrogen	226	226
Nitrogen	351	635
Oxygen	520	790

\*Average of 5 to 10 measurements.

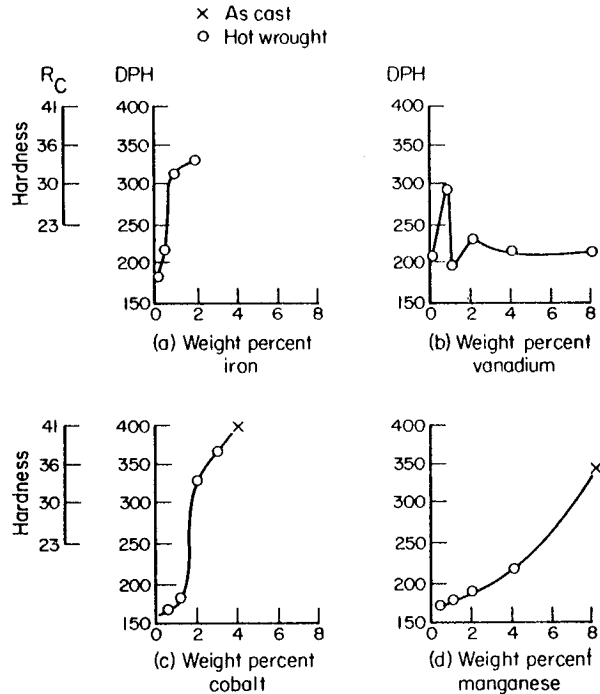


FIGURE 130.—The effect of chemical composition on the hardness of Nitinol alloys at room temperature. (Base alloy contained 55.1 weight % Ni. Except for the two data points marked with an “x”, specimens were tested in the hot-wrought condition. Specimens designated by x were tested in the as-cast condition.)

lowered the hardness from 43.5 to 41.0 R<sub>A</sub>, (ref. 89). Wang related the drop to an increase in free electron concentration, and compared the hardness vs electron concentration of other intermetallic compounds with titanium. This comparison is shown in figure 137.

IMPACT TOUGHNESS

Table 10 shows the Charpy-unnotched impact strength for undersized specimens of 54.5 and 55.1 weight percent Ni alloy (ref. 12). The impact strength of notched and unnotched standard-sized bars is shown in table 11 (ref. 94). It is evident that the alloy displays some notch sensitivity below the transition-temperature range. No data were found for impact properties above the transition-temperature range.

FATIGUE STRENGTH

Very few data are available on the fatigue strength of 55-Nitinol. Buehler (ref. 68) reported the results of a standard R. R. Moore rotating-beam fatigue test on

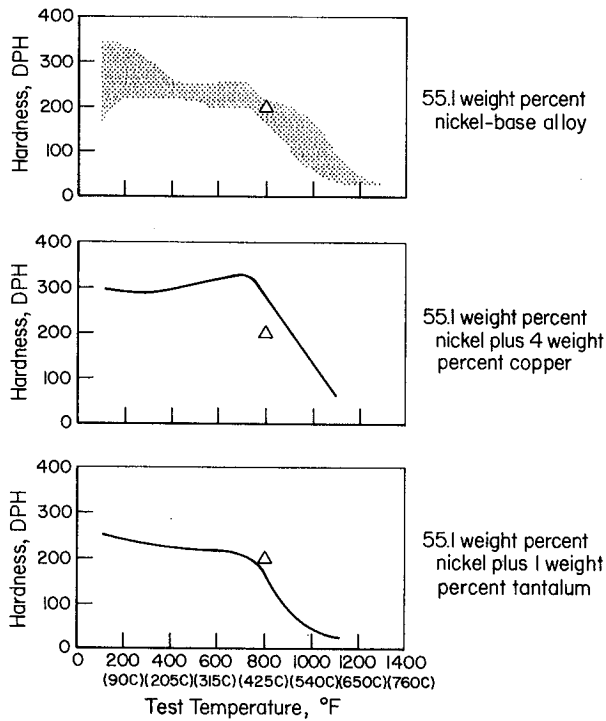


FIGURE 131.—The effect of temperature on the hardness of 55-Nitinol (55.1 weight % Ni) containing selected alloying additions.

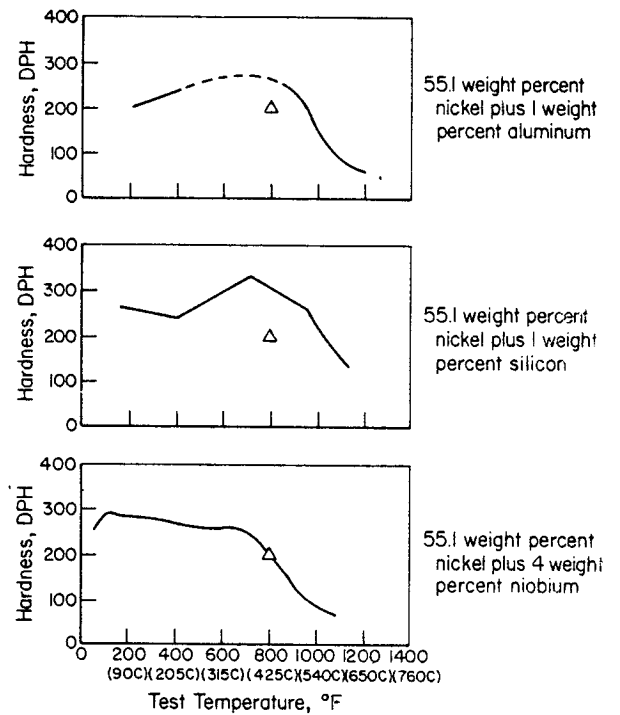


FIGURE 133.—Hardness at elevated temperatures for ternary alloys based on 55-Nitinol (55.1 weight % Ni).

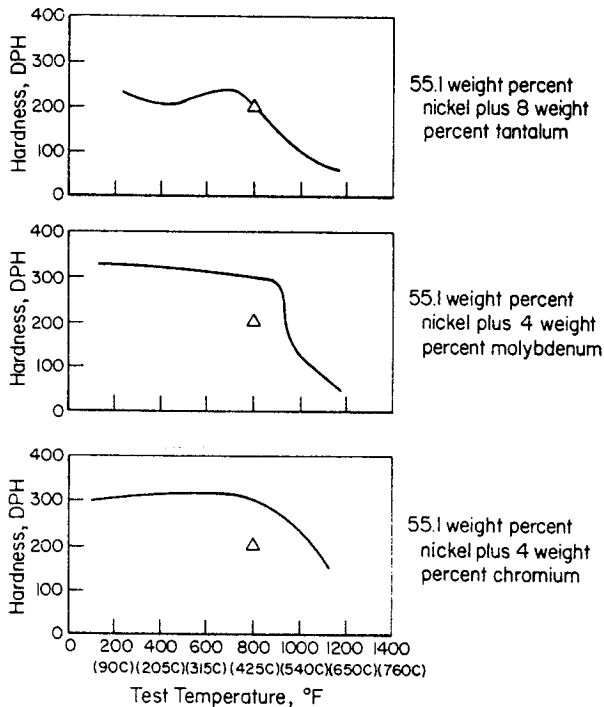


FIGURE 132.—The effect of temperature on the hardness of 55-Nitinol (55.1 weight % Ni) containing selected alloying additions.

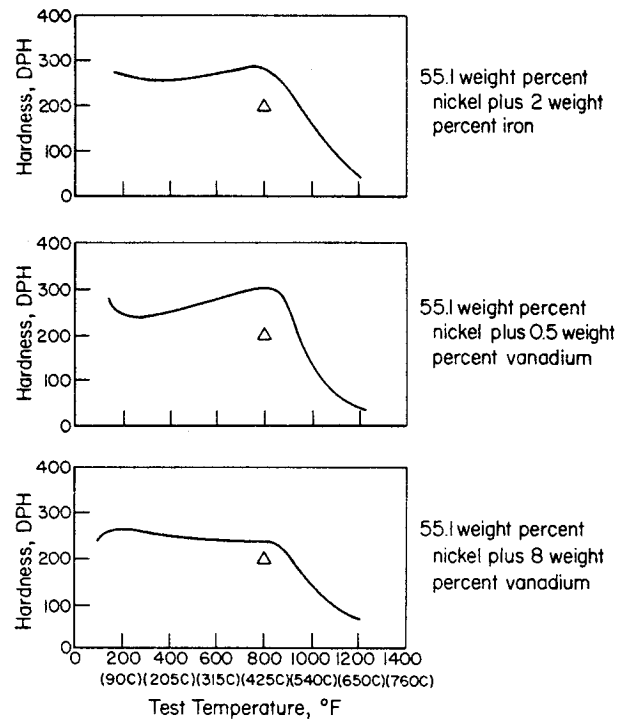


FIGURE 134.—Hardness at elevated temperatures for ternary alloys based on 55-Nitinol (55.1 weight % Ni).

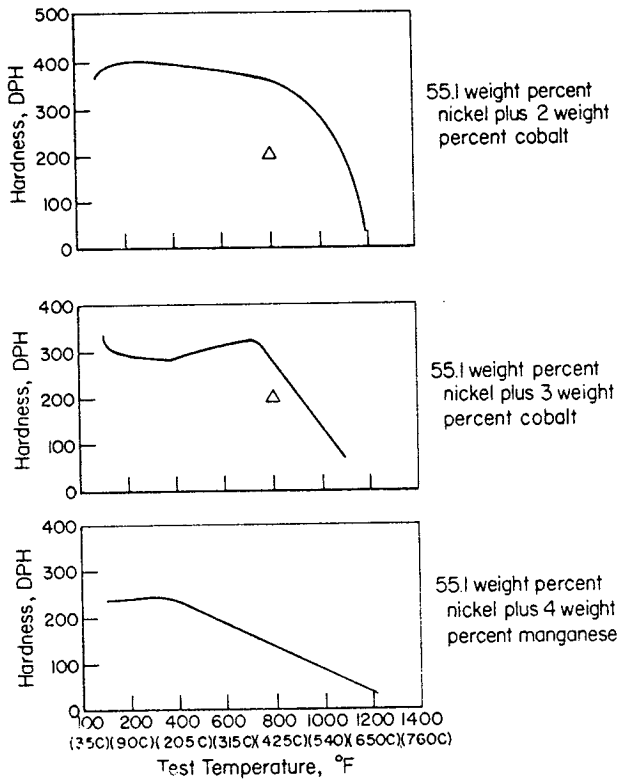


FIGURE 135.—Hardness at elevated temperatures for ternary alloys based on 55-Nitinol (55.1 weight % Ni).

hot-wrought material containing 56 weight percent Ni at room temperature (which was below the transition-temperature range). He found that the specimen endured  $2.5 \times 10^7$  cycles at 70 000 psi. It should be noted that 70 000 psi is well above the yield strength of the material.

**MACHINABILITY**

The machining characteristics of 55-Nitinol have been studied by Gould (ref. 95). Tool life tests were conducted in turning, face milling, drilling and tapping operations. Grinding tests were also conducted. It was found that tool wear is rapid and that the cutting speed, feed, tool material, tool geometry, and type of cutting fluid have a great effect on the results obtained. Specifically, Gould reported that

(1) Nitinol alloys can be turned 10 to 20 times faster with carbide tools than with high-speed steel tools. It is not practical to turn some Nitinol compositions with high-speed steel tools.

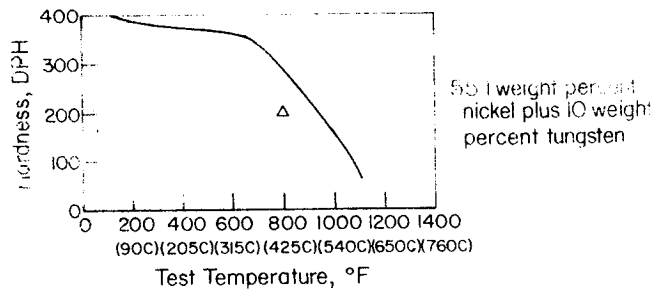


FIGURE 136.—Hardness at elevated temperatures for 55-Nitinol (55.1 weight % Ni) containing 10 weight % W.

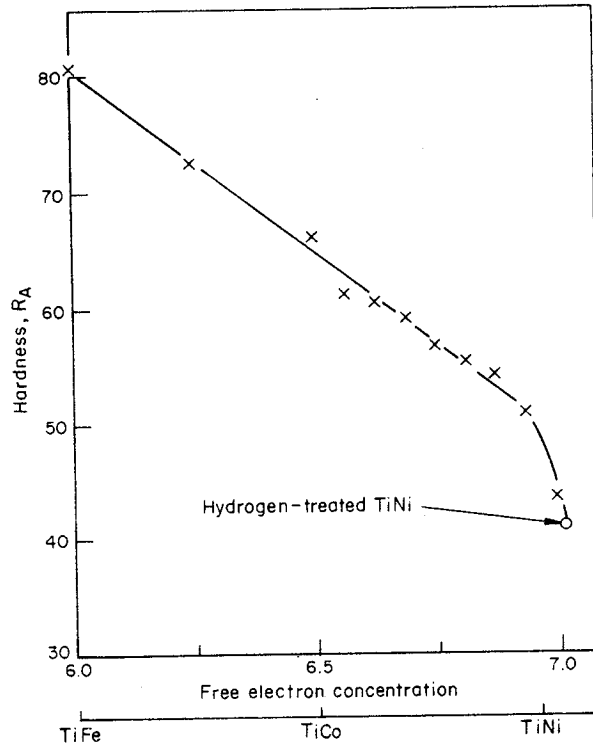


FIGURE 137.—The effect of chemical composition and free electron concentration on the hardness of the ternary phases Ti ( $Ni_xCo_{1-x}$ ) and Ti ( $Co_x, Fe_{1-x}$ ).

- (2) Feeds of 0.003 to 0.005 in./rev. should be used in turning.
- (3) The optimum tool geometry for face milling these alloys is  $0^\circ$  axial rake and  $0^\circ$  radial rake.
- (4) A feed of 0.005 in./tooth should be used in face milling. At higher and lower feeds, tool life decreases very rapidly.
- (5) Maximum tool life in face milling a 55 weight percent Ni alloy (in the "as-received" condition; hardness 217 BHN) was attained at a cutting speed of

TABLE 10.—Impact Data for NiTi

Nominal Nickel Content, weight %	Specimen section Size, <sup>a</sup> in.	Test conditions	Charpy impact, ft-lb
54.5	<sup>b</sup> 0.296×0.296	Test temperature: 24° C (room temperature)	28
54.5	<sup>b</sup> 0.296×0.296	Test temperature: 52° C	32
54.5	<sup>b</sup> 0.296×0.296	Test temperature: 93° C	29.5
54.5	<sup>b</sup> 0.296×0.296	Test temperature: -80° C	40
54.5	<sup>b</sup> 0.296×0.296	Cooled to -80° C, warmed in room-temperature water, held 15 mins. in room-temperature air. Test temperature not given.	23
54.5	<sup>b</sup> 0.296×0.296	Cooled to -112° F, warmed in room-temperature water, held 15 mins. in room-temperature air. Test temperature: 71° C	25
55.1	<sup>c</sup> 0.297×0.297	Test temperature: 24° C (room temperature)	24
55.1	<sup>c</sup> 0.297×0.297	Test temperature: 93° C	28
55.1	<sup>c</sup> 0.297×0.297	Test temperature: -80° C	43

<sup>a</sup>Unnotched bars of square cross section were employed.

<sup>b</sup>Specimens prepared from hot-swaged (900° C) bars.

<sup>c</sup>Specimens prepared from hot-rolled (900° C) plate.

TABLE 11.—Impact Properties of 55 Weight Percent Nickel Nitinol

Composition	Test temperature, ° C	Impact strength, ft-lb	
		Unnotched	Notched
"55-Nitinol"	Room	117	24
	-80	70	17
55.1 Ni-0.08 Fe	Room	155	
	-80	160	

220 ft/min, while for a 56 weight percent Ni alloy (furnace cooled, 321 BHN, or quenched, 363 BHN) the optimum cutting speed was 125 ft/min.

(6) The drilling speed of Nitinol alloys was found to be 5 to 10 times greater when a carbide drill was used than when the drill was made of M-33 high-speed steel.

(7) Drilling speed is very critical. A deviation in cutting speed of only 5 ft/min from the optimum will result in a decrease in tool life of over 50 percent.

(8) Light feeds must be used in drilling Nitinol alloys. Feeds greater than 0.002 in./rev. will result in very short tool life.

(9) An active cutting oil is required in order to obtain a reasonable drill life. Drill life is extremely short with a soluble oil cutting fluid.

(10) Silicon carbide wheels should be used in surface grinding Nitinol alloys.

(11) A highly chlorinated oil is far more effective than soluble oil in surface grinding.

(12) With most compositions tested, the grinding ratio\* was found not to change significantly with changes in wheel speed over a range of 2000 to 5000 ft./min.

(13) In surface grinding, a down feed of 0.002 in./pass provided the best grinding ratio on all of the alloys tested, except the 55 weight percent Ni alloy. The maximum grinding ratio on a 55 weight percent Ni alloy occurred at a down feed of 0.001 in./pass.

(14) In most cases, a cross feed of 0.050 in./pass produced the best grinding ratio.

(15) Abrasive sawing appears to be the only satisfactory method of cutting off.

(16) Tapping these alloys is very difficult. At best, one or two holes can be obtained before the tap breaks.

Drennen and Jackson found that the 54 weight percent Ni alloy can be machined readily by electrical discharge machining (ref. 65).

$$*\text{Grinding ratio} = \frac{\text{Volume of metal removed}}{\text{Volume of wheel removed}}$$

# Chemical Properties

## RESISTANCE TO CORROSION

Early tests by Buehler (ref. 68) showed that 55-Nitinol was not corroded during a 96-hr salt spray test (35° C, 20 percent salt solution). Neither was it attacked by sea water, a normal air atmosphere, or during normal handling; details of these three tests were not given. In a later paper, Buehler and Wang reported the results of additional experiments to evaluate the resistance of Nitinol alloys to a sea water environment (ref. 5). These tests were carried out by the Naval Ship Research and Development Center, Annapolis, Maryland; the U.S. Naval Applied Science Laboratory, Brooklyn, New York; and the Naval Ship Research and Development Center, Caderock, Maryland. The research involved studies of the resistance of Nitinol alloys to (1) impingement by high-velocity sea water, (2) cavitation erosion, (3) stress corrosion, and (4) crevice corrosion.

In the high-velocity impingement tests, commercial-purity specimens of 55-Nitinol (55 and 56 weight percent Ni nickel) were subjected to impingement by sea water at 15 to 26 ft/sec for a period of 60 days. The weight loss varied from nil to a few mg; the size of the specimens was not given. After testing, all specimens retained the appearance that they had prior to testing.

Rectangular radius-nosed bars with transverse holes downstream were used for the cavitation-erosion tests; once again, commercial-purity alloys containing about 55 and 56 weight percent Ni were used. The specimens were subjected to sea water at 117 ft/sec for a period of 30 days. At the end of this period, the 55 weight percent Ni alloy had lost about 0.092 g and the 56 weight percent Ni alloy had lost 0.050 g. The former value is about the same as found for MST 821 titanium alloy under similar test conditions.

The susceptibility of Nitinol (55 weight percent Ni) to stress corrosion in sea water was measured on

bar specimens containing a fatigue crack at the root of a V-notch. Such specimens, stressed at up to 100 percent of their yield stress while immersed in sea water, showed no tendency toward the propagation of the crack. The duration of the test was not noted.

Both commercial and laboratory-prepared specimens of 55-Nitinol (containing 55 weight percent Ni), as well as a commercial-purity specimen containing 56 weight percent Ni, were exposed to stagnant sea water. The commercial-purity material of both compositions became pitted during a one-year exposure to this environment; however, the pitting may have been related to inhomogeneities and segregation which were found in the specimens near the pitted areas. No pitting was found on the laboratory-prepared samples in a similar environment, but a comparison cannot be made here because the exposure time was not given in the reference. As noted by Buehler and Wang, additional tests in stagnant sea water will be necessary before a definite conclusion can be reached regarding the resistance of 55-Nitinol to this environment.

## RESISTANCE TO OXIDATION

Buehler (ref. 68) studied the resistance of 55-Nitinol (nominal composition, 55 weight percent Ni) to oxidation at 600°, 800°, and 1000° C. The results of his experiments are given in figure 138. It may be seen that the rate of oxidation of 55-Nitinol increases rapidly with increasing temperature between 600° and 1000° C. Buehler noted spalling of the oxide coating at 800° and 1000° C.

Buehler found that the resistance of 55-Nitinol to oxidation at 1000° C can be improved substantially by electroplating the alloy with chromium (outer layer) and nickel (inner layer) (ref. 69).

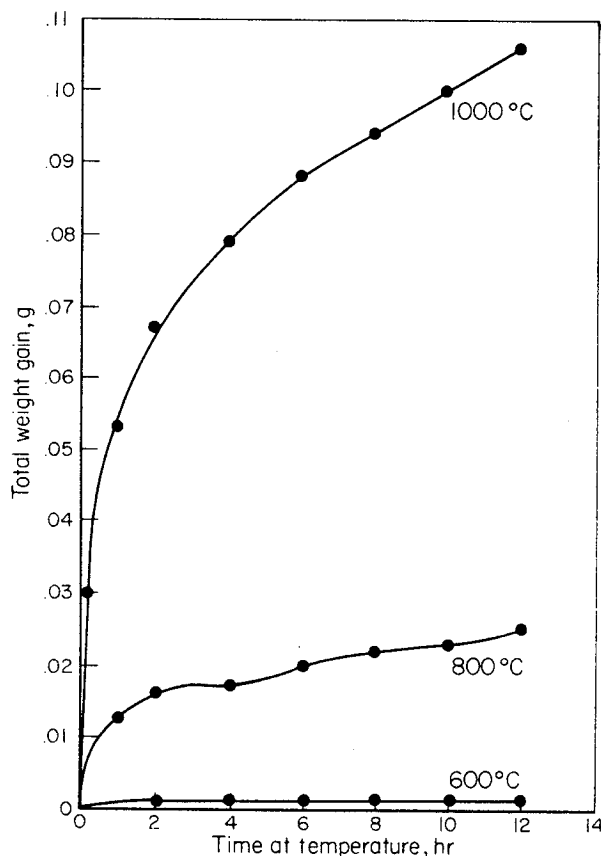


FIGURE 138.—The effect of temperature and time on the oxidation of 55-Nitinol (55.1 weight % Ni). (The initial weight of each specimen was approximately 6.5g. The surface area of the specimens was not given.)

### EFFECT OF HYDROGEN ABSORPTION

Buehler and Wang conducted an experiment to study the absorption of hydrogen by 55-Nitinol and the effect of this absorption on the properties of the alloy (refs. 54 and 89). A 0.020-in.-thick strip of 55-Nitinol was outgassed at  $10^{-7}$  torr for 24 hr at  $900^{\circ}$  C and then cooled to room temperature. Hydrogen was then introduced to a pressure of  $8 \times 10^{-2}$  torr, after which the specimen was heated to  $800^{\circ}$  C. It was found that no hydrogen was absorbed at temperatures up to about  $500^{\circ}$  C. Between  $500^{\circ}$  and  $625^{\circ}$  C, hydrogen was absorbed. After the specimen was cooled to room temperature, it was found that the pressure had decreased to  $4 \times 10^{-2}$  torr. It was concluded that the specimen had absorbed enough hydrogen to correspond to a concentration of about 150 ppm in the strip.

Furthermore, it was found that the hardness decreased from  $R_A$  43.5 to  $R_A$  41 and the transition-temperature range increased somewhat as a result of the treatment. What portion of this change might have been caused by the heating cycle and possible vaporization of nickel or titanium during the long holding period at  $900^{\circ}$  C, and how much of the effect was actually caused by hydrogen absorption cannot be ascertained from the published information.

Beuhring, Jackson and Wagner (ref. 64) studied the effect of absorbed hydrogen on the tensile properties, shape recovery, recovery force, electrical resistance, and internal friction of 55-Nitinol (chemical analysis: 45.9 weight percent Ti). Specimens of 0.089-in.-diameter wire were cathodically charged with hydrogen in an electrolytic cell having a platinum anode. The electrolyte was an aqueous solution of 0.02 wt percent sulfuric acid containing 5 drops of poison per liter of solution. The poison consisted of 2 g of phosphorus dissolved in 40 ml of carbon disulfide. Experiments indicated that charging the specimens for 1 hr at a current density of 200 mA/in<sup>2</sup> resulted in the desired hydrogen content of about 100 ppm.

The results of tests conducted immediately after hydrogen charging indicated that the ultimate tensile strength and the curves of shape recovery vs temperature, recovery force vs temperature, and electrical resistance vs temperature were essentially the same before and after hydrogen absorption. On the other hand, hydrogen charging did reduce the tensile elongation from 10 to 5.8 percent, reduce the reduction of area from 10.9 to 4.0 percent, and increase the yield strength from 12 500 to 15 000 psi.

There was some indication that internal friction was affected by hydrogen absorption. A characteristic maximum, which occurred at the same temperature as did the rapid shape recovery in uncharged 55-Nitinol, seemed to have been shifted to a slightly lower temperature in hydrogen-charged specimens. Scatter in the data prohibited a definite conclusion, but, if the phenomenon is real, it could indicate that hydrogen exerts an effect at the atomic level that is not detectable by the other measurements.

Beuhring et al. on the same program also carried out experiments which suggest that 55-Nitinol is not subject to delayed brittle failure (hydrogen-stress cracking) as a result of the absorption of over 2000 ppm of hydrogen (ref. 64).

## Applications for 55-Nitinol

Many and varied applications have been envisioned for alloys based on the NiTi intermetallic compound. Most of these applications are based on the mechanical (shape) memory properties of such alloys, which are unique in engineering alloy systems.\* The memory properties that are of most interest are the ability of the alloys to return to a present shape upon heating, the force that is generated, and the mechanical work that can be done by the alloy as it attempts to regain its preset shape. Some applications are based on other properties of the alloy; for instance, its excellent damping characteristics at temperatures below the transition-temperature range, its corrosion resistance, its nonmagnetic nature, its low density and its high fatigue strength.

Repeatability is required in some applications. In these cases, it is desirable that the Nitinol part return to its deformed shape upon cooling (after heating to effect a change from the deformed shape to the memory shape), so that it can revert to its memory shape again in successive heating cycles. As usually heat treated, 55-Nitinol is not reversible; the memory shape is retained upon cooling through the transition-temperature range. However, because the yield strength of Nitinol is low at temperatures below the transition-temperature range, reversibility can be effected by biasing the Nitinol element with a common spring. When the Nitinol is heated, it exerts sufficient force to overcome the spring completely and perform the desired operation. On the other hand, as soon as the Nitinol part cools through its transition-temperature range, the spring is strong enough to form the Nitinol into the deformed shape.

---

\*Although, as mentioned in the section on "Physical Metallurgy," certain compositions in the gold-cadmium and indium-thallium systems also show a memory effect, these alloy systems cannot be considered to be engineering alloy systems. Furthermore, it is understood that the force exerted and work done as the memory shape is recovered on heating is very much less than with NiTi-base alloys.

In this way, the Nitinol is ready to operate on the next heating cycle.

Research at Battelle-Columbus has indicated that reversibility can also be "built into" the alloy so that the use of a biasing spring or similar device is not necessary.

It should be pointed out that Nitinol is superior to thermostatic bimetals for three reasons:

(1) The force exerted by Nitinol is much greater than that exerted by bimetals.

(2) To obtain the same planar movement with bimetals as that obtained with Nitinol, the bimetals would have to be heated over a very much greater temperature range. In fact, in many cases it would be impossible to obtain the same shape change with bimetals as that possible with Nitinol.

(3) With Nitinol, the force and shape changes occur over a selected and relatively narrow temperature range; above and below this range the force and shape remain constant. With bimetals, the force and shape changes occur gradually over the entire temperature range of operation.

Many possible applications for Nitinol alloys have been disclosed in the literature. Others, still undisclosed, are being examined at this time in industrial and Government research laboratories. The primary applications that have been made public are listed in table 12. Space does not permit describing in detail the manner in which Nitinol might be used in all the applications listed in table 12. Two representative applications will, however, be described.

The first commercial application of 55-Nitinol is in the area of self-actuating fasteners; the application is a heat-shrinkable hydraulic coupling (trade-marked Cryofit). In this application, a tube of a Nitinol alloy with a transition-temperature range between liquid-nitrogen temperature and  $-54^{\circ}\text{C}$  is given a memory shape and then expanded to a larger diameter. In use, the expanded coupling is removed from a bath of

TABLE 12.—*Suggested Applications for 55-Nitinol*

Self-actuating fasteners	Military applications
Connector	Ordnance fuze (refs. 2, 92, 101)
Blind rivet (refs. 2, 55)	Nonmagnetic parts for mine craft (sweeping and servicing) (refs. 11, 12)
Self-spreading cotter pin (ref. 2)	Armor
Self-locking nut (ref. 2)	
Self-erectable structures for aerospace hardware (refs. 2, 54, 55, 67, 96, 97)	Bioengineering devices
Antenna (refs. 2, 54, 98)	Device to restrain inaccessible body parts during surgery (ref. 2)
Gravity gradient boom (ref. 54)	Recorder of temperature change during shipment of blood (ref. 99)
Passive satellite (refs. 54, 96)	Small motor to power artificial heart (ref. 99)
Aerial (ref. 97)	Device to ease intermittent occlusion (ref. 99)
Carrier of solar battery (ref. 97)	Self-tightening wire for jaw fixation following fracture of mandible (ref. 99)
Reflector or carrier of reflector (ref. 97)	Device to aid reduction and assure approximation of long bone fractures (ref. 99)
Stabilizing element (ref. 97)	
Rotation-reducing element (ref. 97)	Vibration-damping structures
Tubes, hinged or not hinged (ref. 67)	Machine mounting (ref. 54)
Multistage column (ref. 67)	Towing cable (ref. 54)
Compression-resistant strut (ref. 67)	Hydrofoil (ref. 68)
Other aerospace hardware	Advertising novelties (ref. 2)
Shutter to control temperature of satellite (ref. 67)	
Sun follower, including a continuous rotary drive (ref. 67)	Accumulator bottle used to maintain fluid pressure (ref. 2)
Sun seeker (ref. 67)	
Hydrospace hardware	Binding to compressively stress massive glass and concrete (ref. 54)
Magnetometer boom (ref. 54)	
Undersea structure (ref. 54)	Clock mechanism (ref. 54)
	Timer (ref. 54)
Replacement for a solenoid (ref. 2)	
Thermally actuated switch	Cryogenic components (ref. 54)
Force element in a circuit breaker (ref. 2)	
Current-actuated relay with a minimum of mechanical linkage (ref. 2)	liquid nitrogen and the hydraulic lines are inserted in both ends. As the coupling warms through its transition-temperature range, it contracts to its memory shape and firmly joins the two hydraulic lines with very significant force. The joint is completed at a temperature below $-54^{\circ}$ C.
Valve (refs. 91, 99)	The coupling may be removed from the hydraulic lines, if necessary, by cooling it in liquid nitrogen. It is understood that these couplings have successfully passed the test procedure specified in MIL-F-18280 and are being evaluated for use in the F-14 aircraft.
Thermal- or electrical-to-mechanical energy transducer (refs. 55, 91)	The advantages of Cryofit couplings are
Safety devices (ref. 100)	(1) Nondependence on operator skill for proper installation
Actuator of fire sprinkler system (refs. 54, 55, 91)	(2) Smaller and lighter than threaded couplings
Fire alarm (ref. 54)	(3) Elimination of costly, complicated tooling and set-up time
Temperature throttle (ref. 54)	(4) Ease of replacement of coupling or hydraulic line
Stored-energy devices	
Jack (ref. 54)	
Tool for forming metals and plastics (ref. 54)	
Temperature-sensing devices (refs. 11, 12, 54, 68, 91)	
Toys	

(5) Elimination of necessity to clean surface and purge line, as when brazing or welding is used

(6) Elimination of possibility of annealing hydraulic line, as when brazing or welding is used.

Another type of application of 55-Nitinol is in self-erectable structures for aerospace applications. While in the previous application both the shape recovery and the force aspects of the memory phenomenon are used, this class of application exemplifies primarily the shape recovery effect. A typical example is an antenna for use in space satellites; this application was first examined by Goodyear Aerospace Corporation, Akron, Ohio, under Air Force Contract F33615-67-C-1132 (ref. 98). In their research, Cross et al. constructed a large antenna that could be folded into a compact space. When heated by radiant energy, the antenna unfolded

and became erect. Although the Nitinol material that was used in this research had not been refined in accordance with the more recent advances in the state of the art of memory-heat treatment, the antenna nevertheless was an important proof-of-principle device. Antennas, or other hardware listed in table 12, could be compacted effectively in a satellite during launch and later expanded to full size by solar energy when in orbit.

These two applications, and those suggested in table 12, are only the beginning for 55-Nitinol. Creative design engineers are learning more and more about the unique properties of 55-Nitinol every day. They are finding that this alloy provides a new dimension for them, and they are endeavoring to learn more about its unusual properties. Accordingly, 55-Nitinol appears to have a very bright future in both industrial and Government applications.



## Conclusions and Recommendations

From the preceding discussions and data, it is clear that the potential for 55-Nitinol in industrial and Government applications is great. Nevertheless, in the time since the early 1960's when Buehler and Wiley at NOL discovered the unique "memory" of this series of alloys 55-Nitinol has not come into wide use. Two reasons are apparent: lack of commercial suppliers and lack of understanding of Nitinol's properties by design engineers.

Within the past year, steps have been taken to overcome both difficulties, and 55-Nitinol is now available from two sources:

- (1) Titanium Metals Corporation of America  
P.O. Box 309  
Toronto, Ohio 43964  
Cognizant Individual:  
Mr. Joseph Patrick  
Toronto Technical Laboratory
- (2) Battelle Memorial Institute  
Columbus Laboratories  
505 King Avenue  
Columbus, Ohio 43201  
Cognizant Individual:  
Dr. Curtis M. Jackson  
Associate Chief  
Nonferrous Metallurgy Division

Titanium Metals Corporation of America is marketing the material on a developmental basis, and Battelle-Columbus, not being a manufacturer, has prepared well-characterized research samples on a special-order basis.

The major step forward in making data on the alloy available to potential users has been the research carried out by Goodyear Aerospace Corporation and Battelle-Columbus (ref. 63). A significant number of industrial organizations and Government agencies are also now investigating the properties of 55-Nitinol in

their own laboratories or having such work performed by others. Nevertheless, additional research is required to characterize 55-Nitinol more completely before the alloy can be used extensively in industrial and Government applications. Moreover, it is important that those who perform this research be cognizant of the sensitivity of the alloy to chemical composition and processing, and design their experiments accordingly. The authors know of quite a few industrial organizations that, because they overlooked this important fact, were unable to reproduce their original results. Later research, carried out after the processing and composition sensitivity of the alloy was brought to their attention, yielded reproducible results.

The specific properties and characteristics that must be known to make 55-Nitinol effective in engineering applications vary, of course, with the application. Many of these properties have been investigated in the NASA-Langley program and have been summarized in this report. However, it should be understood that these properties were found for three particular alloy compositions that were processed in a particular manner; because of the composition processing sensitivity of 55-Nitinol, these properties should be regarded as "ball-park" figures, which indicate what 55-Nitinol can do, and not necessarily the properties that one will obtain from any batch of 55-Nitinol regardless of chemical composition and the procedures used to process it.

There are several important properties of 55-Nitinol that apparently have not been investigated to date. It is recommended that research be conducted on these properties:

- (1) Fatigue strength above the transition-temperature range.
- (2) Impact strength above the transition-temperature range.
- (3) Shelf life after memory heat treatment, while in (a) the "memory configuration" and (b) the

“intermediate shape” (fig. 1).

A variety of other properties should also be examined, depending on the particular application that is envisioned.

Because of the strong dependence of the properties of 55-Nitinol on the effects of processing, the optimization of the properties of the alloy should include studies of the effect of processing variables such as the state of stress imposed during deformation of the memory configuration to the intermediate shape (fig. 1), the time and temperature of the memory heat treatment, and the applied stress during the memory heat treatment. These and other processing variables can strongly affect the properties of 55-Nitinol.

The aforementioned recommendations have concerned the empirical characterization of 55-Nitinol. However, as noted in the section entitled “Physical Metallurgy,” neither the atom movements responsible for the “memory” in 55-Nitinol nor the equilibrium structures in Nitinol alloys have yet been proven

conclusively. Until these problems are solved, the optimization of the properties of the alloy must, of necessity, be carried out in a strictly empirical manner. To obtain basic information that is needed as a guideline for applied research, basic research must be conducted to identify the equilibrium phases in 55-Nitinol and the atomic mechanism responsible for the memory properties. It is important that this research be carried out over a range of chemical composition on alloys which are melted, cast, and processed under very carefully selected and well documented procedures, and that at least two (more than two would be preferable) properties be measured. The research should include not only macroscopic property measurements but also examinations by means of light and electron microscopy and X-ray and/or electron diffraction. Although much of the research can be carried out by using polycrystalline specimens, additional single-crystal research on very rigorously characterized material seems essential for the firm determination of equilibrium structures.

## References

- Buehler, W. J.; and Wiley, R. C.: Nickel-Base Alloys. U. S. Patent 3,174,851, Mar. 23, 1965.
- Wagner, H. J.; and Jackson, C. M.: What You Can Do With That "Memory" Alloy . . . . Materials Engineering, Vol. 70, No. 4, Oct. 1969, pp. 28-31.
- Drennen, D. C.; Jackson, C. M.; and Wagner, H. J.: Metallurgical Services in Connection With Nitinol Wire. Summary Rept., Contract NAS 1-7522, Battelle Memorial Institute, June 14, 1968.
- Cross, W. B.; Kariotis, A. H.; and Stimler, F. J.: Nitinol Characterization Study. NASA CR-1433, Sept. 1969.
- Buehler, W. J.; and Wang, F. E.: A Summary of Recent Research on the Nitinol Alloys and Their Potential Application in Ocean Engineering. Ocean Engineering, Vol. 1, 1968, pp. 105-120.
- Laves, F.; and Wallbaum, H. J.: Zur Kristallchemie Von Titan-Legierungen. Naturwissenschaften, Vol. 27, 1939, pp. 674-675.
- Margolin, H.; Ence, E.; and Nielsen, J. P.: Titanium-Nickel Phase Diagram. Transactions of AIME, Vol. 197, 1953, pp. 243-247.
- Poole, D. M.; and Hume-Rothery, W.: The Equilibrium Diagram of the System Nickel-Titanium. J. Inst. Metals, Vol. 83, 1954, pp. 473-480.
- Duwez, P.; and Taylor, J. L.: Structure of Intermediate Phases in Alloys of Titanium With Iron, Cobalt, and Nickel. Transactions of AIME, Vol. 188, 1950, pp. 1173-1176.
- Purdy, G. R.; and Parr, J. G.: Study of Titanium-Nickel System Between  $Ti_2Ni$  and TiNi. Transactions of AIME, Vol. 221, 1961, pp. 636-639.
- Buehler, W. J.; and Wiley, R. C.: TiNi - Ductile Intermetallic Compound. Transactions of ASM, Vol. 55, 1962, pp. 269-276.
- Buehler, W. J.; and Wiley, R. C.: The Properties of TiNi and Associated Phases. Rept. NOLTR 61-75 (AD 266607), U.S. Naval Ordnance Laboratory, Aug. 3, 1961.
- Buehler, W. J.; Gilfrich, J. V.; and Wiley, R. C.: Effect of Low-Temperature Phase Changes on the Mechanical Properties of Alloys Near Composition TiNi. J. Appl. Phys., Vol. 34, 1963, pp. 1475-1477.
- Gilfrich, J. V.: X-ray Diffraction Studies on the Titanium-Nickel System., Vol. 6. Advances in X-ray Analysis. Proceedings of the Eleventh Annual Conference on Application of X-ray Analysis, Plenum Press (New York), 1963, pp. 74-84.
- Koskimaki, D.; Marcinkowski, M. J.; and Sastri, A. S.: Solid State Diffusional Transformations in the Near-Equiatomic Ni-Ti Alloys. Transactions of the Metallurgical Society of AIME, Vol. 245, 1969, pp. 1883-1890.
- Wasilewski, R. J.: Elastic-Modulus Anomaly in TiNi. Transactions of AIME, Vol. 233, 1965, pp. 1691-1693.
- Wang, F. E.; Buehler, W. T.; and Pickart, S. J.: Crystal Structure and a Unique "Martensitic" Transition of TiNi. J. Appl. Phys., Vol. 36, 1965, pp. 3232-3239.
- Dautovich, D. P.; and Purdy, G. R.: Phase Transformations in TiNi. Canadian Metallurgical Quarterly, Vol. 4, 1965, pp. 129-143.
- Rozner, A. G.; and Wasilewski, R. J.: Tensile Properties of NiAl and NiTi. J. Inst. Metals, Vol. 94, 1966, pp. 169-175.
- Zijderveld, J. A.; deLange, R. G.; and Verbraak, C. A.: La Transformation Martensitique des Alliages Titane-Nickel Au Voisinage de La Composition Equiatomique. Memoires Scientifiques Revue de Metallurgie, Vol. 63, 1966, pp. 885-888.
- Wasilewski, R. J.; Butler, S. R.; and Hanlon, J. E.: On the Martensitic Transformation in TiNi. Metal Sci. J., Vol. 1, 1967, pp. 104-110.
- Hanlon, J. E.; Butler, S. R.; and Wasilewski, R. J.: Effect of Martensitic Transformation on the Electrical and Magnetic Properties of NiTi. Transactions of the Metallurgical Society of AIME, Vol. 239, 1967, pp. 1323-1327.
- Wasilewski, R. J.; Butler, S. R.; Hanlon, J.; and Worden, D.: Discussion of "Solid State Diffusional Transformations in the Near-Equiatomic NiTi Alloys. Metallurgical Transactions, Vol. 1, 1970, pp. 1459-1460.
- Wasilewski, R. J.; Butler, S. R.; Hanlon, J. E.; and Worden, D.: The Structure Homogeneity Range in TiNi. J. Metals, Vol. 21, No. 3, 1969, pp. 41A-42A. Submitted to Metallurgical Transactions, 1970.
- Mueller, M. H.; and Knott, H. W.: "The Crystal Structures of  $Ti_2Cu$ ,  $Ti_2Ni$ ,  $Ti_4Ni_2O$ , and  $Ti_4Cu_2O$ . Transactions of the Metallurgical Society of AIME, Vol. 227, 1963, pp. 674-678.
- Rozner, A. G.; Heintzelman, E. F.; Buehler, W. J.; and Gilfrich, J. V.: Effect of Addition of Oxygen, Nitrogen and Hydrogen on Microstructure and Hardness of Cast TiNi Intermetallic Compound. Transactions of ASM, Vol. 58, 1965, pp. 415-418.
- Taylor, A.; and Floyd, R. W.: Precision Measurements of Lattice Parameters of Non-Cubic Crystals. Acta Crystallographica, Vol. 3, 1950, pp. 285-289.
- Laves, F.; and Wallbaum, H. J.: The Crystal Structure of  $Ni_3Ti$  and  $Ni_2Ti$ . Zeitschrift fur Kristallographie, Vol. A101, 1939, pp. 78-93.
- Taylor, A.; and Floyd, R. W.: The Constitution of Nickel-Rich Alloys of the Nickel-Chromium-Titanium System. J. Inst. Metals, Vol. 80, 1952, pp. 577-587.
- Stuwe, H. P.; and Shimomura, Y.: Gitterkonstanten der

- Kubisch Raumzentrierten Phasen FeTi, CoTi, NiTi. *Zeitschrift für Metallkunde*, Vol. 51, 1960, pp. 180-181.
31. Pietrokowsky, P.; and Youngkin, F. G.: Ordering in the Intermediate Phases TiFe, TiCo, and TiNi. *J. Appl. Phys.* Vol. 31, 1960, pp. 1763-1766.
  32. Wang, F. E.; Syeles, A. M.; Clark, W. L.; and Buehler, W. J.: Growth of TiNi Single Crystals by a Modified "Strain-Anneal" Technique. *J. Appl. Phys.*, Vol. 35, 1964, p. 3620.
  33. Buehler, W. J.; and Wang, F. E.: Martensitic Transformations in the TiNi Compound. Reactivity in Solids. Proceedings of the 5th International Symposium (Munich), 1964, Elsevier Publishing Company (Amsterdam), 1965, pp. 79-89.
  34. Kubaschewski, O.: The Heats of Formation in the System Aluminum + Nickel + Titanium. *Transactions of the Faraday Society*, Vol. 54, 1958, pp. 814-820.
  35. Chang, L. C.; and Read, T. A.: Plastic Deformation and Diffusionless Phase Changes in Metals—The Gold-Cadmium Beta Phase. *Transactions of AIME*, Vol. 191, 1951, pp. 47-52.
  36. Sastri, A. S.; Marcinkowski, M. J.; and Koskimaki, D.: Nature of the NiTi Martensite Transformation. *Physica Status Solidi*, Vol. 25, 1968, pp. K67-K69.
  37. Marcinkowski, M. J.; Sastri, A. S.; and Koskimaki, K.: Martensitic Behaviour in the Equi-Atomic NiTi Alloy. *Phil. Mag.*, Vol. 18, 1968, pp. 945-958.
  38. Sastri, A. S.; and Marcinkowski, M. J.: Deformation Behavior in the Near-Equiatomic NiTi Alloys. *Transactions of the Metallurgical Society of AIME*, Vol. 242, 1968, pp. 2393-2398.
  39. Pfeifer, H-U.; Bhan, S.; and Schubert, K.: Zum Aufbau Des Systems Ti-Ni-Cu Und Einiger Quasihomologer Legierungen. *J. Less Common Metals*, Vol. 14, 1968, pp. 291-302.
  40. Dautovich, D. P.; Melkvi, Z.; Purdy, G. R.; and Stager, C. V.: Calorimetric Study of a Diffusionless Phase Transformation in TiNi. *J. Appl. Phys.*, Vol. 37, 1966, pp. 2513-2514.
  41. Wasilewski, R. J.: Personal communication to G. R. Purdy, 1965.
  42. Freise, E.: Personal communication to R. J. Wasilewski, Northwestern University, 1967.
  43. Starke, E. A.; and Lee, E. U.: Observations of "Side-Bands" on X-ray Patterns of the Intermetallic Compound TiNi. *Materials Res. Bull.*, Vol. 2, 1967, pp. 231-239.
  44. Wang, F. E.; DeSavage, B. F.; Buehler, W. J.; and Hosler, W. R.: The Irreversible Critical Range in the TiNi Transition. *J. Appl. Phys.*, Vol. 39, 1968, pp. 2166-2175.
  45. Lieberman, D. S.; Wechsler, M. S.; and Read, T. A.: Cubic to Orthorhombic Diffusionless Phase Change—Experimental and Theoretical Studies of AuCd. *J. Appl. Phys.*, Vol. 26, 1955, pp. 473-484.
  46. Burkart, M. W.; and Read, T. A.: Diffusionless Phase Change in the Indium-Thallium System. *Transactions of AIME*, Vol. 197, 1953, pp. 1516-1524.
  47. Chang, L. C.: On Diffusionless Transformation in Au-Cd Single Crystals Containing 47.5 Atomic Percent Cadmium: Characteristics of Single-Interface Transformations. *J. Appl. Phys.*, Vol. 23, 1952, pp. 725-728.
  48. Lieberman, D. S.: Phase Transformations. ASM Seminar (Detroit), 1968.
  49. Ball, A.; Bergersen, S. G.; and Hutchison, M. M.: Effect of Room-Temperature Prestrain on the Tensile Properties of the Intermetallic Compound NiTi in the Temperature Range 150° to 370° C. Proceedings of the International Conference on the Strength of Metals and Alloys, transactions of the Japan Institute of Metals, Vol. 9 (supplement), 1968, pp. 291-295.
  50. DeLange, R. G.; and Zijdeveld, J. A.: Shape-Memory Effect and the Martensitic Transformation of TiNi. *J. Appl. Phys.*, Vol. 39, 1968, pp. 2195-2200.
  51. Chandra, K.; and Purdy, G. R.: Observations of Thin Crystals of TiNi in Premartensitic States. *J. Appl. Phys.*, Vol. 39, 1969, pp. 2176-2181.
  52. Iwasaki, K.; and Hasiguti, R. R.: Antiphase Boundaries in Ti50-Ni50 Alloys. Paper presented at the 3rd Bolton Landing Conference on Ordered Alloys (Lake George, N. Y.) 1969.
  53. Otsuka, K.; and Shimizu, K.: Precipitation Process in Ti-50Ni. Paper presented at the 62nd Annual Meeting of the Japan Institute of Metals, 1968.
  54. Buehler, W. J.; and Wang, F. E.: Study of Transition Element Intermetallic Compounds. Paper presented at the Ninth Navy Science Symposium (Washington, D.C.) 1966.
  55. Buehler, W. J.; and Cross, W. B.: 55-Nitinol, Unique Wire Alloy with a Memory. *Wire J.*, Vol. 2, June 1969, pp. 41-49.
  56. Drennen, D. C.; Jackson, C. M.; and Wagner, H. J.: The Development of Melting and Casting Procedures for Nitinol Nickel-Base Alloys. Rept. SC-CR-69-3070, Contract 16-7540, Battelle Memorial Institute, Dec. 1968.
  57. Buehler, W. J.; and Cross, W. B.: 55-Nitinol, Unique Wire Alloy with a Memory. *Wire J.*, Vol. 2, June, 1969, pp. 41-49.
  58. Drennen, D. C.; Jackson, C. M.; and Wagner, H. J.: A Study of the Homogeneity of a Large Ingot of a Nitinol Alloy. Final Rept., Contract FAO-16-8835, Battelle Memorial Institute, Nov. 21, 1969.
  59. Hanlon, J. E.; Butler, S. R.; and Wasilewski, R. J.: Effect of Martensitic Transformation on the Electrical and Magnetic Properties of NiTi. *Transactions of the Metallurgical Society of AIME*, Vol. 239, 1967, pp. 1323-1327.
  60. Wang, F. E.; Syeles, A. M.; Clark, W. L.; and Buehler, W. J.: Growth of TiNi Single Crystals by a Modified "Strain-Anneal" Technique. *J. Appl. Phys.*, Vol. 35, 1964, p. 3620.
  61. Wang, F. E.; Syeles, A. M.; Clark, W. L.; and Buehler, W. J.: Method for Growing Single Crystals. U.S. Patent 3,352,722, Nov. 14, 1967.
  62. Buehler, W. J.; and Wang, F. E.: Martensitic Transformations in the TiNi Compound. Reactivity in Solids, Proceedings of the 5th International Symposium (Munich), 1964, Elsevier Publishing Company (Amsterdam), 1965, pp. 79-89.
  63. Cross, W. B.; Kariotis, A. H.; and Stimler, F. J.: Nitinol

- Characterization Study. NASA CR-1433, Sept. 1969.
64. Beuhling, V. F.; Jackson, C. M.; and Wagner, H. J.: The Effect of Thermal Cycling and Hydrogen Absorption on Selected Properties of 55-Nitinol. Final Rept. BMI-X-579, Contract SANL 613/040 on AEC Contract W-7405-eng-92, Battelle Memorial Institute, Sept. 15, 1969.
  65. Drennen, D. C.; and Jackson, C. M.: The Preparation of Research Samples of 55-Nitinol. Final Rept., Contract SANL 613/066 on AEC Contract W-7405-eng-92, Battelle Memorial Institute, Oct. 18, 1969.
  66. Cooper, J. E.; Bowker, D. E.; and Cross, W. B.: Investigation of the Unique Memory Properties of 55-Nitinol Alloy. Materials and Processes for the 1970's. Proceedings of the 15th Annual Symposium of the Society of Aerospace Material and Process Engineers, 1969.
  67. Schuerch, H. U.: Certain Physical Properties and Applications of Nitinol. NASA CR-1232, Nov. 1968.
  68. Buehler, W. J.: "Intermetallic Compound Based Materials for Structural Applications." Proceedings of the Seventh Navy Science Symposium, Rept. ONR-16, vol. 1 (AD 421708), 1963, pp. 1-30.
  69. Buehler, W. J.: Personal communication to D. C. Drennen and C. M. Jackson. U. S. Naval Ordnance Laboratory, 1968.
  70. Cooper, J. E.; Bowker, D. E.; and Cross, W. B.: Investigation of the Unique Memory Properties of 55-Nitinol Alloy. Materials and Processes for the 1970's. Proceedings of the 15th Annual Symposium of the Society of Aerospace Material and Process Engineers, 1969.
  71. Drennen, D. C.; Jackson, C. M.; and Wagner, H. J.: Metallurgical Services in Connection With Nitinol Wire. Summary Rept., Contract NAS 1-7522, Battelle Memorial Institute, June 14, 1968.
  72. Buehler, W. J.; Gilfrich, J. V.; and Wiley, R. C.: Effect of Low-Temperature Phase Changes on the Mechanical Properties of Alloys Near Composition of TiNi. *J. Appl. Phys.*, Vol. 34, 1963, pp. 1475-1477.
  73. Rozner, A. G.; and Buehler, W. J.: Low Temperature Deformation of the TiNi Intermetallic Compound. Rept. NOLTR 66-38, U.S. Naval Ordnance Laboratory, Mar. 1, 1966.
  74. Buehler, W. J.; and Wiley, R. C.: The Properties of TiNi and Associated Phases. Rept. NOLTR 61-75 (AD 266607), U.S. Naval Ordnance Laboratory, Aug. 3, 1961.
  75. Goff, J. F.: Thermal Conductivity, Thermoelectric Power, and the Electrical Resistivity of Stoichiometric TiNi in the 3° to 300° K Temperature Range, *J. Appl. Phys.*, Vol. 35, 1964, pp. 2929-2927.
  76. Gilfrich, J. V.: X-ray Diffraction Studies on the Titanium-Nickel System. Vol. 6: Advances in X-ray Analysis. Proceedings of the Eleventh Annual Conference on Application of X-ray Analysis, Plenum Press (New York), 1963, pp. 74-84.
  77. Wang, F. E.; DeSavage, B. F.; Buehler, W. J.; and Hosler, W. R.: The Irreversible Critical Range in the TiNi Transition. Symposium on TiNi and Associated Compounds, NOLTR 68-16, U.S. Naval Ordnance Laboratory, Feb. 20, 1968, pp. 8-1-8-24.
  78. Allgaier, R. S.: Analysis of the Hall Coefficient Behavior in TiFe, TiCo, TiNi, and Their Alloys. Symposium on TiNi and Associated Compounds, NOLTR 68-16, U.S. Naval Ordnance Laboratory, Feb. 20, 1968, pp. 121-126.
  79. Bradley, D.: Sound Propagation in Near-Stoichiometric TiNi Alloys. *J. Acoust. Soc. Am.*, Vol. 37, no. 4, 1965, pp. 700-702.
  80. Rozner, A. G.; and Spinner, S.: Some Consideration of the Elastic Properties of TiNi in the Vicinity of Transformation Temperature. Symposium on TiNi and Associated Compounds, NOLTR 68-16, U.S. Naval Ordnance Laboratory, Feb. 20, 1968, pp. 6-1 - 6-19.
  81. Spinner, S.; and Rozner, A. G.: Elastic Properties of NiTi as a Function of Temperature. *J. Acoust. Soc. Am.*, Vol. 40, No. 5, 1966, pp. 1009-1015.
  82. Hasiguti, R. R.; and Iwasaki, K.: Internal Friction and Related Properties of TiNi Intermetallic Compound. Symposium on TiNi and Associated Compounds, NOLTR 68-16, U.S. Naval Ordnance Laboratory, Feb. 20, 1968, pp. 4-1 - 4-12.
  83. Hasiguti, R. R.; and Iwasaki, K.: Correlations Between Plastic Deformation and Phase Change in the Compound TiNi with Special Reference to Internal Friction. Proceedings of the International Conference on the Strength of Metals and Alloys, transactions of the Japan Institute of Metals (supplement), Vol. 9, 1968, pp. 288-291.
  84. Berman, H. A.; West, E. F.; and Rozner, A. G.: Anomalous Heat Capacity of TiNi. *J. Appl. Phys.*, Vol. 38, 1967, 4473-4476.
  85. Bragg, W. L.; and Williams, E. J.: The Effect of Thermal Agitation on Atomic Arrangement in Alloys. Proceedings of the Royal Society, Vol. A145, 1934, pp. 699-730.
  86. Bragg, W. L.; and Williams, E. J.: The Effect of Thermal Agitation on Atomic Arrangement in Alloys - II. Proceedings of the Royal Society, Vol. A151, 1935, pp. 540-566.
  87. Goff, J. F.: Dependence of the Transport Properties of Transition Metal Alloys and Compounds on the Electron Number. Symposium on TiNi and Associated Compounds, NOLTR 68-16, U.S. Naval Ordnance Laboratory, Feb. 20, 1968, pp. 9-1 - 9-7.
  88. Rozner, A. G.; and Buehler, W. J.: Effect of Cold Work on Room Temperature Tensile Properties of TiNi Intermetallic Compound. Transactions of ASM, Vol. 59, 1966, pp. 350-352.
  89. Wang, F. E.: The Mechanical Properties as a Function of Temperature and Free Electron Concentration in Stoichiometric TiNi, TiCo and TiFe Alloys. Proceedings of the International Conference on Fracture (Sendai, Japan), 1965, pp. 899-908.
  90. Scholl, R.; Larson, D. J., Jr.; and Freise, E. J.: A Study of the Relative Ductilities of TiFe, TiCo and TiNi. Symposium on TiNi and Associated Compounds, NOLTR 68-16, U.S. Naval Ordnance Laboratory, Feb. 20, 1968, pp. 18-1 - 18-14.
  91. Buehler, W. J.; and Goldstein, D. M.: Conversion of Heat

- Energy to Mechanical Energy, U.S. Patent 3,403,238, Sept. 24, 1968.
92. Marks, R.: Personal communication to C. M. Jackson and H. J. Wagner. U.S. Army, Harry Diamond Laboratories, Sept. 1968.
  93. Goldstein, D. M.; Buehler, W. J.; and Wiley, R. C.: Effects of Alloying Upon Certain Properties of 55.1 Nitinol. Rept. NOLTR 64-235, U.S. Naval Ordnance Laboratory, May 28, 1965.
  94. Anon.: 55 Nitinol Alloys. U.S. Naval Ordnance Laboratory, Apr. 1967.
  95. Gould, J. V.: Machinability of Nickel-Titanium Alloys. Contract N60921-6814 (AD 419009), Metcut Research Associates, Inc., June 24, 1963.
  96. Johnson, J. F.; Reiser, D.; and Ovrevik, G. S.: Erectable Structure for a Space Environment. U.S. Patent 3,391,882, July 9, 1968.
  97. Anon.: Improvements in or Relating to Space Vehicles. Nederlandse Organisatie voor Toegepastnatuurwetenschappelijk Onderzoek ten Behoeve van Nijverheid, Handel en Verkeer. British Patent 1,116,158, June 6, 1968.
  98. Cross, W. B.: Personal communication to C. M. Jackson. Jan. 25, 1968.
  99. Heisterkamp, C. A., III; Buehler, W. J.; and Wang, F. E.: 55-Nitinol—A New Biomaterial. Paper presented at the 8th International Conference on Medical and Biomedical Engineering (Chicago), 1969.
  100. Frei, E. H.; Leibinzohn, S.; and Shtrikman: Thermally Actuated Devices. U.S. Patent 3,285,470, Nov. 15, 1966.
  101. Rothwarf, F.; Auerbach, A.; and Ford, D. R.: Feasibility of Using Memory Metal Effects for Fuze Applications: A. The Use of Martensite Materials in the Design of Thermally Activated Springs. Memorandum Rept. M68-38-1, Department of the Army, Frankford Arsenal, Nov. 1968.